Université de Neuchâtel Faculté des Sciences

Molecular Arene Ruthenium Cages: New Vectors to Deliver Drugs to Cancer Cells

Thèse présentée à la Faculté des Sciences par

Johan Mattsson

Chimiste diplômé de l'Université de Mälardalen (Suède)

Pour l'obtention du grade de Docteur ès Sciences

Membres du jury:

Dr Bruno Therrien	Co-Directeur de thèse, Université de Neuchâtel
Prof. Georg Süss-Fink	Co-Directeur de thèse, Université de Neuchâtel
Prof. Paul J. Dyson	Rapporteur, Ecole Polytechnique Fédérale de Lausanne
Prof. Jean-Marc Neuhaus	Rapporteur, Université de Neuchâtel

Université de Neuchâtel

Institut de Chimie de l'Université de Neuchâtel

Mai 2010

Université de Neuchâtel

FACULTE DES SCIENCES
Secrétariat-Décanat de la faculté
- Rue Emile-Argand 11
- CP 158
- CH-2009 Neuchâtel

IMPRIMATUR POUR LA THESE

Molecular Arene Ruthenium Cages : New Vectors to Deliver Drugs to Cancer Cells

Johan MATTSSON

UNIVERSITE DE NEUCHATEL

FACULTE DES SCIENCES

La Faculté des sciences de l'Université de Neuchâtel,
sur le rapport des membres du jury

MM. G. Süss-Fink (co-directeur de thèse), B. Therrien (co-directeur de thèse),
J.-M. Neuhaus et P.J. Dyson (EPF Lausanne)

autorise l'impression de la présente thèse.

Neuchâtel, le 8 juin 2010

Le doyen :
F. Kessler

UNIVERSITE DE NEUCHATEL
FACULTE DES SCIENCES
Secrétariat - décanat de la faculté
Rue Emile-Argand 11 - CP 158
CH-2009 Neuchâtel
Felix Kessler

■ Téléphone : +41 32 718 21 00 ■ E-mail : secretariat.sciences@unine.ch ■ www.unine.ch/sciences

Acknowledgements

The work presented in this thesis has been done in the chemistry laboratory of inorganic chemistry and molecular catalysis of University of Neuchâtel, under the direction of Dr. Bruno Therrien and Prof. Georg Süss-Fink.

First of all I would like to thank Dr. Bruno Therrien. Thank You for giving me the opportunity to do research with you in Switzerland. I've been given many interesting projects and we have had many interesting discussions. I have learned a lot during these years and I thank You for trusting in me to work freely and putting up with me for such a long time.

Prof. Georg Süss-Fink, Thank You for allowing me to work here and incorporating me into your group.

I want to acknowledge the Swiss Science Foundation for being so generous by financing my studies.

Prof. Paul Dyson and Prof. Jean-Marc Neuhaus, Thank you for taking interest in my work and accepting to be in my jury

I direct massive thanks to all collaborators, Prof. Paul Dyson, Dr. Anna Renfrew and Dr Olivier Zava for the biological tests, Petr Stepnicka for electrochemical tests, Julien Furrer for NMR spectroscopy and Yoshihisa Sei and Kentaro Yamaguchi for mass spectroscopy measurements.

Sarah Angus-Dunne, I'm very greatful for all You have done for me. Without You I wouldn't be where I am today with all the great experiences that I've had.

Ex members of this group Ludovic Chahen, Jerome Canivet, Mathieu Tschan and Vladimir Romakh thank you for introducing me to the chemistry world of Neuchâtel and for being patient speaking English to me and for the nice ambience in the lab.

I want to thank my present (future ex) colleagues Tien, Farooq, Julien, Nicolas and Justin for the team work and ambience in the lab.

Former lab partners Anne-Flore Ibao (AFI), Matheiu Auzias and Michaël Gras thank you for all the laughs, singing and other shenanigans that made lab work a bit more fun.

Friends some on and off campus, Anca, Julien Pierron, Yves Casta, Christoph Letondor, Olivier Zava, Mikael Guillomee with respective girlfriend/boyfriend and everyone else of the Cerf gang so that no one is forgotten.

A big thank you to the water hole Café du Cerf and its owners Cathriona, Stephen, Conor and Donal, and as well to all the wonderful people there. Thank you for making the bar better all the time and keeping it a relaxing place where everybody feels at home.

To the waterpolo team, thank you for keeping me in shape, laughs and beer drunk at the same time, without the team I would be fat like a frog.

Michaël Gras. Dude thank you for your friendship in both good and bad times I know I can always count on you. Seriously a massive thanks for these years, you have been an amazing friend.

I want to thank the people down in Cape Town for taking care of me while I was there. Greg, Preshen, Tameryn, Nathan thank you all, hope you all take coffee breaks now.

As well an enormous thanks to the Rochat family, you make me feel like a family member. I am grateful for all the good times I've had with you. It's very nice to have a second family when you are far away from home.

Jason, Thanks for being a good friend and helping me keep my English decent, ARVINIS again next year?

Sam and the Reign of Silence, Thanks for all the partying, concerts and skiing it has been great. I hope we will continue to go to Adelboden even in the future

A big thank you to all friends down here who made my stay a bit more fun and comfortable

The Albini/Liegeois family (David Delphine, Léa), thank you for laughs, dinners, help and fun. Your enourmous generosity has been well appreciated, as well making me babysit for the first time was an experience I will never forget.

To the people in Sweden
Thank you the Västeras mafia, Jan, Martin, Christina (ja du är med där nu), Thomas KW, Patrik, John, Jakob and Erik for always taking me out to have a good time while I'm at home.

Thank you Robban and Becka for always greeting me with an open door (even though sometimes reluctantly) and all the barbeques, especially the Christmas ones. Thank you Rob for the friendship, partying, concerts, akkurat and all music dicussions and of course for being the only friend who came to visit me down here….

I want give an enormous thank you to my family, Mom, Dad, Christian, Anna, Jocke and Mira (miraklet) for always taking care of me while at home and supporting me while I'm away. It was always nice to have Sweden behind me for this endeavour.

Last but not least: Thank you Anne, for your love, your support, your patience and a righteous kick in the butt when needed. I don't think this would have been possible without you. So a million thanks and all my love and appreciation, it's almost as much your thesis as it is mine.

Abstract

Ever since the discovery of cisplatin by Rosenberg in the 1970's metal complexes as anti-cancer drugs have become an increasing subject of research. Ruthenium as a substitute for the toxic platinum metal has received a lot of attention recently. Organometallic compounds such as arene ruthenium complexes are very versatile and have proven to be active against cancer cells. In order to exploit their activity this work consisted in incorporating arene ruthenium compounds in large systems for facilitating transport into cancer cells.

In a first approach, arene ruthenium compounds were combined with dendritic systems to form metalla-dendrimers: The goal of this being to transport the active ruthenium compounds into cancer cells by large dendrimers. The biological activity was measured which revealed that these complexes are taken up by cells, showing moderate to high cytotoxicity.

In a second approach, as arene ruthenium complexes are also interesting supramolecular building blocks, supramolecular rectangles were constructed. The rectangles are tetra-cationic and slightly water soluble. These discrete supramolecular assemblies show moderate to high cytotoxicity depending on the properties of the building blocks used.

In a third approach, supramolecular triangular prisms were investigated. The prismatic structures can encapsulate large planar compounds. Studies showed that the encapsulated compound can not escape the prismatic cage unless it breaks. This property can be useful for drug transport, therefore a series of functionalized pyrenyl derivatives were encapsulated in the prism. Even though the prism itself is moderately cytotoxic, the activity was found to increase with some of the encapsulated pyrenyl derivatives. Fluorescent studies were made on the encapsulated 1-(4,6-dichloro-1,3,5-triazin-2-yl)pyrene. The study agrees with the theory that these complexes are taken up by the cell and then, like a Trojan horse, breaks to release the encapsulated species trapped inside.

Keywords

Arene ruthenium complexes, supramolecular assembly, Trojan horse, anti-cancer activity, pyrene, supramolecular prism, supramolecular rectangle, metalla-dendrimer, EPR effect.

Table of contents

1. Metals in Medicine

1.1 The very beginning

The medically beneficial effects of metals have been explored for centuries. In ancient China dating back to about 2500 BC gold was used to treat small pox, skin ulcers and furuncles [1]. In ancient Rome the wealthy put silver coins in containers for water storage to prevent spoiling due to silver's anti-bacterial property. Since then metals have been used more and more extensively. A metal containing blockbuster medicine called Salvarsan was commercialized at the beginning of the 20th Century [2]. The arsenic containing Salvarsan was the result of the pioneering work of Paul Ehrlich, who screened a library of compounds to find a treatment for syphilis. Even though metals have been successfully employed for medicinal purposes in the past, the approach is still serendipitous and not many rationally designed metal containing drugs have found the market. The major part of industry still focuses on classical drugs built on a carbon framework. Transition metals are different, often of octahedral geometry, and could therefore produce molecules of different properties, impossible to obtain from a carbon framework. Moreover, the solubility could be fine tuned depending on the metal and the ligands used. There is alas a branch of rationally designed pharmaceuticals yet to be explored.

1.2 Cancer therapy: an enormous task

Cancer is one of the greatest threats to humans in the western world, in the U.S. and Europe almost 25% of all deaths are caused by cancer, being second only to heart diseases as a cause of death [3]. According to statistics it has been predicted that 1 in 3 men and 1 in 4 women in Europe will be directly affected by cancer before they are 75

years old [4]. Alas the numbers are grim although after a peak around 1991 they are decreasing, both cancer incidence and death, especially cases of lung cancer has diminished. This might be due to better information and habits of the population but that is only the author's speculations.

Cancer as such is not one single disease but a collective name of mutated cells that grow uncontrollably. As there are over 50 oncogenes and the types of cells affected differ from each case, just one general treatment for cancer as such is difficult. What cancer cells do have in common is rapid cell division, because of this, DNA has been the target for chemotherapy as this will affect cancerous cells more than normal ones. In general in cancer treatment the tumorous tissue is removed by surgery followed by treatment with drugs and radiotherapy to remove the last traces of cancerous cells, but as mentioned this depends on the cancer type.

The greatest challenge in designing anti-cancer drugs is selectivity. As anti-cancer drugs are in general cytotoxic, they are also a threat to normal cells which is why side effects are often severe. With massive research focusing on cancer the discovery of specific targets in cancer cells has been made: Specific proteins, often protein kinases, and growth factors being upregulated, such as epidermal growth factor receptor (EGFR), vascular endothelial growth factor (VEGF). With these types of localized targets, drugs can be developed to be very selective towards these signaling pathways. This is called targeted chemotherapy and some highly selective compounds have been produced such as Sunitinib, specific for metastatic renal cancer [5].

A slight problem with targeted chemotherapy lies in the specificity, as there are many types of cancer a specific drug will have to be developed for each, a time consuming process. In the meantime classical chemotherapy will have to suffice, and possibly be improved beyond the need of specifically targeted drugs.

1.3 Cisplatin a salvation?

The serendipitous discovery of cisplatin or *cis*-dichlorodiamineplatinum(II) was a great discovery for cancer therapy, and inorganic chemistry as well for that matter. Barnett Rosenberg was studying the effect of electric current on E. Coli in different media. When these tests were done in medium containing ammonia an elongation of E. Coli was taking place. It was later discovered that it was due to release of platinum from the electrodes reacting with ammonia that lead to this phenomenon [6]. From this discovery cisplatin was developed, being among the most active of the platinum compounds tested so far.

Figure 1. The two isomers of dichlorodiamineplatinum(II)

Cisplatin is a square planar complex, and thus there is another isomer, transplatin (Figure 1). Cisplatin is several orders of magnitude more active than transplatin due to its mode of action in the cell. It is widely believed that cisplatin slowly hydrolyzed to produce an aqua species which in turn reacts with the base pairs of DNA, binding two of them covalently to produce a kink in the DNA [7]. If enough platinum is bound without repair the cell will die through apoptosis.

Cisplatin was approved for clinical use in 1978 and together with its derivatives have been used readily in chemotherapy ever since being deployed in about 60% of cancer cases [8]. Even though commonly used and effective, cisplatin suffers from several problems. It has a high general toxicity, not being very selective for cancer cells, and as a result inflicts severe adverse effects like neurotoxicity and nefrotoxicity. In addition cisplatin also suffers from resistance mechanisms [9]. This has induced massive

research in platinum compounds to improve these problematic features [10-15]. Even though thousands of compounds have been produced only a few have reached clinical trials and only two have been approved worldwide, carboplatin and oxaliplatin (Figure 2). Even though some of the problems were diminished with the introduction of carboplatin and oxaliplatin on the market some still resides and it remains an active field of research.

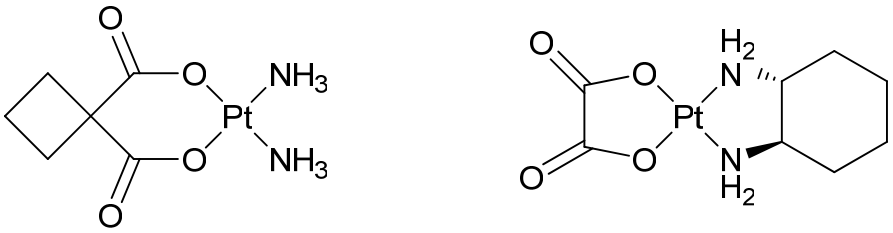

Figure 2. Platinum drugs carboplatin and oxaliplatin

1.4 Ruthenium as a substitute

Ruthenium compounds as biologically active agents have been evaluated in the 1950's by Dwyer and co-workers [16]. They studied the effect of several inorganic ruthenium complexes on bacteria and mice. However these studies did not appeal to the rest of the scientific world and were largely forgotten. After the success of cisplatin and the discovery of its shortcomings, a branch of scientist started to look into the possibility to interchange the toxic platinum with other metals. The interest for ruthenium has increased and it has become a strong candidate for several reasons: It is less toxic in general than platinum [8, 17-18]; it possesses an exchange rate of the chloride ligand similar to platinum compounds which is important for biological applications; moreover ruthenium has a wider range of oxidation states available and can mimic iron, thus profiting from natural transport mechanisms in the body. The latter may be an

explanation to the selectivity for cancer cells exhibited by ruthenium compounds as cancer cells have a higher uptake of iron due to their rapid proliferation.

1.4.1 Inorganic ruthenium compounds

The most successful ruthenium compounds so far are inorganic Ru(III) complexes. After the success of cisplatin, cisplatin analogs of ruthenium such as tetra amine dichloro ruthenium complexes were tested in the pioneer work of Clarke et al. [19-20]. The major drawback with these compounds was their poor water solubility which is essential for biological applications. A method to introduce water solubility is to make charged complexes. This has been applied in the work of Sava and Keppler. Sava's compound NAMI-A is based on an imidazole and a DMSO ligand while Keppler's KP1019 compound contains two indazole ligands (Figure 3).

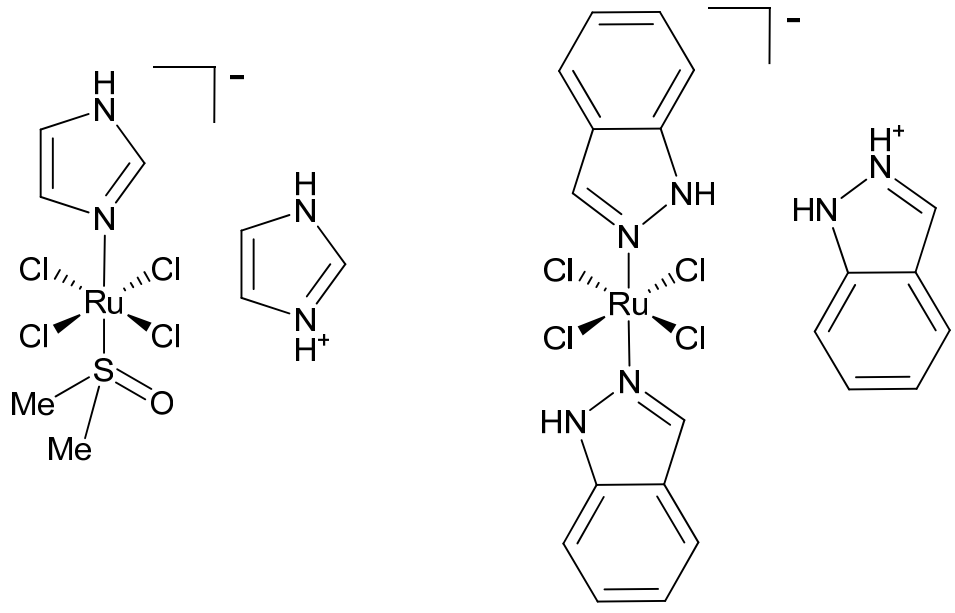

NAMI-A KP1019

Figure 3. Ruthenium compounds in clinical trials, NAMI-A [21] and KP1019 [22]

NAMI-A was developed from ruthenium DMSO type compounds, it is not very active against primary tumors but possesses high anti-metastatic activity. In contrast to cisplatin, NAMI-A only binds weakly to DNA, so it's activity is from another mechanism yet not clear [21]. KP1019 on the other hand is more stable and has high anti-tumoral activity but is not anti-metastatic [22]. It is believed that Ru(III) species are reduced to Ru(II) by reducing agents inside the cancer cells and that Ru(II) is the active species. Both NAMI-A and KP1019 has successfully completed phase I clinical trials [23-24], this brings hope in the future for ruthenium chemistry in the pharmaceutical domain.

1.4.2 Organometallic ruthenium compounds

Arene ruthenium complexes are an organometallic class of compounds that have a face capped arene bound through the π-system to the metal in an η^6 fashion stabilizing the Ru(II) oxidation state, this creates a piano-stool type complex with the arene as a seat and three σ-ligands (XYZ) as legs (Figure 4).

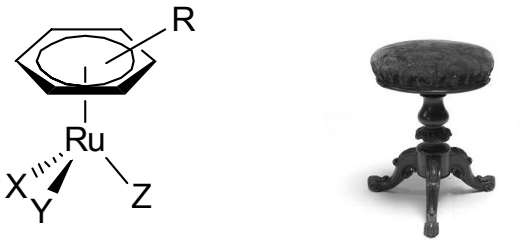

Figure 4. Arene ruthenium compound (piano-stool complex)

The hydrophilic nature of the metal and the hydrophobic nature of the arene ligand dawn for a versatile complex. The arene can be functionalized with many types of groups [25] and in addition the σ-ligands can be tuned for solubility or chosen to achieve

charged complexes to increase solubility in water. Moreover being already in Ru(II) oxidation state, these compounds do not need to be activated by reduction. Arene ruthenium compounds were developed as anti-cancer agents by the groups of P. J. Sadler [26] and P. J. Dyson [27]. The mechanism of this type of complex is still not completely clear but it is believed that similarly to cisplatin the complex is hydrolyzed in the cell and binds to DNA most favorably to the N7 of guanine [28]. The corner stone compound from Dyson and co-workers is RAPTA-C (Figure 5) from which derivatives have been made, in general derivatizing the arene moiety and having pta (1,3,5-triaza-7-phospha-adamantane) as one of the σ-ligands [8]. The typical arene ruthenium complexes from Sadler and co-workers is $[(\eta^6\text{-biphenyl})Ru(en)Cl]^+$ (Figure 5), which possesses a large hydrophobic arene and a chelating σ-ligand, thus affecting the rate of hydrolysis of the remaining chloro ligand which seems to be an important factor for biological activity. It is important that the complex is hydrolyzed inside the cell to be active, these complexes rely on the higher concentration of chloride in blood plasma, that by equilibrium hinders the hydrolysis from taking place [29-30].

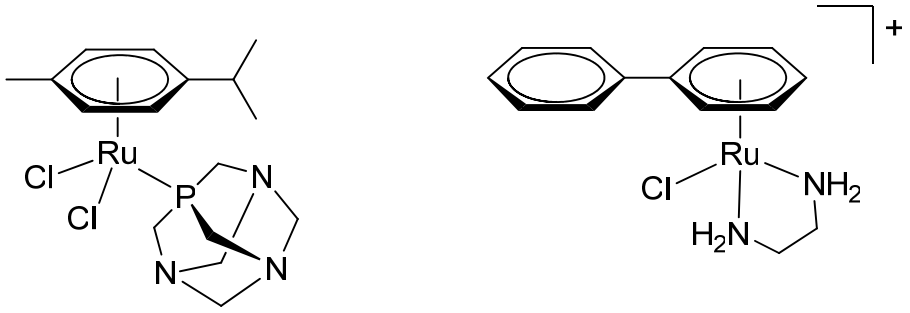

RAPTA-C $[(\eta^6\text{-biphenyl})Ru(en)Cl]^+$

Figure 5. Typical arene ruthenium compounds, RAPTA-C [8] and $[(\eta^6\text{-biphenyl})Ru(en)Cl]^+$ [29-30]

Another approach to create active arene ruthenium compounds is by using multinuclear complexes. Trinuclear arene ruthenium clusters (Figure 6A) have proven to be surprisingly active, having activity 5 times less than cisplatin but 20-30 times more

active than most arene ruthenium complexes [31]. The arenes of the cluster can be interchanged with the same wide variety as general arene complexes, this is important to fine tune solubility and possibly attach biologically active groups. The novelty in these complexes lies in the metal-metal bond which is quite rare in this domain and it can also, being large, target the EPR effect (enhanced permeability and retention) which will be discussed in detail in Chapter 2.

Multinuclear arene complexes can also be in the form of arene complexes connected by an organic linker like in the work of Hartinger and Nazarov [32]: The linker being a maltol derivative connected by an aliphatic chain that binds to the ruthenium as a bidentate ligand (Figure 6B). They studied structure activity relationships (SAR) and came to the conclusion that the length of the linker seems to correlate to activity, probably due to the change in lipophilicity. These complexes were found to bind to DNA and some proteins and were even more active against two oxaliplatin resistant cell lines than native cancer cell lines [33].

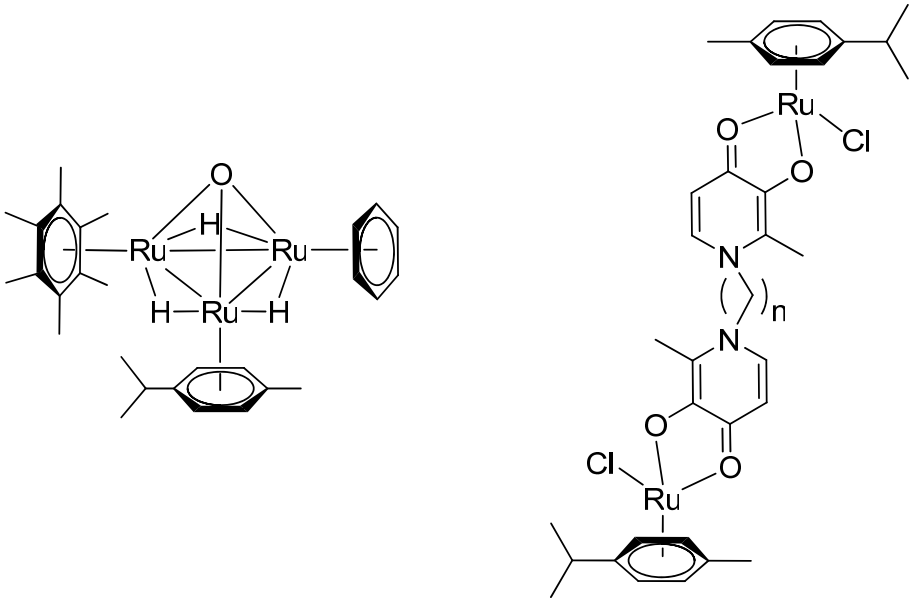

A B

Figure 6. Multinuclear arene ruthenium complexes, A: trinuclear arene ruthenium cluster [31], B: binuclear arene ruthenium complex connected by linkers [32]

Another example, but of different purpose, is the metalla-porphyrins investigated by Therrien and co-workers. It is a porphyrin scaffold with pyridine rings that binds four arene ruthenium moieties (Figure 7). These were developed for photodynamic therapy (PDT) i.e. compounds that are relatively inactive in the dark and can accumulate in cancerous tissue but activated upon irradiation with light. These proved to be strong candidates as in the dark they were not toxic (IC_{50} > 80 μM), while when irradiated they were highly cytotoxic. The utility of the arene ruthenium moiety was proven as the Cp*Rh (Cp* = pentamethylcyclopentadienyl) analogue was not internalized by cancer cells [34-35]. Apparently the arene ruthenium plays an important role to solubilize and induce more selective transport into cancer cells for these systems.

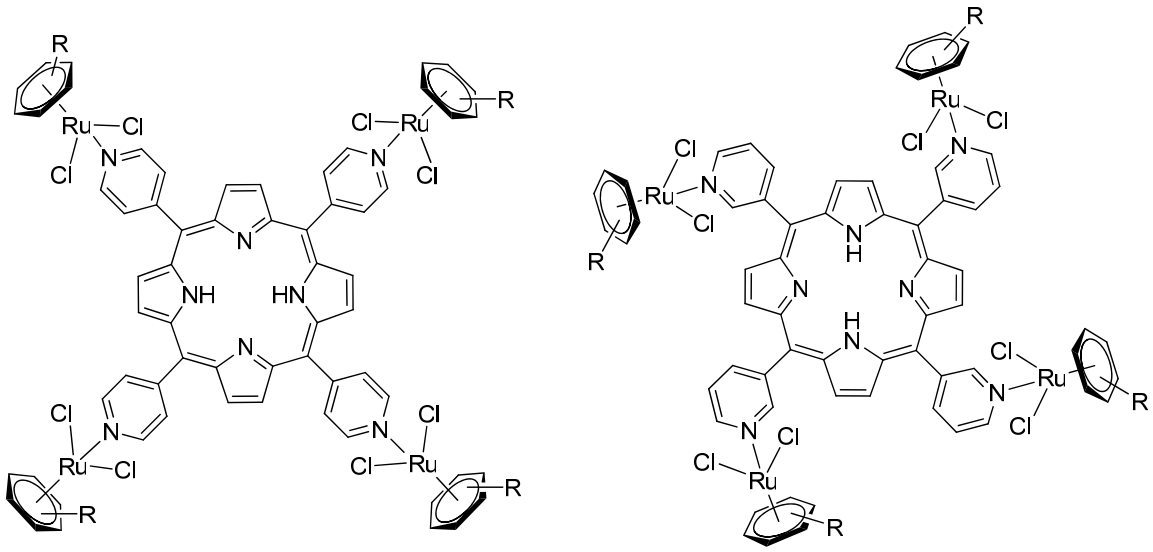

Figure 7. Arene ruthenium metalla-porphyrins [34-35]

2. Drug Transportation

In drug design, one of the problems encountered is to ensure delivery of the drug to its target. In general, drugs are given orally and they have to pass a number of biological systems with harsh conditions, stomach and liver for example, in which they might need protection. Intravenous drugs avoid some of these limitations except for the fact that it has to be given by authorized personnel. Most drugs, depending on their target, have to be water soluble enough to be transported with the blood stream but also lipophilic enough to pass cell membranes and other barriers. Drugs also need to be somewhat specific to their target, a large number of attributes for a single compound. To improve attributes without designing a new drug, delivery by another compound or vector, hidden inside, grafted on the outside or even connected to biomolecules is quite attractive. This changes the biodistribution and clearance of the molecule significantly and drugs which are effective but otherwise sensitive to biomolecules can be used.

2.1 The enhanced permeability and retention effect

Nowadays, research concentrating on putting a large amount of drugs inside or onto large molecules or other systems shows great promises: The reason being the enhanced permeability and retention (EPR) effect of cancer cells. Described by Y. Matsamura and H. Maeda in the 80's when they realized that a polymeric protein was more active than the single product [36]. They came to the conclusion that this effect depends on the special vascular and lymphatic properties of cancer cells. Cancer cells are growing rapidly. They are in higher demand of nutrients for cell division than normal cells. Because of this need of nutrients, the vascular endothelial growth factor (VEGF) is expressed to induce angiogenesis (create new blood vessels to the tumor cells) which increases the permeability of the cell membrane. The increased permeability leads to a higher uptake of large molecules and proteins. However the major difference from

normal cells resides in the lymphatic drainage, which is severely impaired for cancer cells, thus leading to the retention of large molecules and lipids inside the cell [37]. This is an excellent target for the development of anti-cancer agents: Large molecules would almost selectively be taken up by cancer cells and as well retained inside these disease cells whereas if uptaken in normal cells excretion through its healthy lymphatic system might occur.

2.2 Metal drug delivery

With the discovery of potential delivery systems and the EPR effect, attempts to include anti-cancer metal-based drugs in transport vectors have been made. Naturally most attempts have focused on platinum compounds as they are clinically used, very effective but not selective. Therefore, this transport strategy could be a method of increasing efficacy and selectivity.

2.2.1 Dendrimers as drug delivery vectors

Dendrimers can be well controlled in size unlike other polymers. At higher generation they take on a stable globular shape, similar to many biomolecules, and have a tight outer shell. This has made them interesting for biological applications as they are more stable than micelles and lipid bi-layers as transport vehicles [38] and can target the EPR effect. Inside the solid outer shell of dendrimers, cavities of different sizes which can accommodate drugs, are used for transport. Moreover drugs can also be connected to the outer shell via binding to the end-groups of the dendrimer. Duncan et al. reported the conjugation of cisplatin to a polyamido amine (PAMAM) dendrimer, modified on the periphery with sodium carboxylate functionalities (Figure 8) [39]. The dendrimer-platinate is water soluble and displayed anti-tumor activity when administered

intravenously against a B16F10 melanoma, whereas cisplatin was inactive. Dendrimers are nowadays commercially available and incorporation of drugs and diagnostic agents is a hot topic.

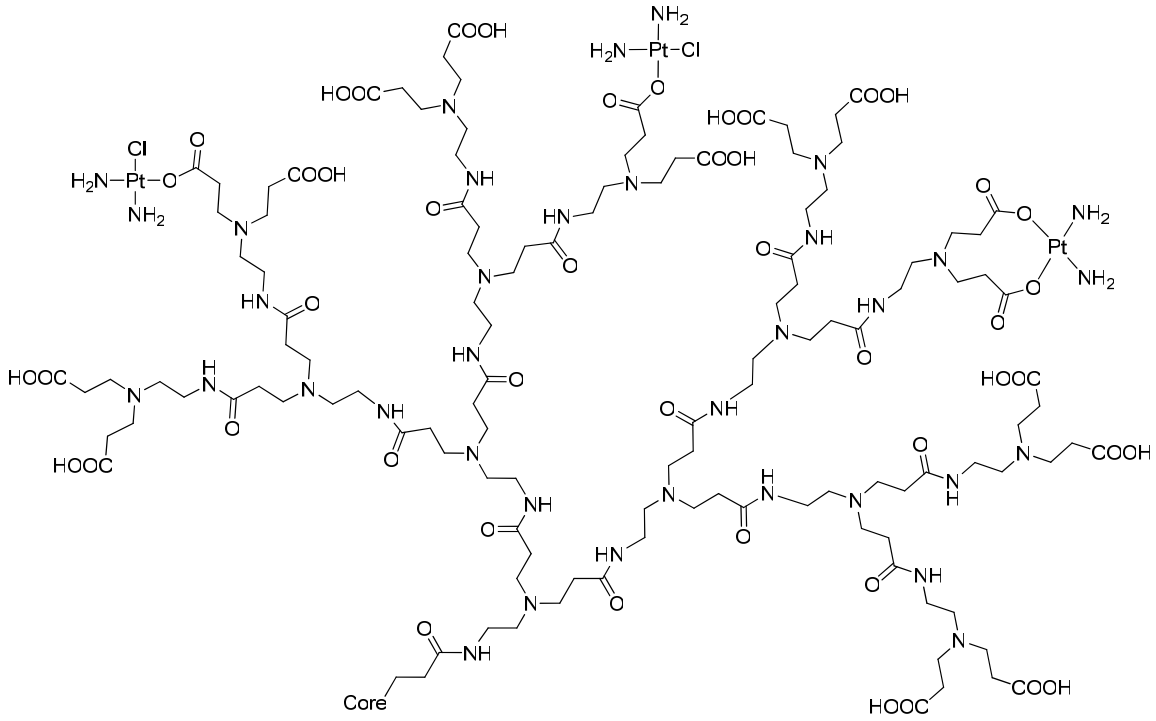

Figure 8. Cisplatin conjugated to PAMAM dendrimer, one branch of a greneration 3.5 dendrimer synthesized by Duncan [39]

2.2.2 Carbon nanotubes

Carbon nanotubes are tubular carbon frameworks that have recently received attention because of their ability to travel across cell membranes [40-42]. This has lead to research with the goal to incorporate drugs inside their cavity for transportation. Single wall nanohorns (SWNHs) filled with platinum compounds, which cluster together to give large spherical structure has proven to increase activity of cisplatin (Figure 9) [43].

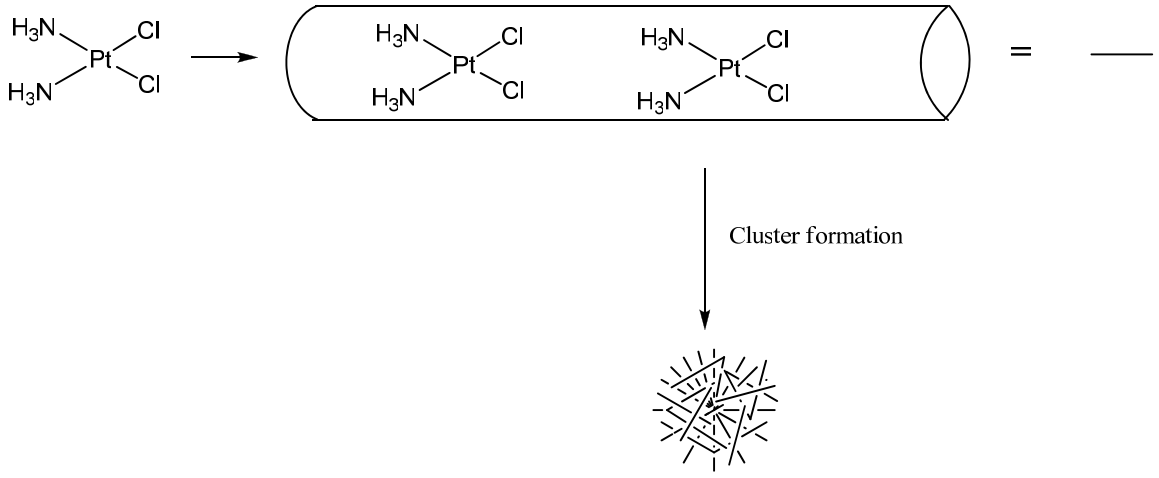

Figure 9. Cisplatin inserted into SWNH which then cluster into spherical aggregates [43]

Single wall nanotubes (SWNTs) have been functionalized by covalently tethered platinum compounds. The toxicity towards testicular cancer was increased with up to 25 fold of the parent complex (Figure 10) [44]. However they were taken up by the cell through an endocytotic process and did not target the EPR effect. It still proves that these systems, although biologically unorthodox, can be used as transport vectors.

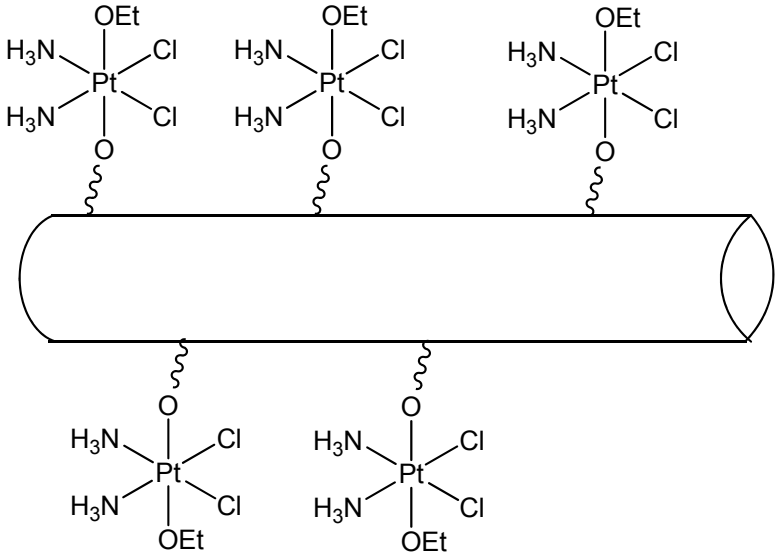

Figure 10. SWNT with tethered platinum compounds [44]

2.2.3 Liposomes

Liposomes are spherical structures made up of a lipid bi-layer and an aqueous core (Figure 11). They form spontaneously in aqueous solution by lipids having hydrophobic tails and hydrophilic heads. They can be loaded with drugs and target the EPR effect by being large and retained in the cell because of their lipid nature. However cisplatin was not successfully loaded into these systems as it is not lipophilic enough, thus more lipophilic derivatives like Aroplatin (Figure 11) were made and eventually successfully loaded into the bi-layer. The effects were positive and a system like this is in phase II clinical trials [45].

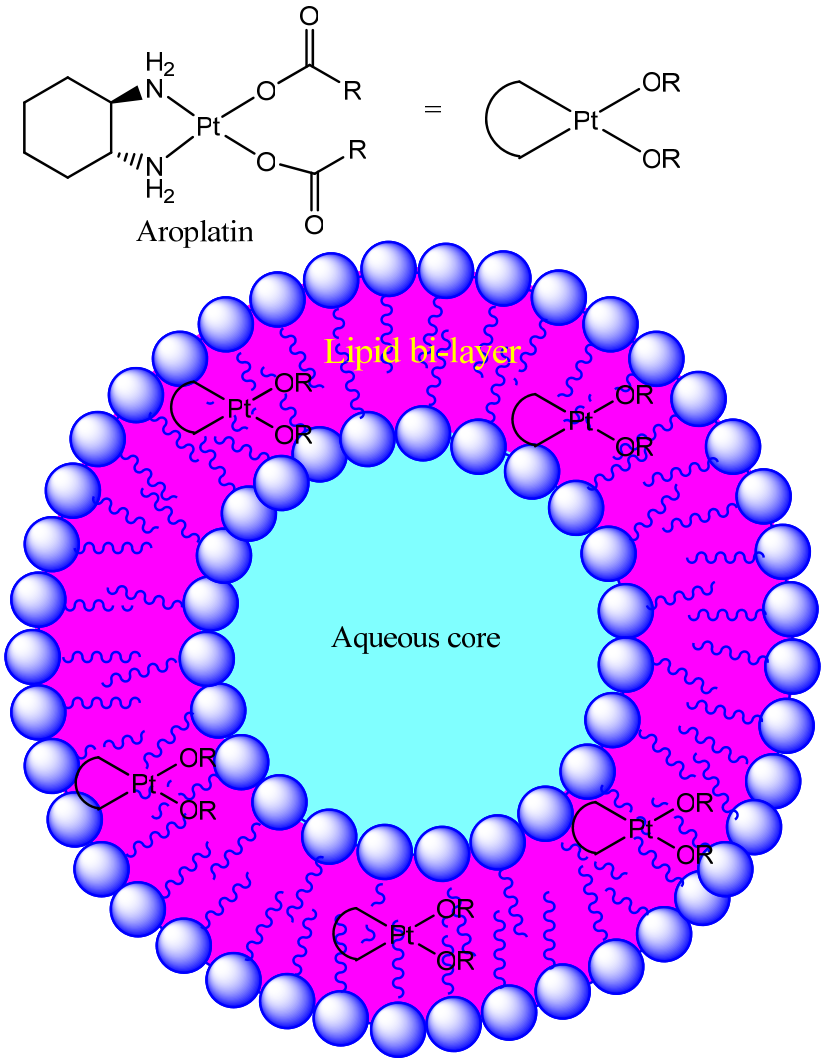

Figure 11. Cross section of a liposome with Aroplatin loaded into the bi-layer [45]

2.2.4 Large systems which do not target the EPR effect

Even though the EPR effect is an attractive target not all drug delivery systems focus on this opportunity. Indeed the macrocyclic system cucurbit[n]uril (Figure 12A) protect highly active platinum compounds that would otherwise be deactivated before reaching their target (Figure 12B).

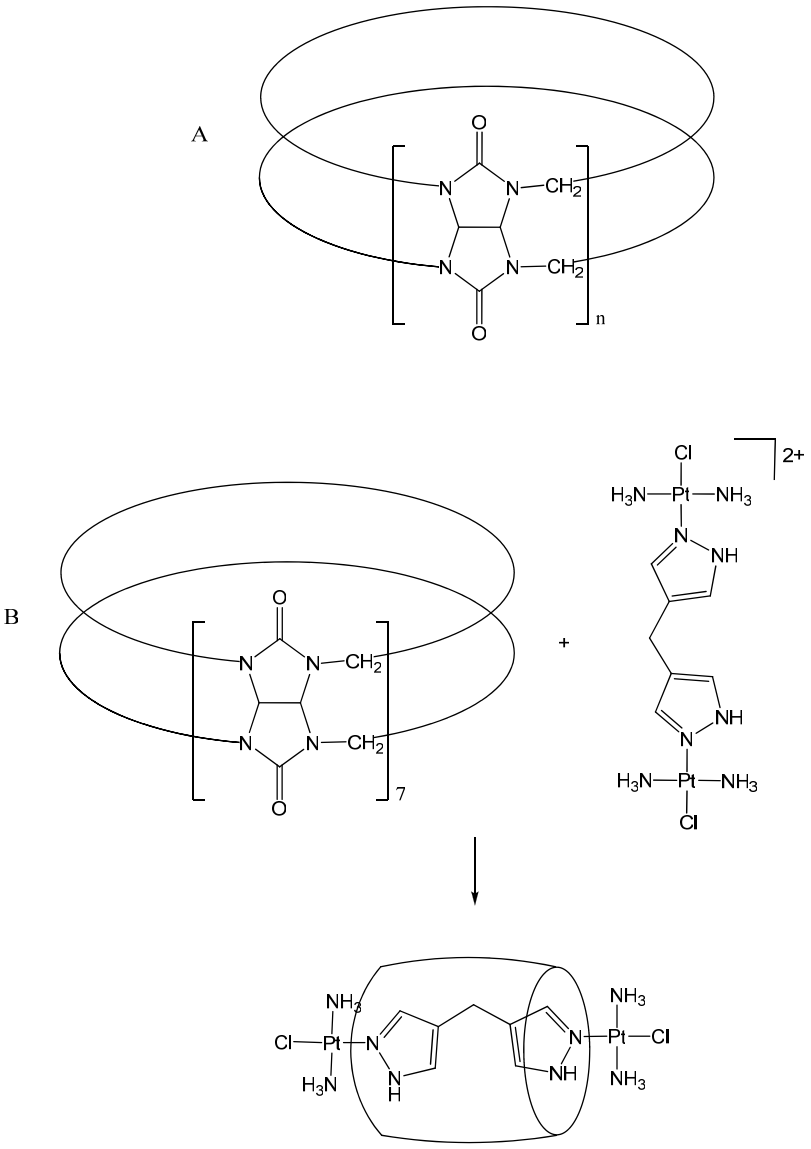

Figure 12. A: Cucurbit[n]uril, B: Insertion of a dinuclear platinum complex into a cucurbit[7]uril [46-47]

They also prevent resistance from the glutathione protein mechanism [46-47]. Incorporation in ceramic materials has been investigated for slow release close to the tumorous tissue. Another system is incorporation into or onto biomolecules which are large but taken into the cell by endocytosis and not through the membrane. These are in general equipped with antibodies or receptors to target cancer cells specifically [48].

2.3 Goals of this project

Even though drug delivery vectors are well known, a supramolecular approach remains rare. Discrete supramolecular assemblies are versatile and their charge and solubility can be controlled, moreover there is a possibility for host guest chemistry which can be used for transport and release of drugs. Arene ruthenium compound have, as mentioned, received a lot of attention for their biological activity, and in recent years as well for the possibility to use them as supramolecular building blocks. Discrete systems are as well advantageous in medicinal chemistry as they are well defined.

This work has aspired to investigate the versatility of arene ruthenium chemistry, incorporating them into large systems like discrete supramolecular assemblies and dendrimers. Making such compounds renders large water soluble systems, an important factor for biological activity making them bio-available. The presence of several metal centers should give high activity and may give rise to selectivity as ruthenium compounds have shown some selectivity for cancer cells. Moreover it is possible to encapsulate hydrophobic species in discrete supramolecular assemblies; this could serve as a drug delivery system for drugs with low solubility. As these systems are large selectivity might be increased if the enhanced permeability and retention (EPR) effect can be exploited.

3 Dendritic Systems

3.1 Introduction

Arene ruthenium complexes are air stable, soluble and versatile organometallic compounds that defy the notion that organometallic compounds are air and moisture sensitive. They are prepared in a dimeric form from the reaction of $RuCl_3$ with a cyclic diene, first synthesized by Winkhaus and Singer in 1967 [49]. However the structure was thought to be in polymeric form and the dimeric form was not discovered until later by Baird [50] and Bennett [51]. The chloro-bridged dimeric species formed can easily be broken up by the addition of a ligand (L) (Scheme 1).

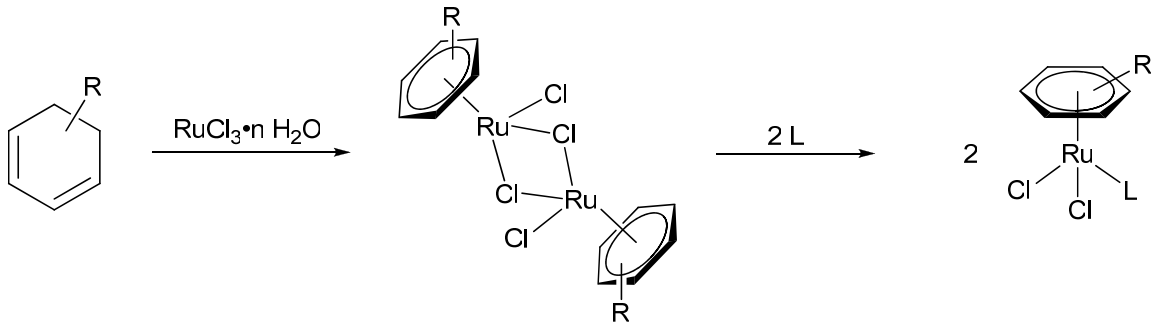

Scheme 1. General synthesis of arene ruthenium complexes

Some arene ruthenium dimers cannot be obtained through the reaction of $RuCl_3$ with the corresponding diene as electron rich systems like hexamethylbenzene and durene can not be reduced to dienes. However the arene ruthenium dimer can be obtained from an arene exchange reaction by reacting the *p*-cymene dimer with the aromatic system at high temperature (Scheme 2) [51].

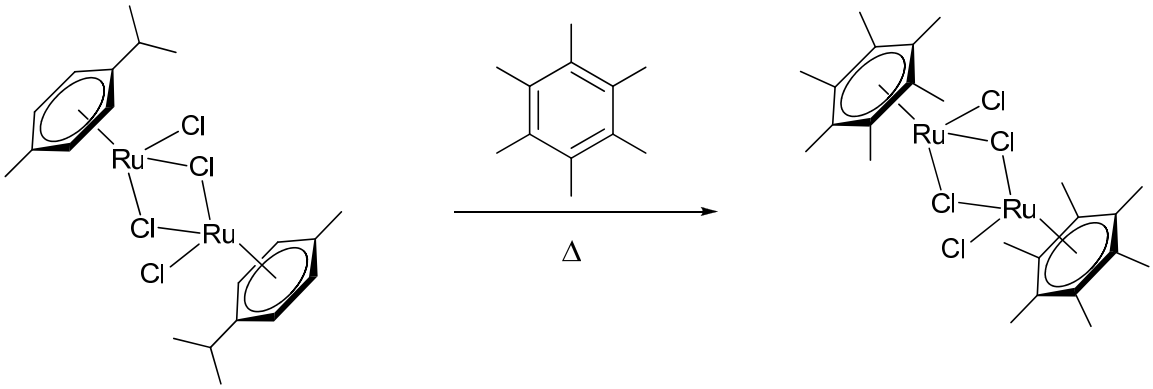

Scheme 2. Arene exchange reaction of *p*-cymene with hexamethylbenzene

As previously mentioned arene ruthenium complexes have recently caught attention as biologically active agents, mostly for anti-cancer activity.

Dendrimers are a polymer class of compounds which are highly branched starting from a core. They are synthesized by two methods, the divergent and the convergent method: The divergent method being the first introduced by Tomalia and co-workers [52], starting from the core adding branching segments outwards (Figure 13A), each layer of branching segment being called a generation (G). In the convergent method, developed by Fréchet and co-workers [53], the synthesis starts from the end groups, then connecting the branching segments inwards and connecting the large segments to the core in the final step (Figure 13B).

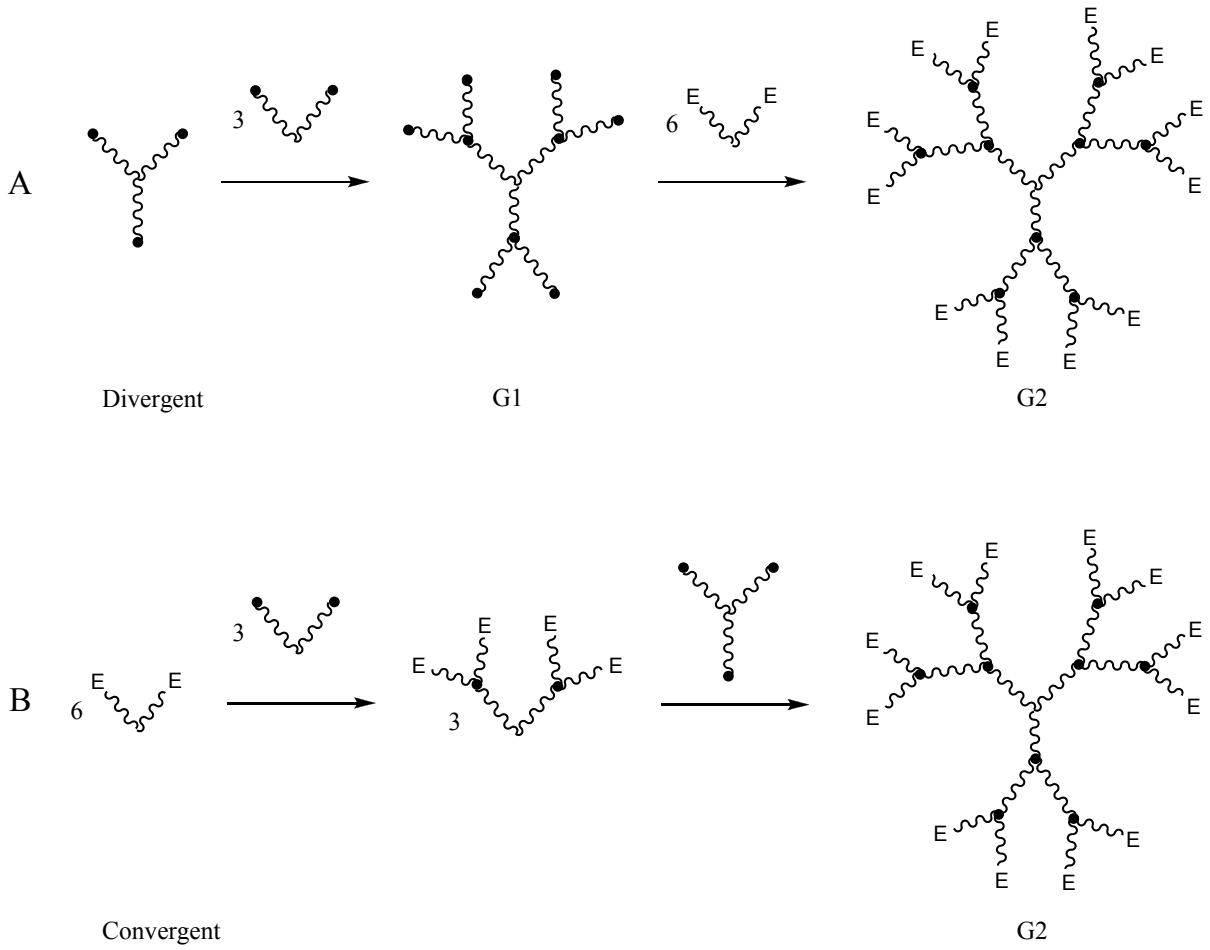

Figure 13. Divergent (A) and convergent (B) methods to prepare dendrimers [38]

In order to exploit size selective uptake of drugs into tumor cells effectively, large compounds are required, and in recent years, dendrimers have found potential as molecular tools in biological applications [54-56], especially as nano-carriers [57], diagnostic agents [58] and as chemotherapeutics [59-61]. Moreover, another advantage of dendrimers is their multivalency, which leads to increased interaction between a dendrimer-drug conjugate and a target bearing multiple receptors, further improving the selectivity to cancer cells. With the aim of reducing the inherent problems related to cisplatin such as poor water solubility, high toxicity and side effects, the combination of platinum-based drugs with dendritic systems is very appealing. However, transition metal complexes with anti-cancer activity, based on a dendritic scaffold are quite rare. Using

the commercially available butanediamine poly(propyleneimine) dendrimer ($DAB(PA)_4$) (Figure 14) which provides four peripheral amine groups a series of tetranuclear platinum compounds were synthesized.

The cationic compound $[DAB(PA)_4\{Pt(NH_3)_2Cl\}_4]^{4+}$ was designed to overcome cisplatin resistance [62], while the neutral derivative $DAB(PA)_4\{Pt(dmso)(L)\}_4$ (L = meso-1,2-bis(4-fluorophenyl)ethylenediamine) was prepared to increase selectivity for breast cancer cells [63]. With the established anti-cancer activity of arene ruthenium complexes and the current interest in dendrimers for biological applications, we decided to explore the synthesis of multinuclear ruthenium complexes based on a poly(propyleneimine) scaffold and investigate their cytotoxicity against A2780 human ovarian cancer cell line.

As far as we are aware these studies are the first to exploit arene ruthenium compounds using this approach although tumor targeting of arene ruthenium compounds via covalent attachment to recombinant human serum albumin via a pH cleavable linker has been reported [64].

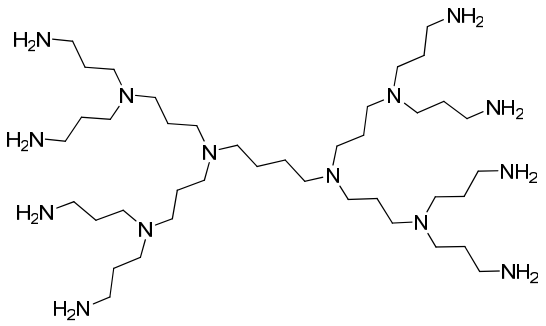

Figure 14. Second generation of a DAB dendrimer

3.2 Synthesis and characteristics

3.2.1 Synthesis and characterization of iminopyridyl-functionalized dendritic ligands G1 and G2

In collaboration with Dr Gregory Smith and co-workers at the University of Cape Town (South Africa) a first- (G1) and second-generation (G2) iminopyridyl dendrimer based on a poly(propyleneimine) scaffold were synthesized via a standard Schiff-base reaction. The 4-pyridylimine-functionalized dendritic ligands (G1–G2) were prepared by the reaction of 4-pyridinecarboxaldehyde with DAB-$(NH_2)_n$ (n = 4, 8 for G1 and G2, respectively) (Scheme 3). The dendritic ligands are isolated as orange-yellow oils, in moderate yields. They are soluble in dichloromethane, chloroform, methanol, diethyl ether and tetrahydrofuran.

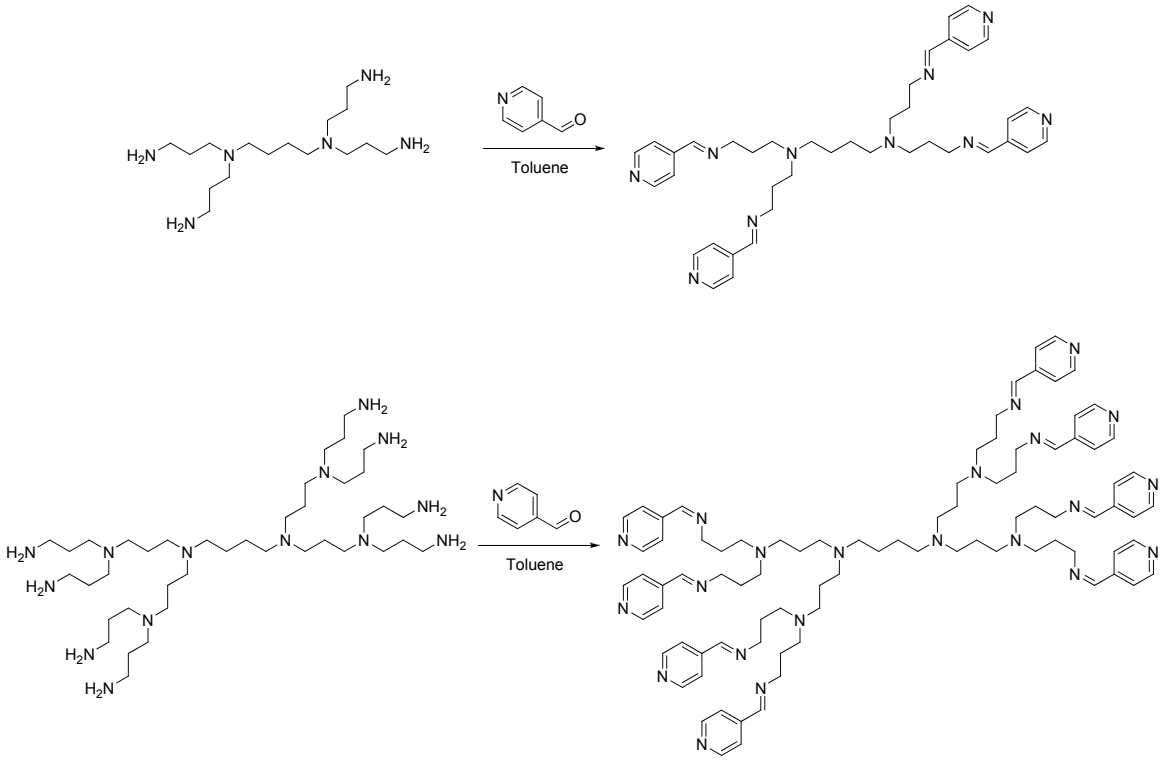

Scheme 3. Synthesis of iminopyridyl dendrimer G1 (top) and G2 (bottom)

The Schiff base condensation reaction is confirmed by appearance of a peak in the range 8.17 and 8.23 ppm assigned to the imine protons for G1 and G2, respectively. Two distinct doublets (^3J ~ 6.00 Hz) are observed for the aromatic protons on the 4-pyridyl rings. $^{13}C\{^1H\}$ NMR spectra for both ligands (G1–G2) show similar signal patterns. Aliphatic carbons were seen in the region of 25–60 ppm and aromatic carbons in the region of 120–150 ppm for both generations. As expected for both ligands the imine carbon was the most deshielded signal at 159 ppm. For both G1 and G2, the IR spectra show two absorption bands of strong intensity at ~1647 and 1599 cm^{-1} assigned to the (C=N) imine and (C=N) aromatic vibrations respectively.

3.2.2 Synthesis and characterization of metalla-dendrimers

The dinuclear arene ruthenium complexes $[(\eta^6\text{-arene})RuCl_2]_2$ (arene = *p*-cymene, hexamethylbenzene) react with the dendritic ligands G1 and G2 at room temperature in dichloromethane to yield the neutral tetranuclear (**1**-**2**) (Figure 15) and octanuclear (**3**-**4**) (Figure 16) ruthenium metalla-dendrimers. The yellow-orange solids (**1**-**4**) are isolated as air-stable solids in high yields (79-98%). The complexes are soluble in most organic solvents such as dichloromethane, chloroform, ethanol, dimethylsulfoxide, acetone, acetonitrile, diethyl ether and tetrahydrofuran.

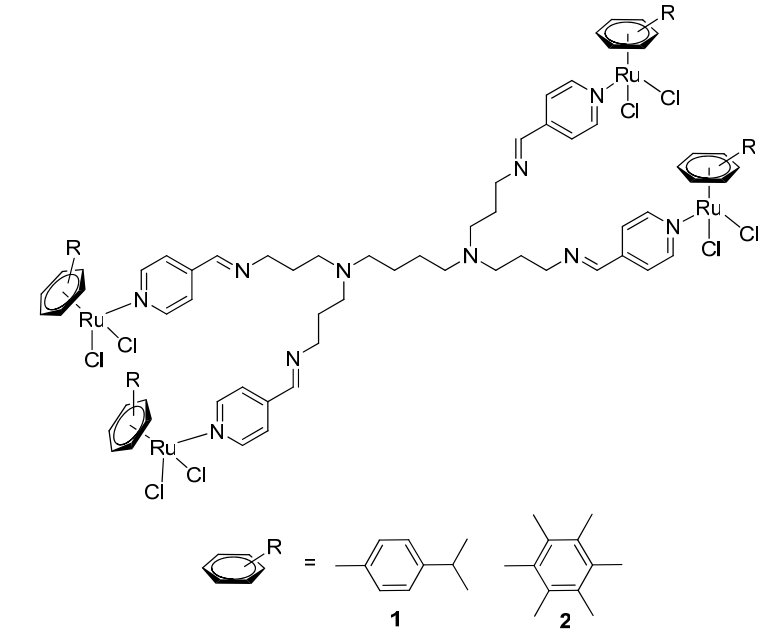

Figure 15. Metalla-dendrimers G1, tetranuclear **1-2**

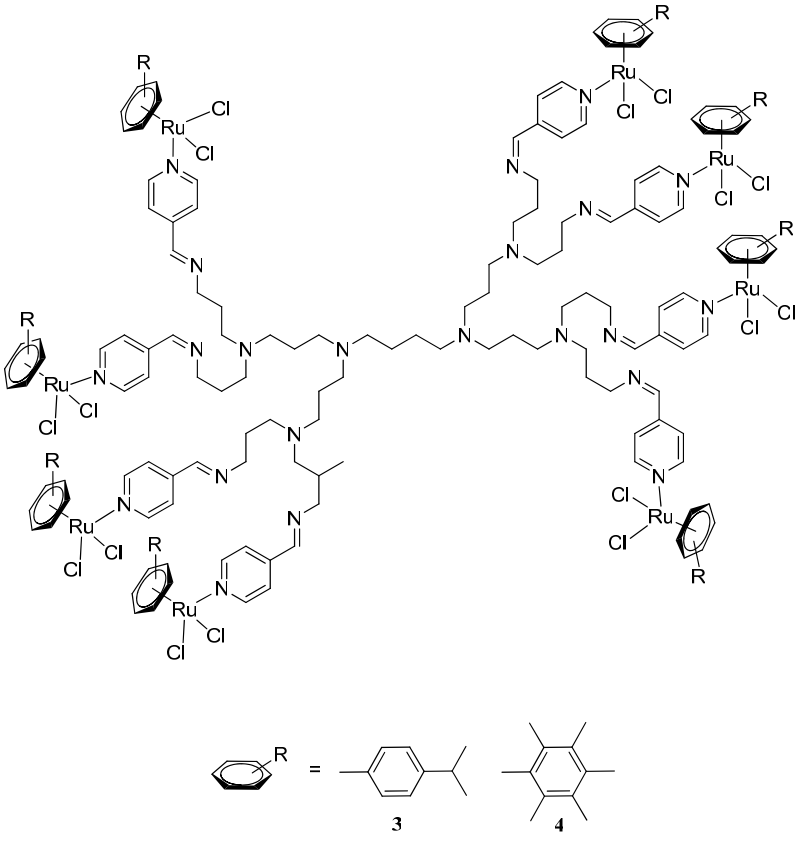

Figure 16. Metalla-dendrimers G2, octanuclear **3-4**

The ^{1}H NMR spectra of **1-4** shows broadened peaks upon complexation of the multinuclear ruthenium moieties. The aliphatic protons of the dendritic core and side arms occur at similar shifts to those of the dendritic ligand precursors. Evidence for the coordination of the ruthenium metal to the aromatic nitrogen atom can be seen by a shift in the doublet (assigned to aromatic protons on the carbon adjacent to pyridyl nitrogen atom) from 8.66 to 9.10 ppm. A shift in the signal is due to the electron-withdrawing effects of the coordinating metal, resulting in the signals being shifted downfield. There is also no distinct shift in the imine proton suggesting no coordination at this position. The ^{1}H NMR spectrum for the second generation of complexes (**3-4**) showed similar shifts to the first generation. This alludes to coordination at the pyridyl nitrogen only and not the imine nitrogen. This is further confirmed by IR spectroscopic studies. Infrared spectroscopic studies show a shift in the (C=N) aromatic peak from a lower wavenumber to a higher wavenumber at around 1615 cm^{-1}. The (C=N) imine absorption band remains unchanged at around 1646 cm^{-1}. The second generation dendritic complexes show similar trends. The ruthenium functionalized dendrimers (**1-4**) were precipitated with the inclusion of solvent, trapped between the dendritic arms. The elemental analysis data correlates with the inclusion of 2 molecules and 4 molecules of dichloromethane for **1** and **3**, respectively.

3.2.3 Synthesis and characterization of mononuclear compounds

For comparison, the analogous mononuclear ruthenium complexes (**5-6**) were synthesized (Figure 17). These were prepared by reacting the ligand, N-(pyridin-4-ylmethylene)propan-1-amine (L), with the dinuclear arene ruthenium complexes $[(\eta^{6}\text{-arene})RuCl_2]_2$ (arene = *p*-cymene, hexamethylbenzene) in dichloromethane at room temperature. The mononuclear ruthenium complexes (**5-6**) are isolated as yellow-orange solids in high yields. They are air-stable and soluble in most solvents.

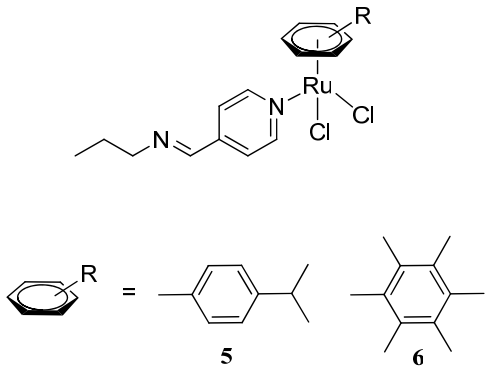

Figure 17. Mononuclear ruthenium compounds **5-6**

The aromatic protons adjacent to the pyridyl nitrogen atom appear more downfield than for the uncoordinated ligand (8.66–9.10 ppm), while the imine protons remain at the same position as for the dendritic ligand (~8.2 ppm). A shift in the (C=N) aromatic absorption band in the IR spectrum of **5** and **6** is seen at around 1550–1615 cm^{-1}. The (C=N) imine absorption band around 1647 cm^{-1} remains constant and confirms that no coordination occurred at this site. The coordination of the ruthenium metal occurred to the aromatic nitrogen atom was further confirmed by the X-ray structure analysis of complex **5**.

X-ray quality crystals for complex **5** are obtained by slow diffusion of hexane into a concentrated dichloromethane solution of **5**. The molecular structure of **5** shows that, like other arene ruthenium complexes [25], the metal center adopts a piano-stool, pseudo-tetrahedral geometry, with ruthenium coordinated by the arene ligand, two chlorides and the iminopyridyl ligand. An ORTEP drawing of **5** is shown in Figure 18 and selected bond lengths and angles are presented in Table 1. The distance between the ruthenium atom and the center of the C_6H_4 aromatic ring of the *p*-cymene ligand is 1.670(4) Å. The Ru–N and Ru–Cl bond distances in **5** are comparable to those reported in the pyridine (py) derivatives [(η^6-1,3,5-trimethylbenzene)$RuCl_2$(py)] [65] and [(η^6-hexamethylbenzene)$RuCl_2$(py)] [66]. Similarly, the Cl–Ru–N and Cl–Ru–Cl bond angles of complex **5** [84.8(2) and 87.0(2)] are similar to those in [(η^6-1,3,5-trimethylbenzene) $RuCl_2$(py)] and [(η^6-hexamethylbenzene)$RuCl_2$(py)]. As suggested previously, only the

aromatic nitrogen atom is found to be coordinated to the ruthenium atom, thus validating the coordination mode proposed in complexes **1-4**.

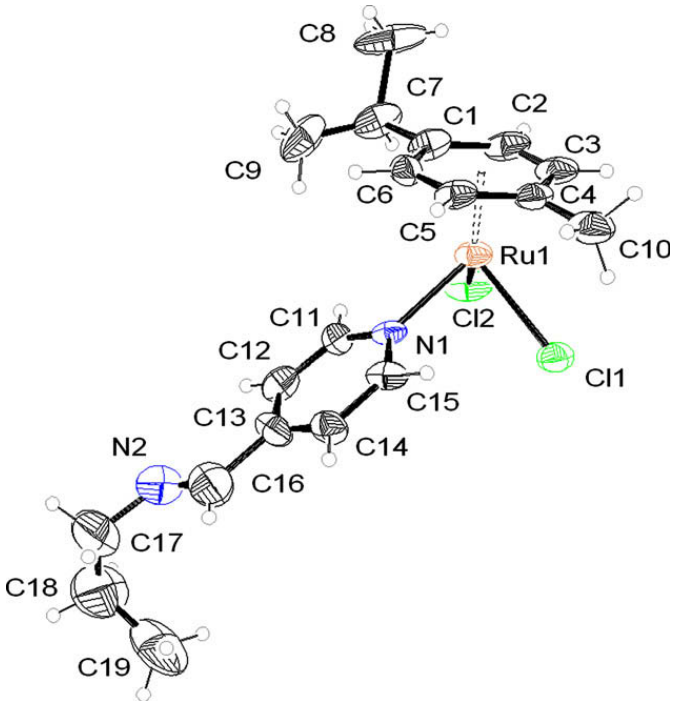

Figure 18. Molecular structure of the mononuclear complex **5** showing ellipsoids at the 50% probability level

Table 1. Selected bond lengths and angles of compound **5**

Bond lengths (Å)		Bond angles (°)	
Ru(1)–N(1)	2.128(9)	N(1)–Ru(1)–Cl(1)	84.8(2)
Ru(1)–Cl(1)	2.406(3)	N(1)–Ru(1)–Cl(2)	87.0(2)
Ru(1)–Cl(2)	2.405(3)	Cl(1)–Ru(1)–Cl(2)	87.6(2)
N(2)–C(16)	1.34(3)	C(13)–C(16)–N(2)	115(2)
N(2)–C(17)	1.49(3)	C(16)–N(2)–C(17)	125(2)

3.3 Biological activity

The biological activity was tested in collaboration with Prof. Paul Dyson and co-workers at the EPFL (Switzerland). The ability of **1-6** to inhibit cancer cell growth was evaluated *in vitro* on A2780 ovarian cancer cell line using the biological MTT assay which measures mitochondrial dehydrogenase activity as an indication of cell viability. The compounds are incubated at various concentrations (in triplicate) in the A2780 cells and cell viability is measured after an incubation period of 72 hours. Each experiment is conducted in duplicate and the IC_{50} values (inhibition of cancer cell growth at the 50% level) listed in Table 2 are calculated as an average over two experiments. All compounds display moderate anti-proliferative activity in the A2780 cell line. While the IC_{50} values determined are higher than that of cisplatin, the most active compounds, **3** and **4**, are relatively low for ruthenium compounds.

Table 2. IC_{50}[a] values for compounds **1-6** measured on A2780 human ovarian cancer cell line[b]

Compound	IC_{50} (μM)
1 [{(η^6-*p*-cymene)$RuCl_2$}$_4$G1]	43
2 [{(η^6-hexamethylbenzene)$RuCl_2$}$_4$G1]	40
3 [{(η^6-*p*-cymene)$RuCl_2$}$_8$G2]	21
4 [{(η^6-hexamethylbenzene)$RuCl_2$}$_8$G2]	20
5 [(η^6-*p*-cymene)$RuCl_2$(L)]	98
6 [(η^6-hexamethylbenzene)$RuCl_2$(L)]	94
cisplatin	1.6

[a] Concentration at which 50% of cell viability is inhibited.

[b] Maximum error is $< \pm 5$ μM.

These are the first examples of arene ruthenium dichloro complexes with an iminopyridyl ligand to be tested for *in vitro* activity. However, analogous hexamethylbenzene and *p*-cymene cyanopyridyl complexes have previously been reported to show significant unwinding of supercoiled DNA and also inhibit haem polymerase activity. In contrast, [(η^6-*p*-cymene)Ru(py)Cl_2] was found to show negligible activity in the TS/A cell line [67]. There is a clear trend between the size of the dendritic compound and cytotoxicity, i.e. the monoruthenium compounds have modest cytotoxicity whereas [{(η^6-*p*-cymene)$RuCl_2$}$_8$G2] **3** and [{(η^6-hexamethylbenzene)$RuCl_2$}$_8$G2] **4** are cytotoxic. Based on this observation, the biological properties of **3** and **4** are worth studying further as they may be able to target cancerous tissues more effectively than smaller compounds by exploiting the enhanced permeability and retention effect, a property that needs to be evaluated *in vivo*. Moreover, the activity shown here for **3** and **4** is not too dissimilar to that of the multinuclear arene ruthenium adduct of recombinant human serum albumin [57], but the facile synthesis and considerably lower cost of the dendrimer system, cannot be overlooked.

3.4 Conclusions

A number of metalla-dendrimers have been produced from G1 and G2 organic dendrimers in a simple and straightforward synthetic route, producing the final metalla-dendrimers in high yields. These derivatives were tested for biological activity and found to be cytotoxic in comparison to a mononuclear reference compound. The simplicity of synthesis and the possibility to target the EPR effect make these compounds favorable for further studies. If these compounds really target the EPR effect has yet to be confirmed, it might be necessary to compare with higher generations of dendrimers to evaluate a potential synergistic effect.

4. Supramolecular Rectangles

Arene ruthenium complexes are as mentioned versatile and have been used for many purposes. One fairly new approach is to use these systems in supramolecular assemblies. Earlier, mostly platinum and other square planar metals centers have been used, but arene ruthenium complexes offer an octahedral complex controllable in its geometry by the blocking of three ligand sites through the arene ligand.

4.1 Introduction

4.1.1 Supramolecular squares, a new dawn in supramolecular chemistry

Self-assembly is a process leading to the formation of discrete nanometer-sized objects or well-defined aggregates in which the overall structure is controlled by the symmetry of the different building blocks [68-72]. In the case of metalla-supramolecular assemblies, the coordination mode of the metal center as well as the symmetry of the ligands needs to be controlled in order to allow the formation of the desired aggregates.

Fujita et al. pioneered the usage of 90° building blocks in the 90's and many other groups subsequently followed. Fujita in early experiments used square planar Pd compounds with ethylenediamine (en) ligand to block two adjacent coordination sites and produce a compound capable of binding bridging ligands in a 90° angle. When these palladium corners react with four linear bidentate ligands molecular squares are formed (Scheme 4).

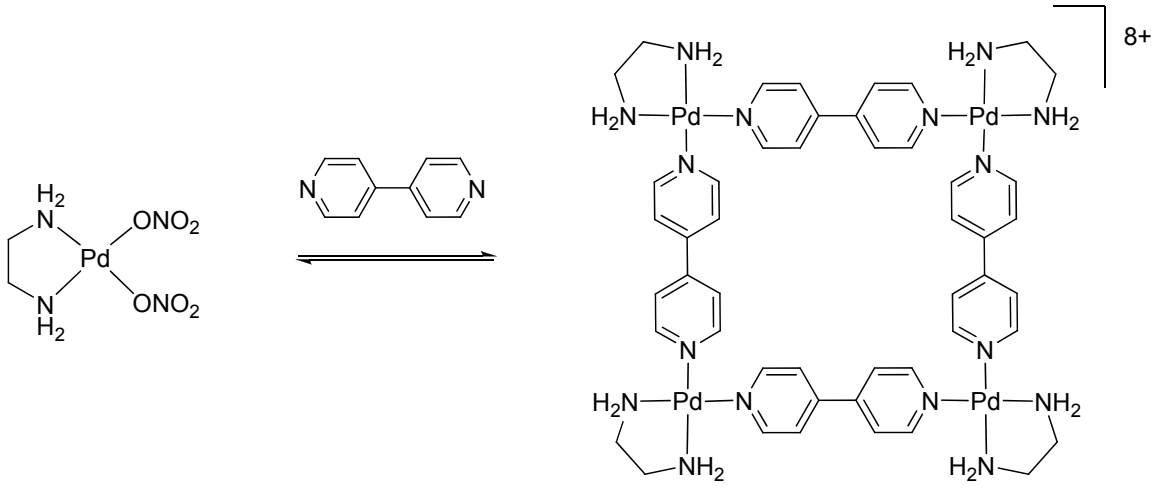

Scheme 4. Synthesis of the square $[\{(en)Pd(4,4'\text{-bipy})\}_4]^{8+}$ [73]

The synthesis is thermodynamically controlled and has an equilibrium favoring the formation of the square. The cavity can host a guest which was seen by NMR spectroscopy upon addition of 1,3,5-trimethoxy benzene in solution [73].

With these types of systems a new branch of supramolecular chemistry started, incorporating dative metal bonds in confined nanosized structures and not large lattices or frameworks as earlier metal containing supramolecular structures. These systems consist of two types of building blocks, an angular unit that contains two coordination sites or bonding possibilities in an angle of choice, and a linear bridging unit with binding sites in 180° relative orientation. The final shape of the molecule is dependent on these angles. A connecting corner with a 60° angle would hence produce a triangle whereas 90° would produce a square, 108° a pentagon and 120° a hexagon (Figure 19) when combined with linear bridging units [74].

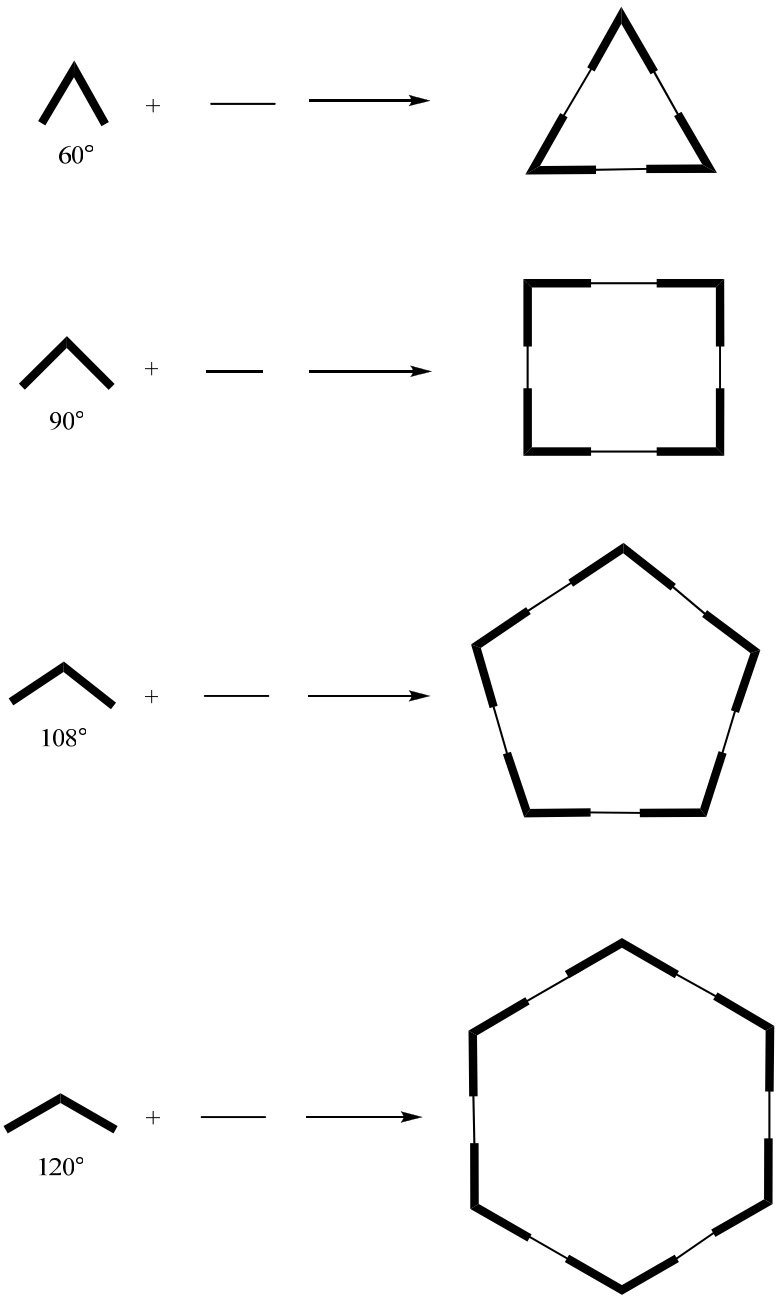

Figure 19. Strategy of producing different shaped 2D supramolecular architectures [74]

It is also possible to combine angular units with other angular units to produce rhombic shapes, squares and hexagons. Stang et al. investigated several rectangular systems and came to the conclusion that there are other forces determining the structure

than the angles. The strength of the dative bond has an impact on the formation: This was found while trying to synthesize Pt and Pd squares with cyanoligands (Scheme 5). While the Pd corners formed the desired squares the Pt counterpart only formed oligomers, due to the weaker bond to Pd which allows reconfiguration to the thermodynamically more stable product [74-75]. The self-assembly of discrete system relies on equilibrium, if the reaction is under kinetic control oligomers will be the main product. However when under thermodynamic control the equilibrium of the reaction will allow for multiple species to form but ultimately the most stable will naturally be favored. If an assembly is broken up or misformed it can thus self repair into the most stable form. This self reparation is quite common in natural systems.

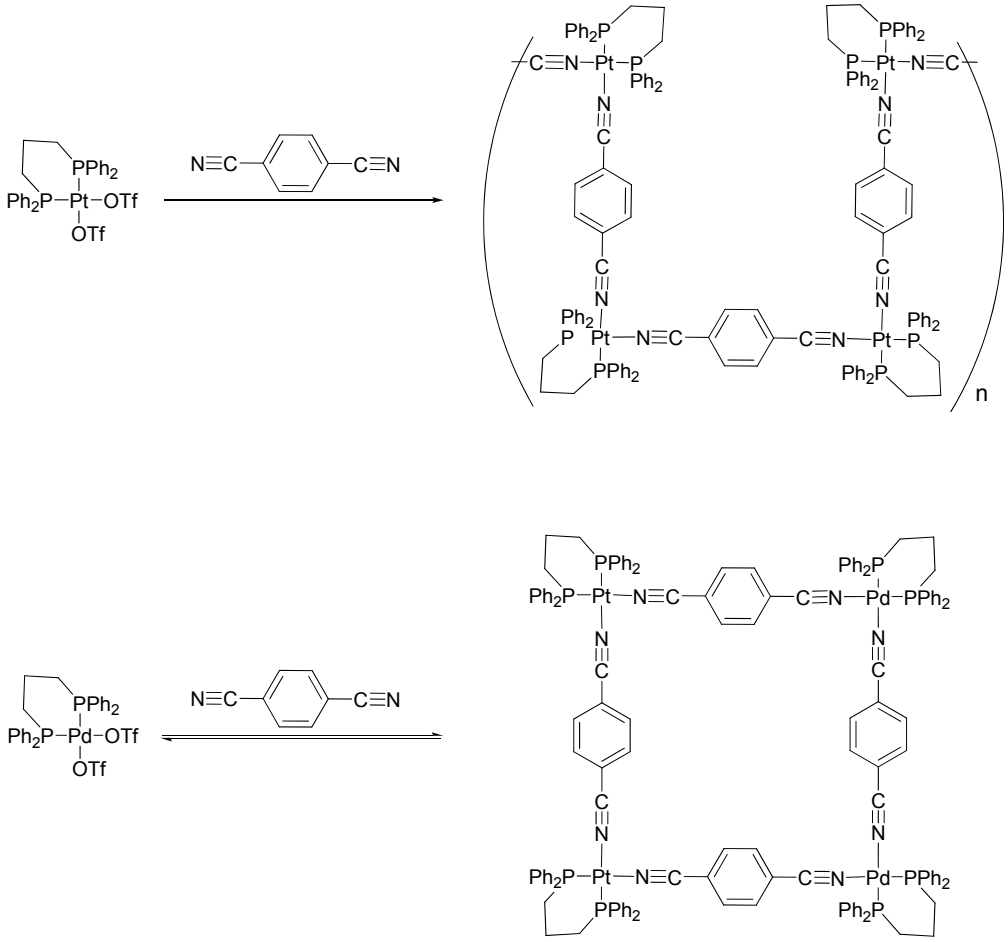

Scheme 5. The formation of Pt oligomers versus thermodynamic product the Pd square [74-75]

Another factor that contributes to the stability of the squares is π-stacking, where in the case of the compounds in Scheme 5 the phenyl in the biphosphine ligand can interact with the bridging ligand. However this interaction is weak in the cynaoligand case but much stronger if a 4,4'-bipyridine bridging ligand is used. Stang also showed that squares of lower symmetry are obtainable by using two different angular units creating bimetallic squares (Figure 20 compound A and B) [76-79], this has as well been done by Hupp in a different fashion (Figure 20 compound D) [80]. Fujita created rhombic structures by an analogous strategy of combining angular units of different types and different angles (Figure 20 compound C) [81].

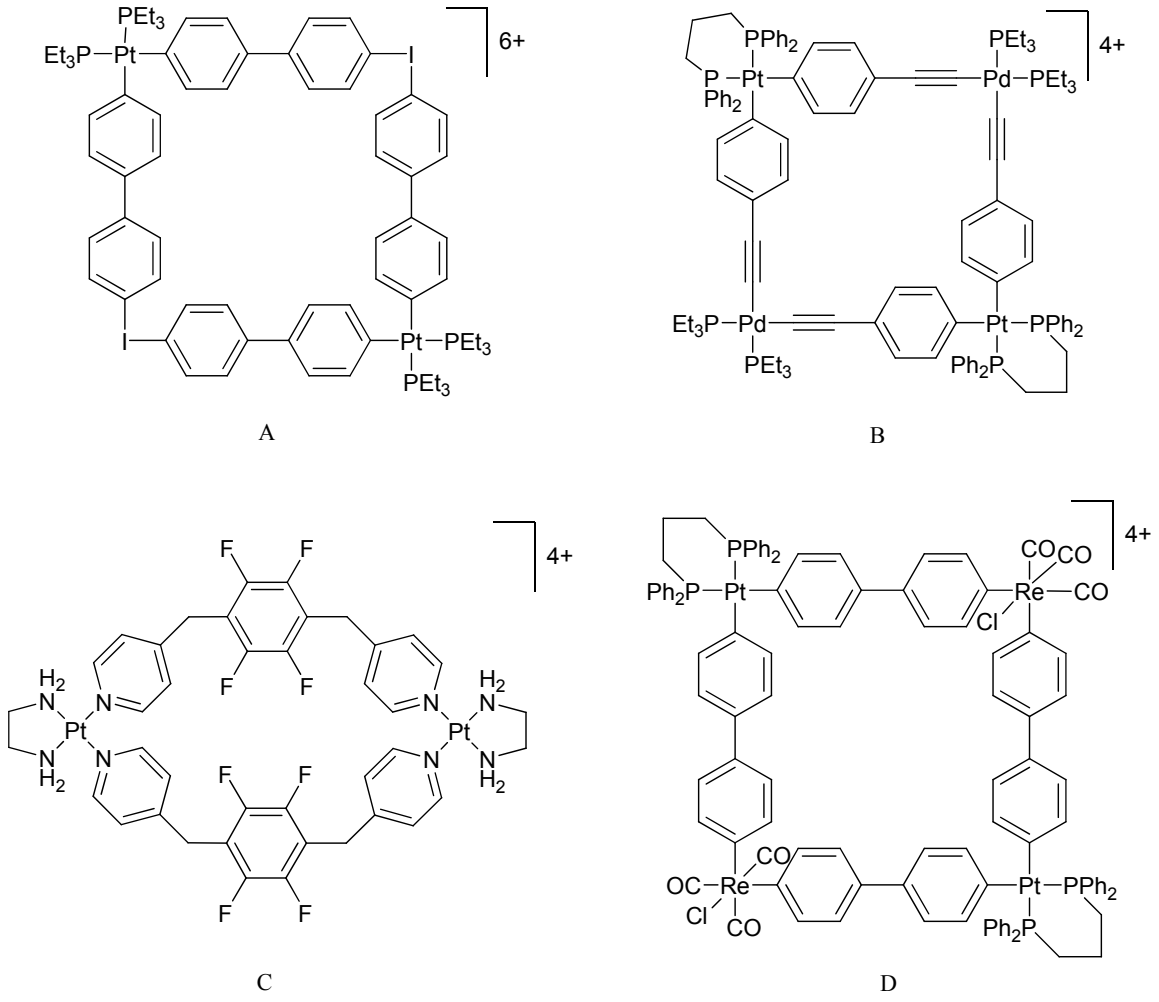

Figure 20. Bimetallic squares by Stang (A [76-77], B [78-79]) rhombic complex by Fujita (C) [81] and bimetallic complex by Hupp (D) [80]

Even though this seems like a simple and straightforward strategy for making rationally designed supramolecular structures there are some exceptions. Rigid ligands combined with 90° metallic corners that form triangular species instead of the expected squares. The combination of the small rigid pyrazine (pyz) ligand with a square planar complex of rhodium produced the triangular complex $[\{Rh(PPh_3)_2(pyz)\}_3]^{3+}$ [82], the same results were observed with a similar platinum complex containing pyrazine resulting in the triangular complex $[\{Pt(PEt_3)_2(pyz)\}_3]^{6+}$ [83].

Alessio and co-workers studied this phenomenon and was the first to produce triangles with octahedral metal corners instead of square planar. It was concluded that even though the reasons for this formation is not completely known, steric effects of the ancillary ligands are important as this narrows the 90° angle and hence makes the triangle the more favorable product as the metal-pyrazine bond also is tilted to relieve strain and minimize energy loss [84].

4.1.2 Supramolecular rectangles: a challenge

Hupp et al. investigated the possibility of forming molecular rectangles by mixing angular corners $Re(CO)_5Cl$ with linear bridging ligands of different sizes such as pyrazine and 4,4'-bipyridine. Even though it is statistically possible to form a rectangle from this mixture, this did not happen, instead they ended up with two different sized squares [85]. This implies that it is thermodynamically unfavorable to form asymmetrical compounds.

To be able to synthesize supramolecular rectangles a change of strategy is needed. A possibility is to make one robust side of the rectangle so that it has two 90° angular coordination sites in one unit, this could then be combined with a linear component of preferred length (Figure 21).

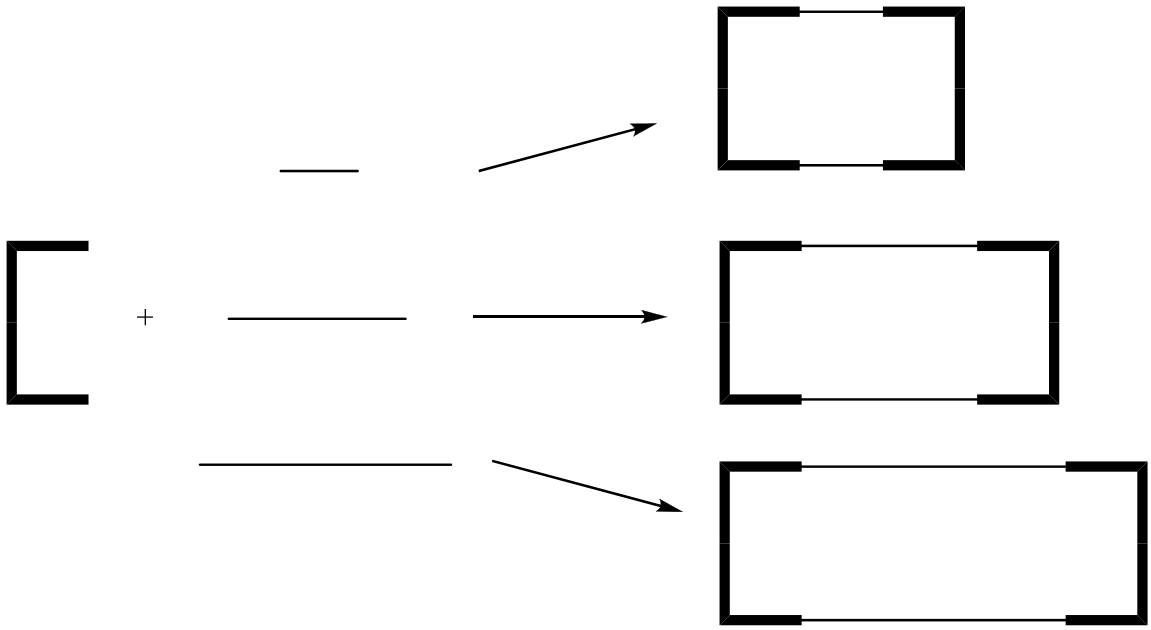

Figure 21. Synthetic strategy to generate supramolecular rectangles

Stang and co-workers developed this strategy, even though a similar approach was used by Süss-Fink and co-workers in 1997 [86], they called the compound with the two 90° angles a "molecular clip". The first test with a biphenyl linker between two platinum complexes was unsuccessful as the biphenyl rotated and the reactive sites ended up on opposite sides. A more rigid anthracene bridge unable to rotate was then developed to produce rectangles of various sizes (Figure 22) [87].

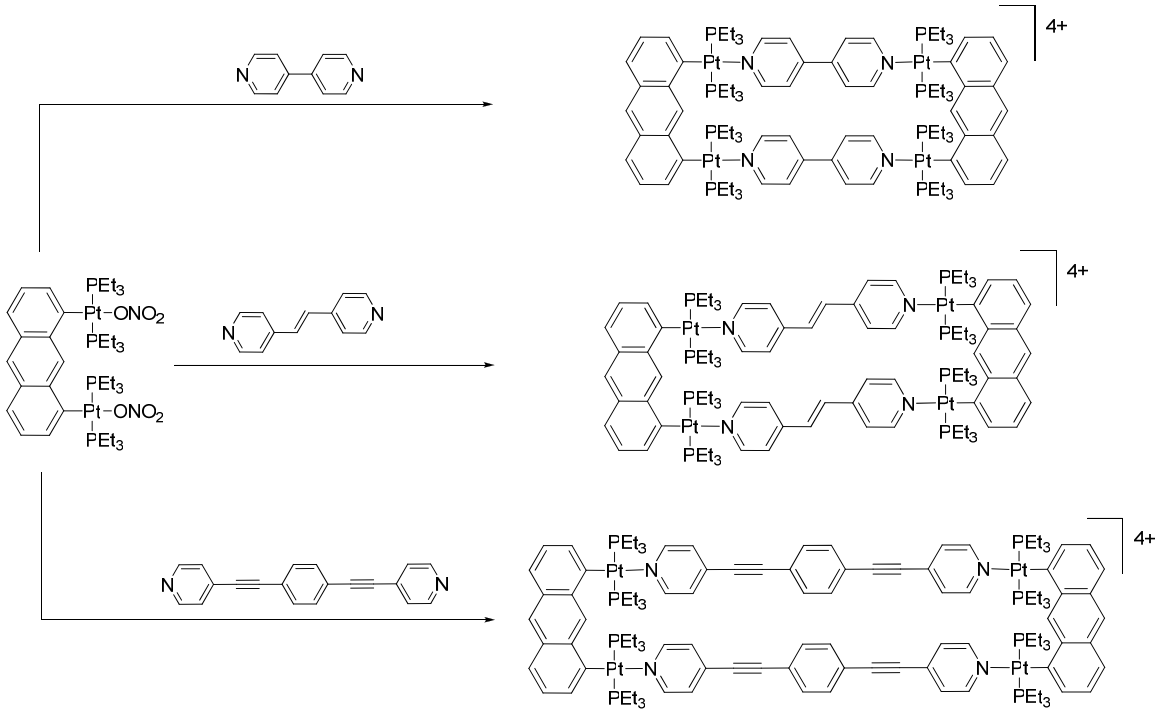

Figure 22. Synthesis of rectangles via anthracene platinum "molecular clip" [87]

4.1.3 Half sandwich compounds in supramolecular assemblies

Half sandwich complexes like arene ruthenium compounds have recently become interesting building blocks in supramolecular chemistry. Their geometry with three coordination sites available at 90° angles is a useful feature in self-assembly. By combining bridging ligands with three donor atoms with half sandwich complexes where the bridge binds as a bidentate ligand to one metal center and the third donor to another metal center, self-assembled macrocycles can be produced.

An early discovery of supramolecular half sandwich structures was one by Wolfgang Beck and co-workers who during their work of studying reactions of bioligands with RhCp* (Cp* = pentamethylcyclopentadienyl) complexes found that by

removing the chloride with Ag^+ these compounds formed chiral trimeric supramolecular structures (Figure 23) [88].

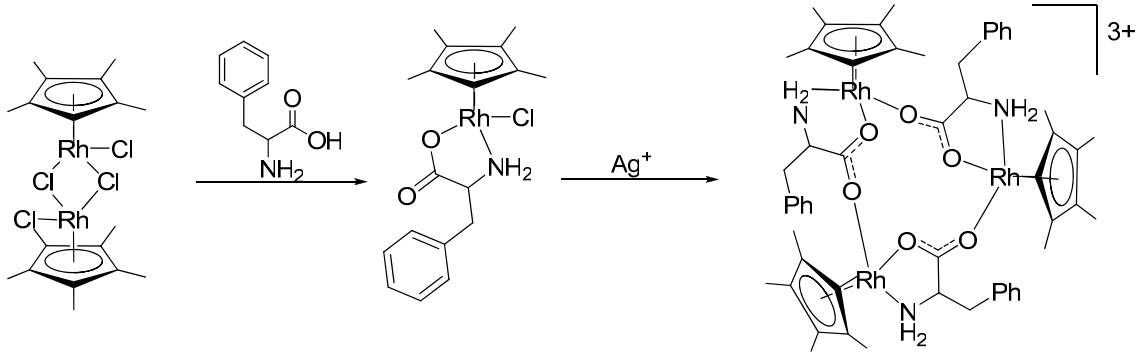

Figure 23. Synthesis of trinuclear half sandwich structure [88]

As well as trimeric complexes, dimeric, tetrameric and hexameric macrocycles are accessible from similar components. Tri, tetra and hexameric structures are all accessible using adenine derivatives as a bridging ligand, small changes on the adenine derivative determining the final structure. Independent studies by Fish, Sheldrick and Yamanari using different half sandwich complexes showed that free adenine (Figure 24, A) forms tetramers whereas its ethyl derivative (Figure 24B) forms trimers [89-90]. With 9-ethyl-hypoxanthine (Figure 24C) a trimeric species is formed [91] while the thio derivative (Figure 24D) produces hexameric macrocycles [92] and its counterpart (Figure 24E) which formed tetrameric species [93].

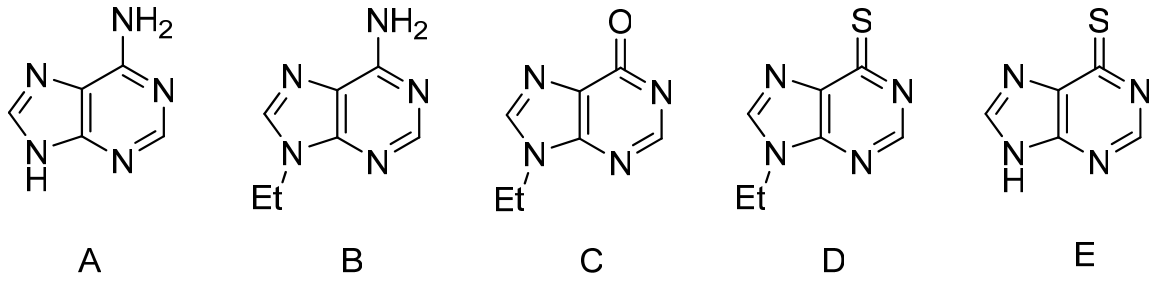

Figure 24. Adenine derivatives used to form different sized macrocycles

Studies by Severin and co-workers came to the same conclusion that rather small changes in the structure of the bridging ligand determine the size of the macrocycle. They also pointed out that too much flexibility in the ligand might lead to the entropically favored dimeric species [94]. These type of macrocycles has found applications as host guest systems to selectively bind lithium [95-96] or fluoride ions [97].

Even though metalla-supramolecular structures are very versatile and have been used to generate confined environments able to encapsulate compounds [98-100], protect and stabilize an otherwise unstable molecule [101-105], inhibit telomerase by stabilizing G-quadruplexes [106], recognize and trap specific guest molecules [107-109], or even act as microreactors for specific reactions [110-113], they are rarely evaluated for their biological activity. A series of trinuclear arene ruthenium compounds bridged by aminomethyl-substituted 3-hydroxy-2-pyridone ligands were recently evaluated *in vitro* which fragmented and gave rise to mononuclear active species [114]. Hannon and co-workers has synthesized self-assembled dinuclear ruthenium compounds with helical shape. These chiral compounds were found to bind in the major groove of DNA inducing intra molecular coiling [115] .

We decided to produce a series of rectangular arene ruthenium rectangles and evaluate their biological activity. Previous research by Süss-Fink and co-workers proved that rectangles from arene ruthenium compounds are obtainable by using a tetradentate oxalato bridging ligand connecting two metal centers and combining this with a bidentate bridging ligand. In the same manner larger rectangles can be produced by changing the size of the tetradentate ligand and by using the "molecular clip" approach to avoid formation of trinuclear species. This chapter will describe the synthesis, characterization, electrochemistry and biological activity of rectangles synthesized with quinonato bridged molecular clips. Even though some of these rectangles were produced in parallel by Jin et al. their biological activity was never before evaluated [116].

4.2 Synthesis and characterization of molecular clips

The chloro-bridged arene ruthenium dimer reacts with the bis-bidentate ligand (dihydroxo benzoquinone and chloranilic acid) at room temperature in methanol over 2 hours to form the bimetallic species $[(\eta^6\text{-arene})_2Ru_2(OO\cap OO)Cl_2]$ (arene = hexamethylbenzene, *p*-cymene; $OO\cap OO$ = 2,5-dihydroxy-1,4-benzoquinonato (dhbq), 2,5-dichloro-3,6-dihydroxo-1,4-benzoquinonato (dchq)) **7**-**10** (Scheme 6). The dark brown purple solids are collected by filtration in high yields. They are soluble in chlorinated solvents and sparingly soluble in most other organic solvents like methanol and acetone.

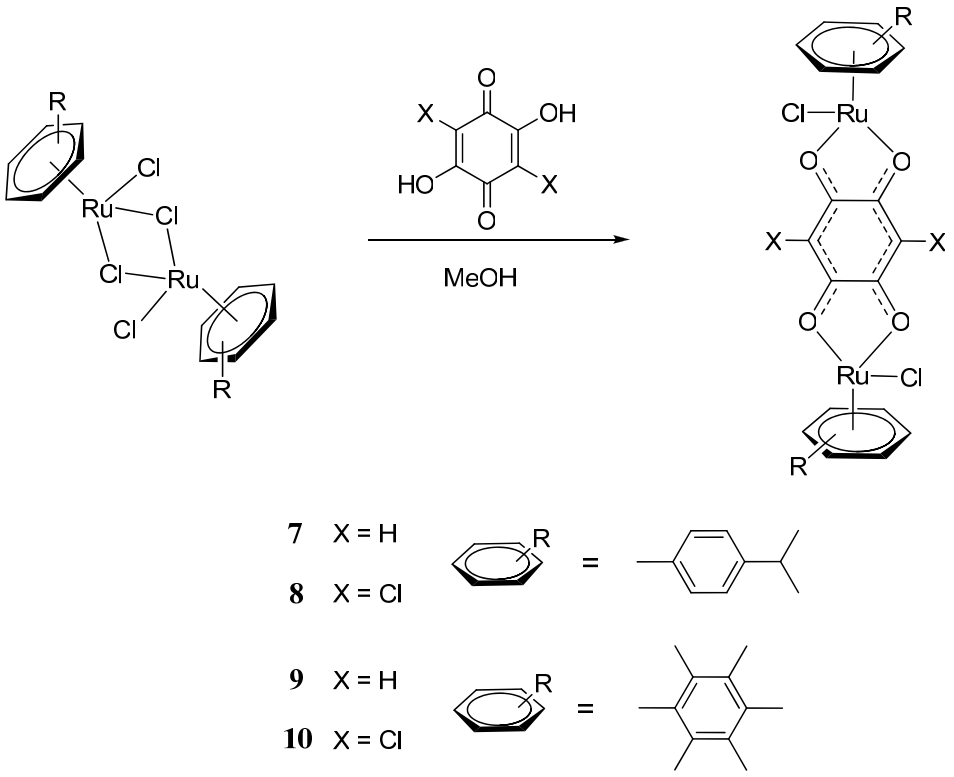

Scheme 6. Synthesis of bimetallic "molecular clip" of the type $[(\eta^6\text{-arene})_2Ru_2(OO\cap OO)Cl_2]$ (**7**-**10**)

In the ^{1}H NMR spectra the signals from the *p*-cymene moiety is in general shifted slightly downfield in comparison to the chloro dimer by about 0.3 ppm. The arene signals are also separated by an additional 0.1 ppm due to the deshielding effect of the quinonato

ligand. The signal of the dhbq protons in compounds **7** and **9** are also shifted upfield in comparison with free dhbq-H_2 by 0.3 ppm.

4.3 Synthesis and characterization of supramolecular rectangles

4.3.1 Pyrazine bridged rectangles

The dinuclear arene ruthenium complexes $[(\eta^6\text{-arene})_2Ru_2(OO\cap OO)Cl_2]$ (**7**-**10**) react in methanol at room temperature with silver triflate to remove the chloride ligands. The activated methanolate species produced *in situ* can adopt a syn symmetry. It then reacts with the $N\cap N$ donor ligand pyrazine to give the metalla-cyclic tetranuclear cations **11**-**14**. The rectangles are obtained as their triflate salts (Scheme 7).

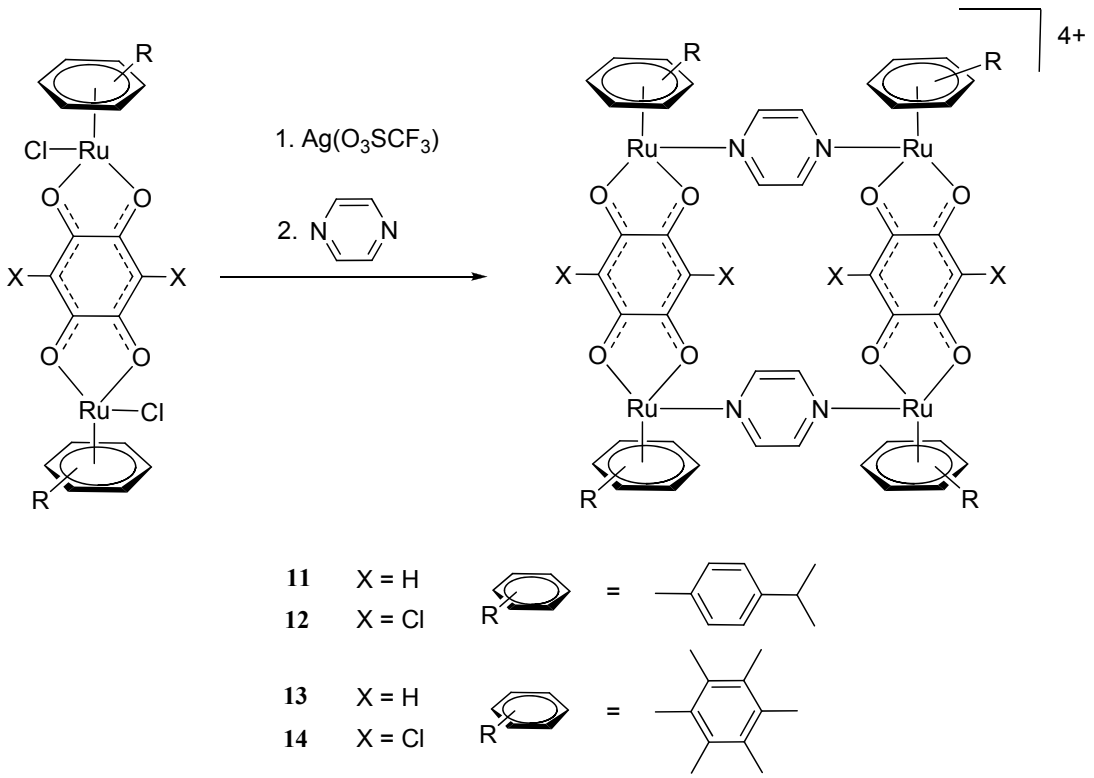

Scheme 7. Synthesis of pyrazine rectangles, compounds **11**-**14**

The tetranuclear compounds [**11-14**][O_3SCF_3]$_4$ dissolve only sparingly in acetone and dichloromethane and show rapid decomposition in dimethylsulfoxide. The ^{1}H NMR spectra of **11-14** display a singlet due to the pyrazine protons. Unlike free pyrazine, where the proton signal is found at 8.61 ppm in acetone-d_6, the signal in **11-14** appears slightly shifted downfield at 8.7 ppm. Upon formation of the cationic tetranuclear metalla-rectangles, the methyl and isopropyl signals of the *p*-cymene ligands in **11** and **12** remain almost unchanged as compared to complexes **7** and **8**, while the aromatic protons of the *p*-cymene ligands are shifted downfield. On the other hand, the proton signal of the dhbq bridging ligands in **11** and **13** is shifted upfield as compared to the parent complexes **7** and **9**. The infrared spectra of **11-14** are dominated by absorptions of the coordinated *N*∩*N* and *OO*∩*OO* ligands, which are only slightly shifted as compared to the free ligands. In addition to the *N*∩*N* and *OO*∩*OO* signals, strong absorptions due to the triflate anions (1260(s), 1030(s), 638(m) cm^{-1}) are also observed in the infrared spectra of the salts.

4.3.2 4,4'-Bipyridine bridged rectangles

The synthesis of these rectangles follows the same procedure as the previous ones. The bimetallic clip reacts in methanol at room temperature in the presence of silver triflate which removes the chloride, and the methanolated clip is then mixed with the bridging *N*∩*N* donor ligand to produce the metalla-rectangles [**15-18**][O_3SCF_3]$_6$ as their triflate salts in good yields as dark red solids (Scheme 8). Compounds [**15-18**][O_3SCF_3]$_4$ are soluble in polar organic solvents such as dichloromethane, acetone, methanol, dimethylsulfoxide and also in water.

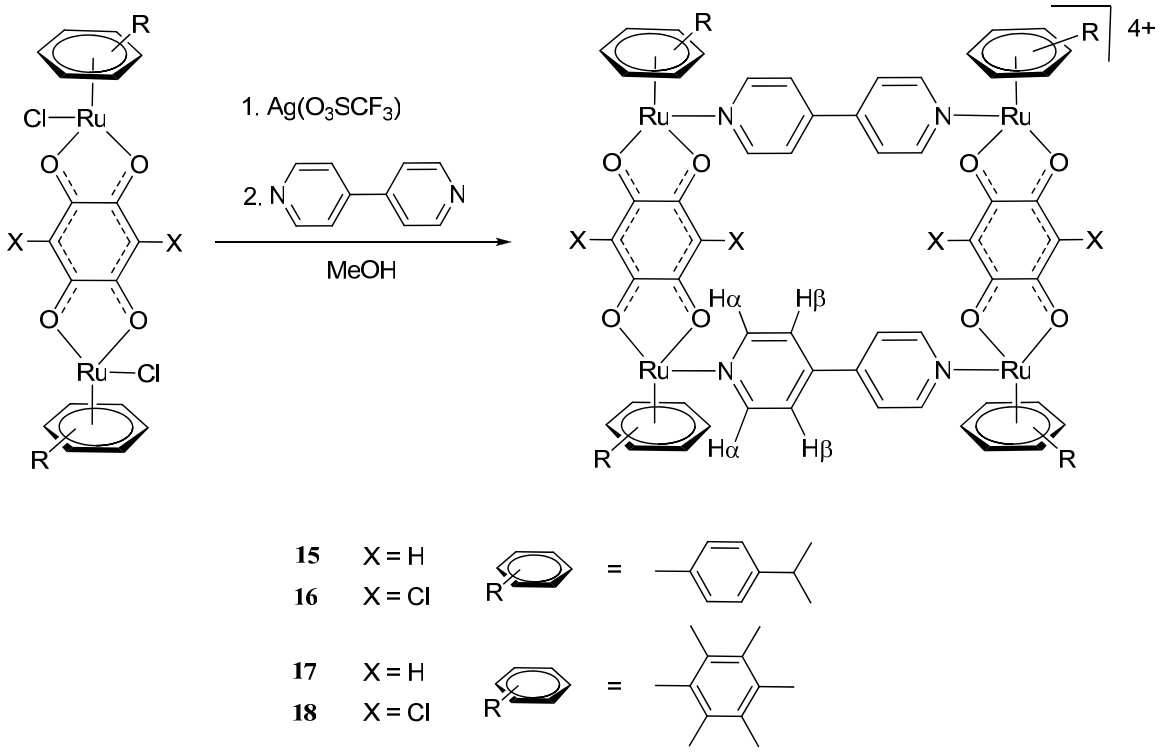

Scheme 8. Synthesis of 4,4'-bipyridine bridged rectangles, compound **15**-**18**

The ^{1}H NMR spectra display two doublets originating from the 4,4'-bipyridine bridging ligand. The signal from the α-proton is found in acetone-d_6 at 8.54 ppm for **15** and **16** and at ~8.40 ppm for **17** and **18** shifted slightly upfield from the free ligand at 8.72 ppm. The β-proton signal is found at ~8.04 ppm (**15**, **16**) and ~8.10 ppm (**17**, **18**) respectively which is as well downfield shifted by about 0.3 ppm from the free 4,4'-bipyridine. Signals from the methyl and isopropyl groups of *p*-cymene and hexamethylbenzene remain virtually unchanged whereas the arene proton signals of *p*-cymene shift downfield, as well the dhbq proton in complex **15** and **17** shifts upfield. The IR spectra are as well dominated by the *N*∩*N* and *OO*∩*OO* ligands with the additional absorptions of the triflate anions.

The single crystal X-ray structure analysis of [**17**][O_3SCF_3]$_4$ confirms the expected rectangular structure. The molecular structure is presented in Figure 25. The

cation **17** contains four ruthenium metal centers bonded to a hexamethylbenzene ligand, which are bridged by the dianionic *OO*∩*OO* ligand through its four oxygen atoms and linked by the neutral *N*∩*N* ligand 4,4'-bipyridine. The Ru-N and Ru-O distances observed in **17** are comparable to those found in the hexacationic metalla-prisms. The 4,4'-bipyridine linkers show a twist of 4.6° between the two pyridyl units, which is comparable to that found in other 4,4'-bipyridine bridged ruthenium complexes [117].

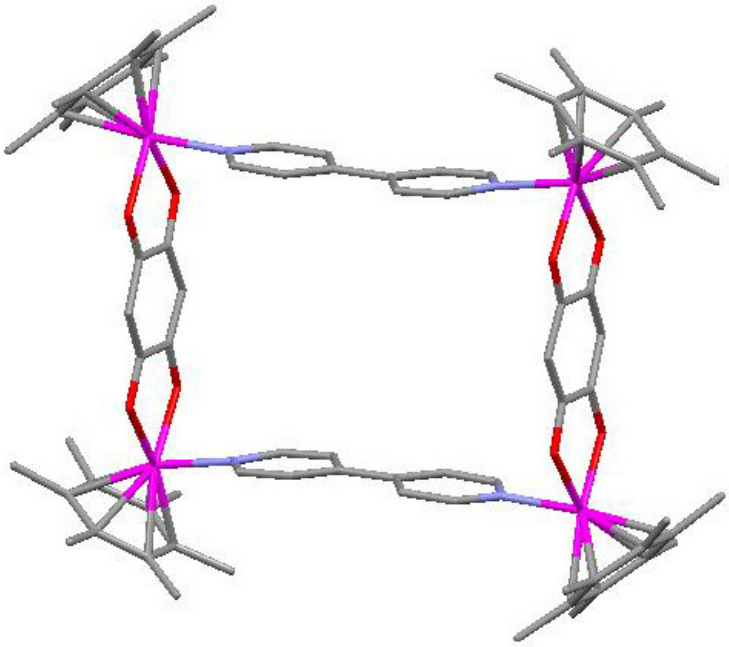

Figure 25. Capped sticks representation of cation **17**, O_3SCF_3 and H atoms omitted for clarity

Interestingly, [**17**][O_3SCF_3]$_4$ forms in the solid state one dimensional channels along the *b* axis with intramolecular Ru-Ru separations of 7.9 and 11.3 Å. A similar arrangement along the *c* axis has been found in the crystal structure of [**16**][O_3SCF_3]$_4$, with almost identical Ru-Ru separations (7.9 and 11.2 Å) [116]. In both structures the triflate anions are located between the rectangular channels. However, in [**16**][O_3SCF_3]$_4$ disordered water molecules are observed in the cationic molecular rectangle as compared to [**17**][O_3SCF_3]$_4$ for which no solvent molecules are observed in the hydrophobic cavity.

4.3.3 1,2-Di(4-pyridyl)ethylene bridged rectangles

The synthesis follows the same procedure using 1,2-di(4-pyridyl)ethylene as *N*∩*N* ligands thus producing the metalla-rectangles [**19-22**][O_3SCF_3]$_4$ as their triflate salts in good yields as dark red solids (Scheme 9). The triflate salts are like the 4,4'-bipyridine bridged compounds soluble in polar organic solvents and in water.

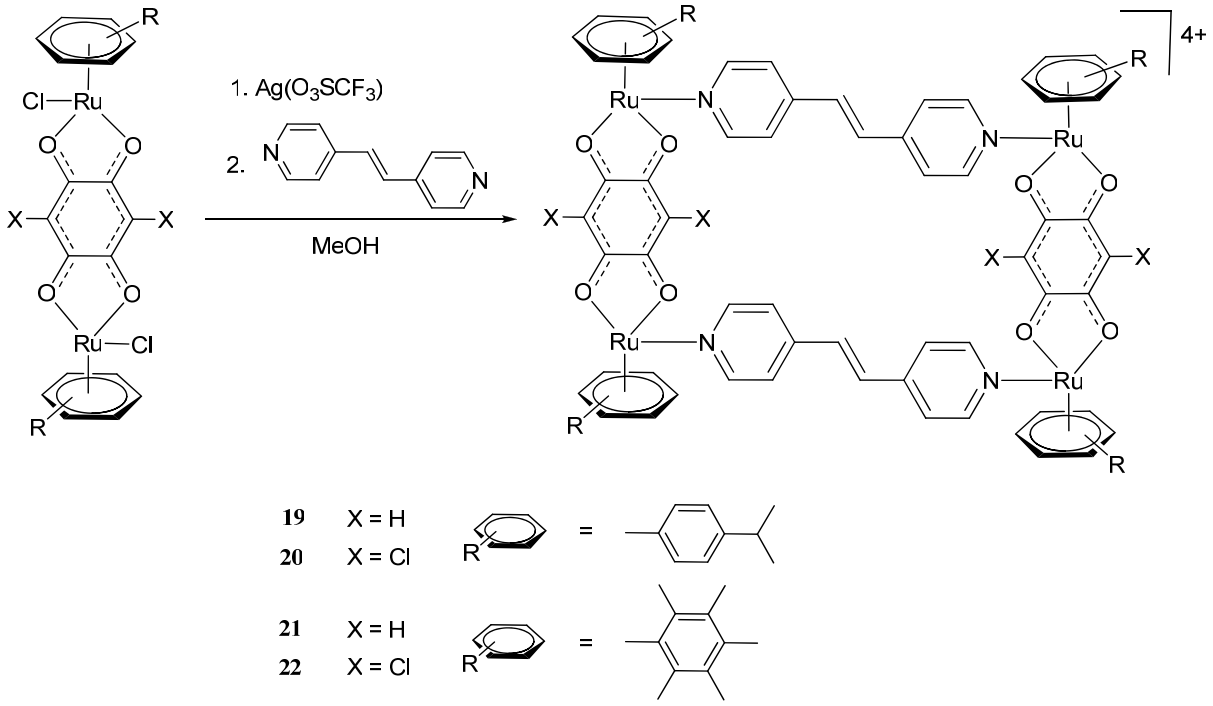

Scheme 9. Synthesis of 1,2-di(4-pyridyl)ethylene bridged rectangles, compound **19-22**

The ^{1}H NMR spectra naturally display two doublets originating from the aromatic ring of the bipyridine bridging ligand but also a singlet from the ethylene protons. The signal of the α-proton appears as a doublet at ~8.33 ppm for the *p*-cymene containing **19** and **20** and at ~8.20 ppm for the hexamethylbenzene containing **21** and **22**. Compared to the 4,4'-bipyridine bridged complexes these shifts are 0.1 ppm larger (0.3 ppm for **19** and **20**, 0.4 ppm for **21** and **22**) in comparison with the free ligand. The signal of the β-proton is in this case as well shifted downfield but by about 0.2 ppm for compounds **19-22**, with

a slightly higher shift for the chloro containing complexes **20** and **22**. As in the case of the 4,4'-bipyridine containing rectangles the signals of the aromatic protons of *p*-cymene complexes are shifted downfield whereas the methyl groups remains virtually unchanged, there is also an upfield shift of the dhbq protons of **19** and **21.** The infrared spectra is as previously mentioned also in this case dominated by the *N*∩*N* and *OO*∩*OO* ligand absorptions and the absorptions of the triflate anions.

The single-crystal X-ray structure analysis of [**22**][O_3SCF_3]$_4$ confirms that the 1,2-di(4-pyridyl)ethylene also forms the expected rectangular structures: The molecular structure being presented in Figure 26. Cation **22** contain four ruthenium metal centers bonded to a hexamethylbenzene ligand, which are bridged by the dianionic *OO*∩*OO* ligand through its four oxygen atoms and linked by the neutral *N*∩*N* ligand. The Ru-N and Ru-O distances observed in **22** and **17** are comparable to those found in the hexacationic metalla-prisms [guest⊂(η^6-arene)$_6$Ru$_6$(4-tpt)$_2$(2,5-dihydroxy-1,4-benzoquinonato)$_3$][O_3SCF_3]$_6$ (guest = pyrene, benzo[e]pyrene, Pt(acetylacetonato)$_2$, hexamethoxytriphenylene) [118-120].

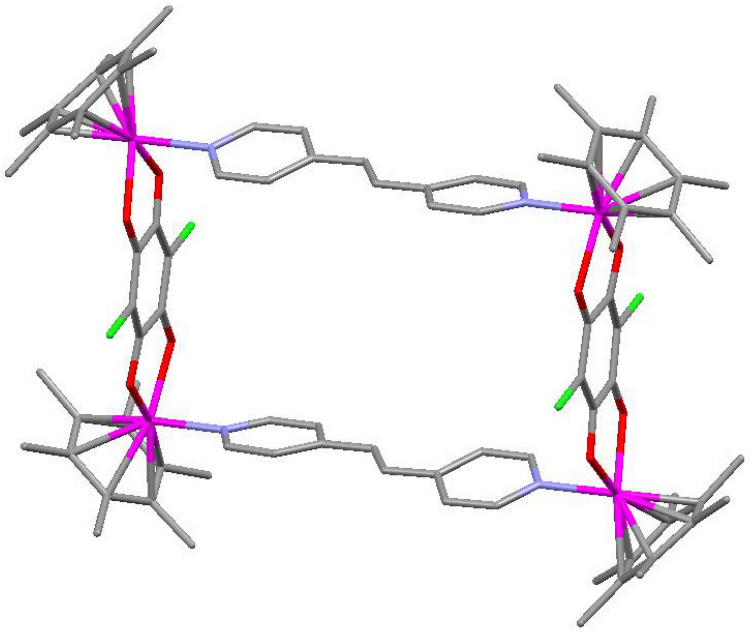

Figure 26. Capped sticks representation of cation **22**, O_3SCF_3, H atoms and solvent molecules omitted for clarity

As expected, the molecular structure of [**22**][O_3SCF_3]$_4$ shows a larger cavity (7.9 × 13.6Å^2). Upon crystallization of [**22**][O_3SCF_3]$_4$ from a chloroform/diethyl ether mixture, two diethyl ether molecules are encompassed in the hydrophobic cavity of cation **22**. A similar crystal packing has been observed in [**20**][O_3SCF_3]$_4$ in which highly disordered solvent molecules were found in the rectangular 7.9 × 13.5 Å^2 cavity [116].

4.4 Electrochemical properties

Electrochemical studies were done in collaboration with Petr Štěpnička of Charles University (Czech Republic). Compounds **7**-**10** and [**15**-**22**][O_3SCF_3]$_4$ have been studied by cyclic voltammetry at a platinum disk electrode. The measurements were performed on ca. 0.5 mM (or saturated) dichloromethane solutions containing 0.1M Bu_4NPF_6 as the supporting electrolyte. Pertinent data are summarized in Table 3.

The redox response of the dinuclear complexes **7**-**10** is roughly similar, the compounds displaying one or two well-separated oxidations and one or two reductions in the accessible potential range. Unfortunately, the reduction waves are difficult to study, as they occur at the upper limit of the potential window provided by the solvent. Complex **7** shows two well-separated irreversible reductions at -1.20 and -1.89 V and an oxidation at around +1.0 V (Figure 27).

Replacement of dhbq with dchq bridges such as in **8** results in a shift of the reductive waves to less negative potentials while making the single oxidation more difficult (Table 3). In addition, the presence of the dchq ligand renders the first reduction wave reversible (Figure 28). The wave is observed with full electrochemical reversibility when recorded with the switching potential set before the second reduction process at scan rates down to 0.1Vs^{-1}. However, upon extending the scan range further beyond the second reduction wave, the anodic peak current due to the first wave becomes lower than its corresponding cathodic counterpeak.

Table 3. Summary of electrochemical data of complexes **7**-**10** and **15**-**22**

Compound	E[V]
7	-1.20 (ir.), -1.89 (ir.); ca. +1.0 (ir.)
8	2 -0.90 (rev.), -1.76 (ir.),[b] ca. +1.1 (ir.)
9	3 -1.37 (ir.), +0.76 (ir.), ca. +1.1 (ir.)
10	-1.06 (rev.), ca. -2.0 (ir.), ca. +0.76 (ir.)
15$[O_3SCF_3]_4$	-0.68 (rev.),[c] -1.39 (ir.), -1.90 (ir.)
16$[O_3SCF_3]_4$	-0.45 (rev.),[c] -1.15 (rev.)[c,d]
17$[O_3SCF_3]_4$	-0.82 (rev.)[c], ca. -1.6 (ir.)
18$[O_3SCF_3]_4$	-0.55 (rev.), -1.35 (rev.)[c]
19$[O_3SCF_3]_4$	-0.70 (rev.), -1.42 (ir.), ca. -1.9 (ir.)
20$[O_3SCF_3]_4$	-0.45 (rev.), -1.19 (rev.)[c], ca. -1.9 (ir.)
21$[O_3SCF_3]_4$	-0.56 (rev.),[c] -1.44 (ir.)
22$[O_3SCF_3]_4$	-0.57 (rev.),[c] -1.41 (rev.)[c], ca. -2.0 (ir.)

[a]Potentials are given relative to ferrocene/ferrocenium. Peak potentials are quoted for irreversible (ir.) processes (E_{pa} or E_{pc}). The potentials for reversible (rev.) couples are defined as the mean of the anodic and cathodic peak potentials: $E°'=1/2(E_{pa} + E_{pc})$. [b]A prepeak is observed at -1.65 V. [c] See text. [d] The most negative peak is hidden by decomposition of the base electrolyte and some decomposition processes.

This points to some coupled chemical processes that consume the electrogenerated species and is in accordance with the fact that the second reduction is accompanied by adsorption processes or decomposition. The replacement of the *p*-cymene ligand for hexamethylbenzene (**7** → **9** and **8** →**10**) leaves the redox pattern virtually unchanged, but the respective waves appear shifted to more negative potentials. Apparently, the higher donor ability of the hexamethylbenzene ligand makes any electron addition more difficult while facilitating the oxidative processes. For **9**, this "shift" allows

for observation of two oxidative waves at +0.76 and ca. +1.1 V, whereas the expected second reduction falls outside the accessible potential range.

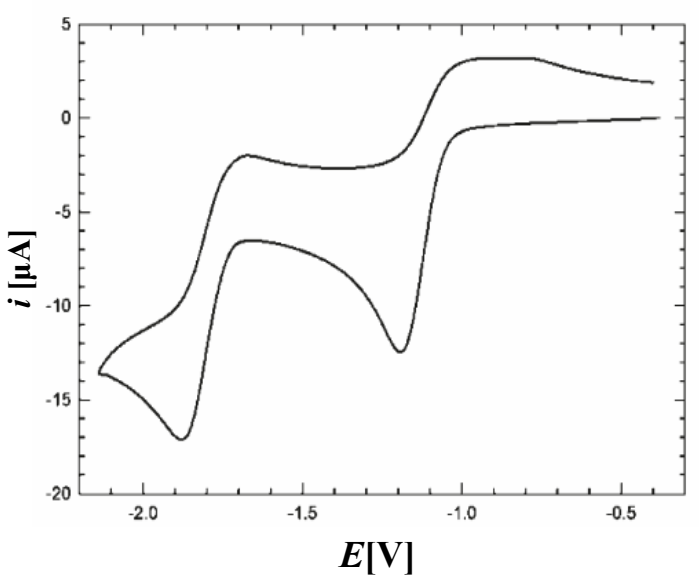

Figure 27. Cyclic voltammograms of **7** (0.5 mM in CH_2Cl_2 at Pt-disk, scan rate $0.1Vs^{-1}$)

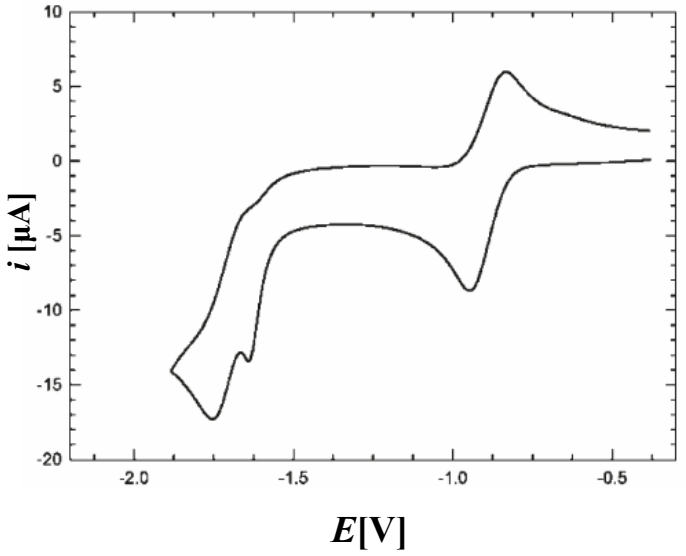

Figure 28. Cyclic voltammograms of **8** (0.5 mM in CH_2Cl_2 at Pt-disk, scan rate $0.1Vs^{-1}$)

In analogy to the previous reports dealing with electrochemistry of diruthenium complexes featuring dhbq and dchq bridges [121-123], we can formally assign the cathodic processes to one-electron reductions that occur predominantly at the bridging ligand and attribute the oxidations to the Ru(II)/Ru(III) couples. Nevertheless, this assignment is only qualitative, particularly if one considers the extensive mixing of the metal-based orbitals with those located at the bridging ligands as established by theoretical calculations [122].

Like in the case of the dinuclear compounds, the overall redox response of the tetraruthenium complexes **15**-**22** is analogous. Compared with their diruthenium precursors, complexes **15**-**22** bear a high positive charge and, hence, are more prone to reduction, whereas their oxidative waves are either observed at the onset of the base electrolyte decomposition (**19**) or not observed at all due to their highly positive redox potentials. The *p*-cymene ruthenium complex possessing 4,4'-bipyridine bridges, compound **15**, undergoes first a reversible reduction at -0.68 V followed by two successive irreversible reductions at -1.39 and -1.90 V (Figure 29). The following redox steps apparently influence the first one: When the scanning is performed just over the first reduction, the first reduction is observed with full electrochemical reversibility. Upon increasing the switching potential so that the scan involves the subsequent redox step(s), the oxidative peak due to the first wave is observed with a significantly lower peak current. This again points to some associated follow-up associated processes that consume the electrogenerated product(s).

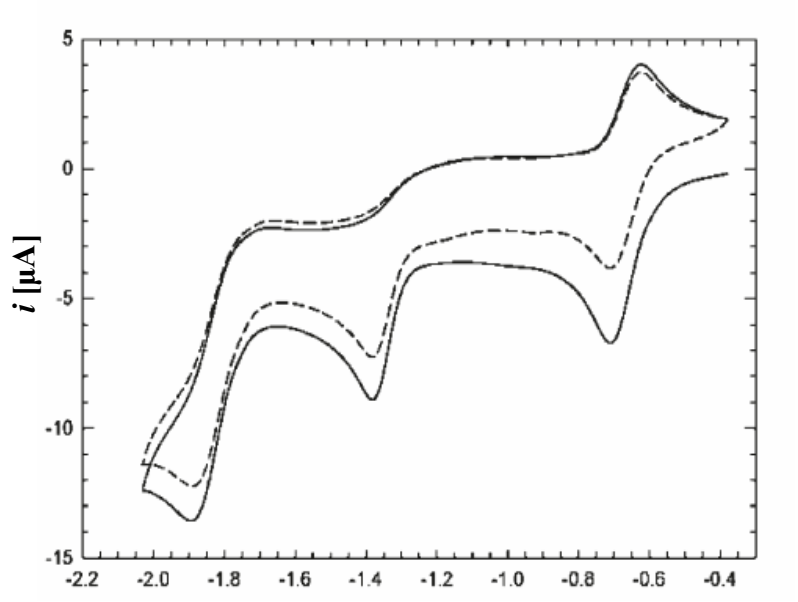

Figure 29. Cyclic voltammograms of **15** (0.5 mM in CH_2Cl_2 at Pt-disk, scan rate 0.1V; first scan — , second scan ----)

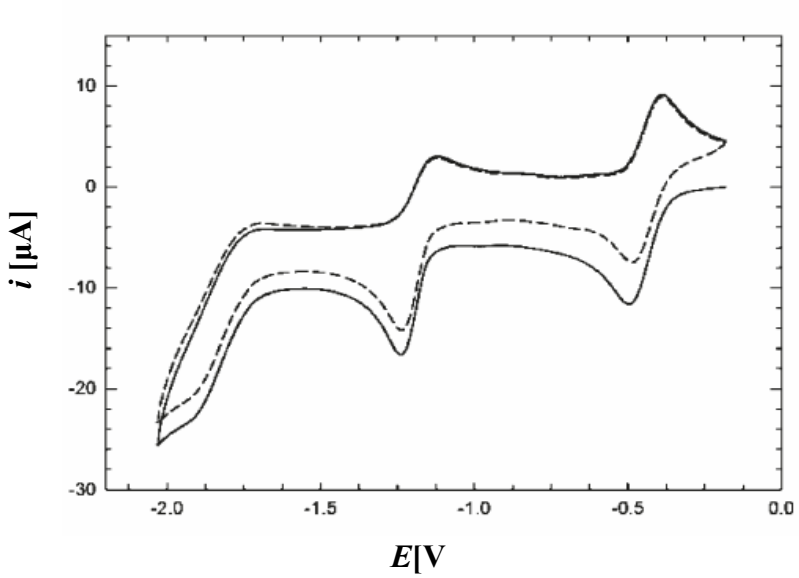

Figure 30. Cyclic voltammogram of **20** (0.5 mM in CH_2Cl_2 at Pt-disk, scan rate 0.1V; first scan — , second scan ----)

The behavior of the analogous compound **19** featuring 1,2-bis(4-pyridyl)ethylene linkers is practically identical, except that all the waves are shifted to slightly more

negative potentials. By contrast, the change of the bridge for the dchq anion has a more pronounced effect. The first two waves in **20** (Figure 30) and **16** are observed shifted to more positive potentials, which is in accordance with the electron-withdrawing nature of the chloride substituents replacing two hydrogen atoms at the *OO*∩*OO* bridging ligand. In addition, both waves bear clear signs of electrochemical reversibility, the first wave being observed with full reversibility when the switching potential is set just after the first reduction. The following wave can be described as quasi-reversible, showing a lower peak current for the back scan peak (anodic) than for the forward (cathodic) peak ($i_{pc}>i_{pa}$). Moreover, scanning further beyond the second wave (i.e., toward more negative potentials) markedly lowers the reversibility of the first redox step, causing an increase in the separation of the counterpeaks and lowering of the current of the respective anodic counterwave. The redox behavior of **17**-**21** and **18**-**22** is complicated by adsorption phenomena that become particularly pronounced upon repeated scanning and reduce the reversibility and reproducibility of the cyclic voltammograms. This is particularly the case of **21**, which shows additional ill-defined reductive peaks and a strong stripping peak in the anodic region.

4.5 Biological activity

The biological activity was tested in collaboration with Prof. Paul Dyson and co-workers at the EPFL (Switzerland). The anti-proliferative activity of the water soluble compounds containing the ligands 4,4'-bipyridine (**15**-**18**) and 1,2-bis(4-pyridyl)ethylene (**19**-**22**) was evaluated against the A2780 ovarian cancer cell line. All complexes exhibit moderate to excellent activity with IC_{50} values in the range 4-66 μM (Table 4). In each case, the hexamethylbenzene complexes exhibit lower IC_{50} values than their *p*-cymene analogues, probably resulting from increased uptake due to their greater lipophilicity. Similarly, complexes containing the dhbq linkers are generally more active than the less lipophilic dchq analogues.

Table 4. IC_{50} values of complexes **15**-**22** on A2780 human ovarian cancer cells after 72h exposure

Compound	IC_{50} (μM)
15$[O_3SCF_3]_4$	66
16$[O_3SCF_3]_4$	43
17$[O_3SCF_3]_4$	27
18$[O_3SCF_3]_4$	33
19$[O_3SCF_3]_4$	6
20$[O_3SCF_3]_4$	29
21$[O_3SCF_3]_4$	4
22$[O_3SCF_3]_4$	23
cisplatin	2

There does not appear to be a correlation between the redox potentials of the compounds and their cytotoxicity, which is perhaps not surprising since it is generally considered that Ru(III) compounds are reduced to Ru(II) compounds inside the reductive environment of a tumor (with Ru(0) not biologically accessible), and therefore the compounds investigated herein are already in the active oxidation state.

Interestingly, the large rectangles incorporating 1,2-bis-(4-pyridyl)ethylene and dhbq linkers (complexes **19** and **21**) are up to an order of magnitude more cytotoxic ($IC_{50} \leq 6$ μM) than the 4,4'-bipyridine containing cations ($IC_{50} \geq 30$ μM). The reason for this effect is not clear but it could be linked to the increased flexibility of the 1,2-bis(4-pyridyl)ethylene linker that may allow the rectangular structures to adapt their shape to better fit with a molecular target. However, it cannot be ruled out that the tetranuclear cations fragment once inside a cell and that the fragments induce the cytotoxic effect, it is even quite likely that fragmentation occurs based on a study of chemically similar compounds [124]. Another study of similar metalla-rectangles by Navarro and Barea treated interactions with DNA and showed that these types of complexes induce changes in the shape of DNA strands. They also proposed possible binding in the major groove of

DNA which might be responsible for the shape changing properties, however if these complexes are able to enter the nucleus has yet to be proven alas another mechanism might be responsible for their activity. The chlorinated clip was found inactive whereas the triflate activated species exhibited some activity. These rectangles were as well found active against the A2780 cell line but much less against a lung cancer cell line which suggests low general toxicity [125].

4.6 Conclusions

With the goal to produce supramolecular assemblies with biological activity we have produced a series of supramolecular rectangles in good yields soluble in most polar organic solvents and water. Some of these complexes have shown high biological activity even though the mechanism of their activity is still unknown, whereas some were not sufficiently stable for such studies. Tests on similar compounds suggest low general toxicity. The positive biological results prove the possibility to use these systems for biological applications although selectivity has yet to be proven.

5. Supramolecular Prismatic Carceplexes

5.1 Introduction

Three dimensional assemblies are obtained following the same strategy as for the two dimensional systems by mixing angular units with linear or planar ones. However in this case one of the two components needs to have three connecting points. Fujita and co-workers were the first to synthesize this type of system using the same $[Pd(en)]^{2+}$ corners but connected with the tritopic ligand 2,4,6-tris(4-pyridyl)-1,3,5-triazine (tpt) to produce a three dimensional cage structure (Figure 31) [126].

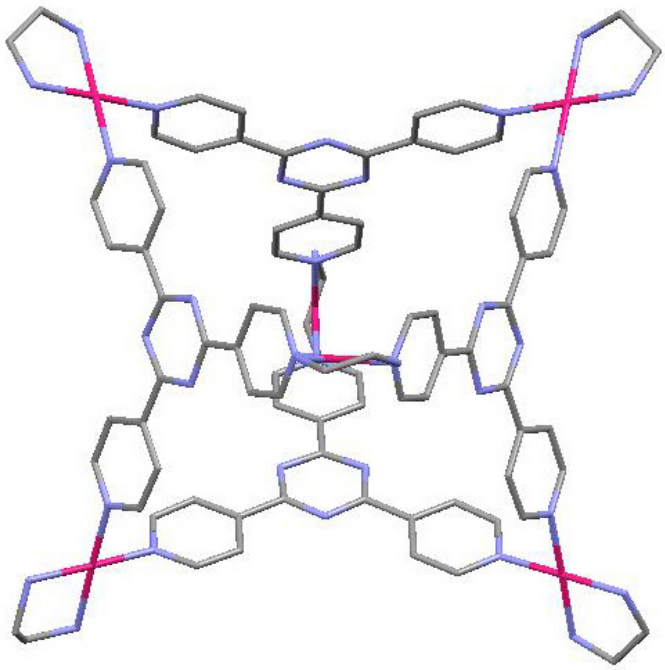

Figure 31. Three dimensional Pd cage $[Pd_6(en)_6(tpt)_4]^{12+}$ synthesized by Fujita [126]

They investigated the host guest chemistry of this octahedron which is able to encapsulate adamantane, the hydrophobic cavity can also be used to carry out reactions

for example Diels Alder catalytic reactions for which acceleration by a factor of 100 was observed [127].

Stang and co-workers followed shortly after and successfully synthesized a chiral octahedron based on the slightly larger tritopic ligand 1,3,5-tris[(4-pyridyl)-ethynyl]benzene and chiral corners in the form of [(*R*-(+)-BINAP)M(O_3SCF_3)$_2$] (M = Pt, Pd, and BINAP = 2,2'-bis(diphenylphosphino)-1,1'-binaphthyl). This complex was as expected found to be optically active [128].

So even for three dimensional structures given specific angles of the units a variety of structures could theoretically be obtained through rational design. A mixture of tridentate planar and linear ligands with 90° corners would produce a triangular prism (Figure 32A), planar tridentate ligands with 78-84° angle units would give the fore mentioned octahedron (Figure 32B), tridentate 90° angular units in combination with linear units would form a cube (Figure 32C), planar tridentate ligands with an angular unit of 109.5° bonding angle would take the shape of a cuboctahedron (Figure 32D) whereas tridentate tetrahedral units 109° combined with linear units would take the shape of a dodecahedron (Figure 32E) .

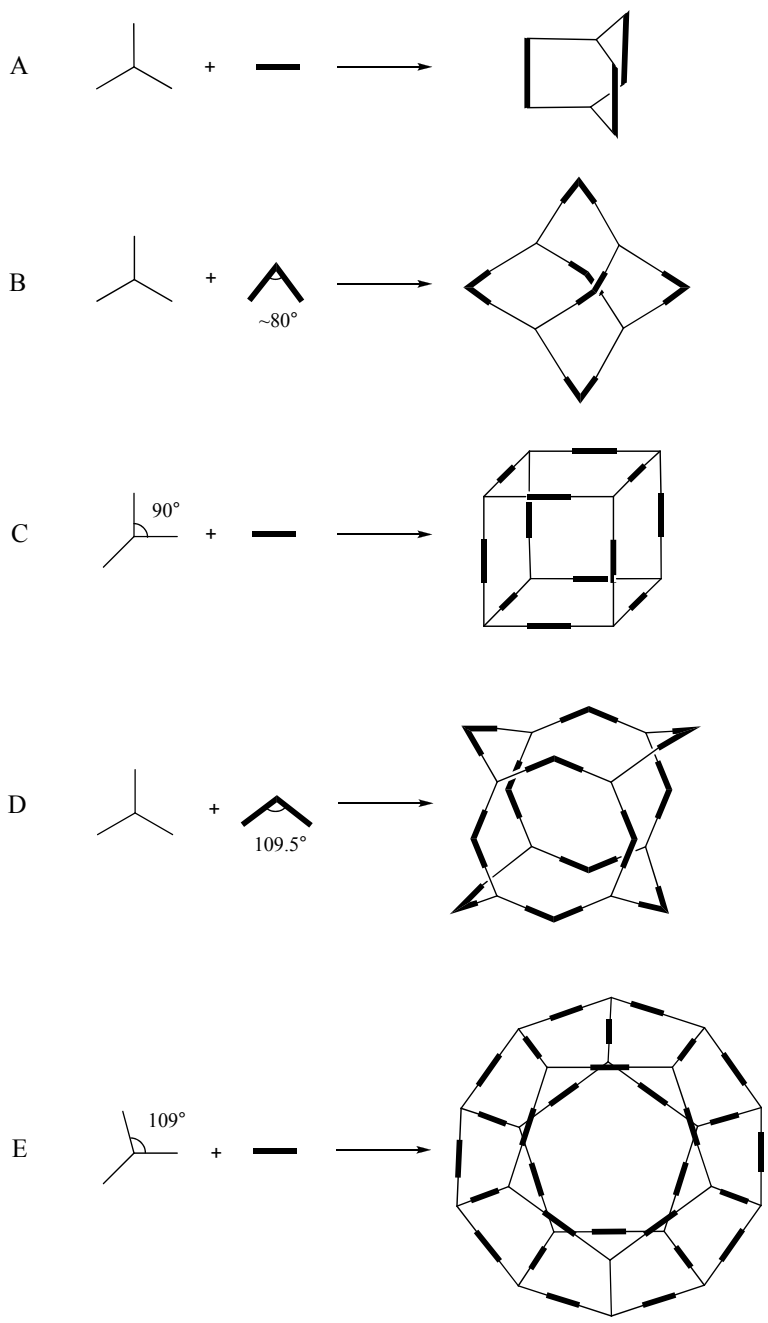

Figure 32. Three dimensional shapes by supramolecular building blocks through rational design [74]

Although the angles are important they will not alone determine the final structure, as mentioned before where components that geometrically should form squares, very often triangles will be obtained instead. The formation of larger structures is

determined by the angle but also the type of the building block, if the building block is flexible these degrees of freedom are frozen upon complexation, an energy loss which is acceptable for small structures but not in larger ones. The key to producing large structures is rigid building blocks with few degrees of freedom. Concentration of the building blocks and solvent choice are two other important factors as they affect the entropy of formation for the complex [129].

Cubic structure is large and demands many components, 8 corner units and 12 linear units. By rational design using the fairly rigid 4,4'-bipyridine ligand with Ru([9]aneS_3) corners, which does not sterically affect the bond angles of the ligands, Thomas and co-workers managed to assemble a molecular cube (Figure 33) [130].

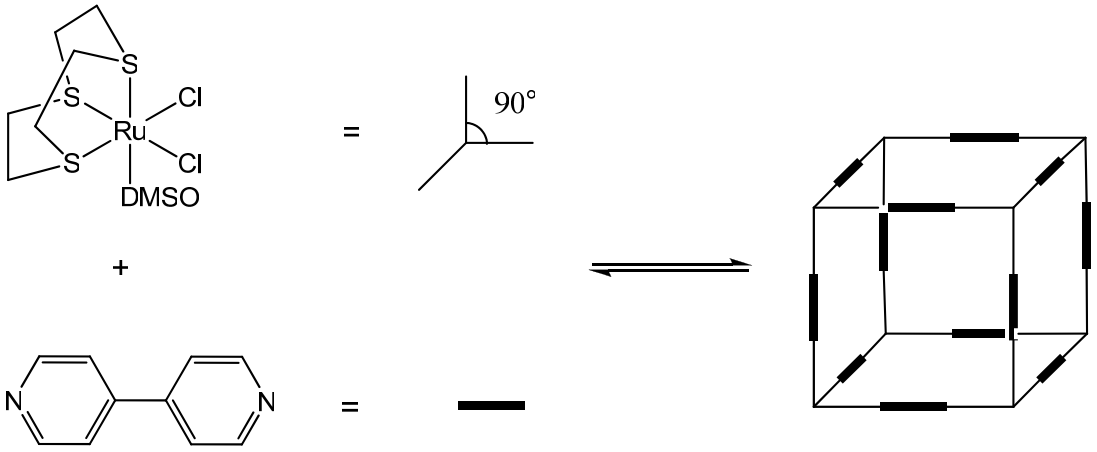

Figure 33. Synthesis of a molecular cube [130]

Three dimensional supramolecular structures can also be obtained from other types of systems than two building block assemblies. Lehn and co-workers produced a cylindrical assembly in 1993, before Fujita's octahedron, from three different types of building blocks, three linear tetradentate, two planar hexadentate ligands and six Cu^+ ions (Figure 34). If building blocks are mixed in the correct stoichiometry (3:2:6) the cylinder is the only product obtained [131].

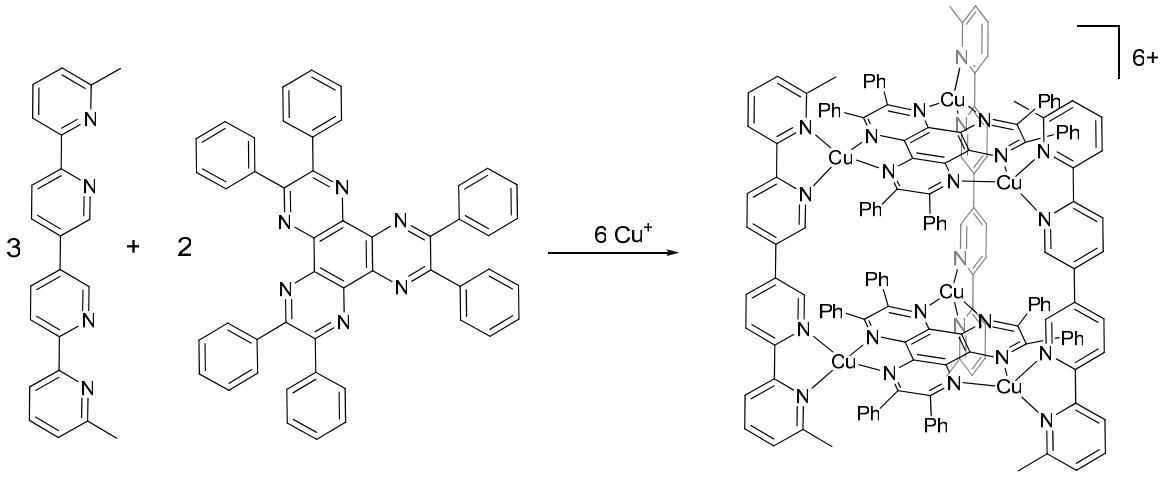

Figure 34. Cylindrical assembly from three different building blocks [131]

Another system that involves three different building blocks is a prismatic assembly by Fujita and co-workers. It is built up by two tpt panels, six Pd corners and three pyrazine bridging ligands (Figure 35). However this prism needs a template to form quantitatively. A template is a molecule that the building blocks can organize themselves around but does not bind to. In the synthesis of the prism in Figure 35 hexamethoxytriphenylene was used, after the prism formed the template could be removed and the cage still remaining stable (Figure 35) [132].

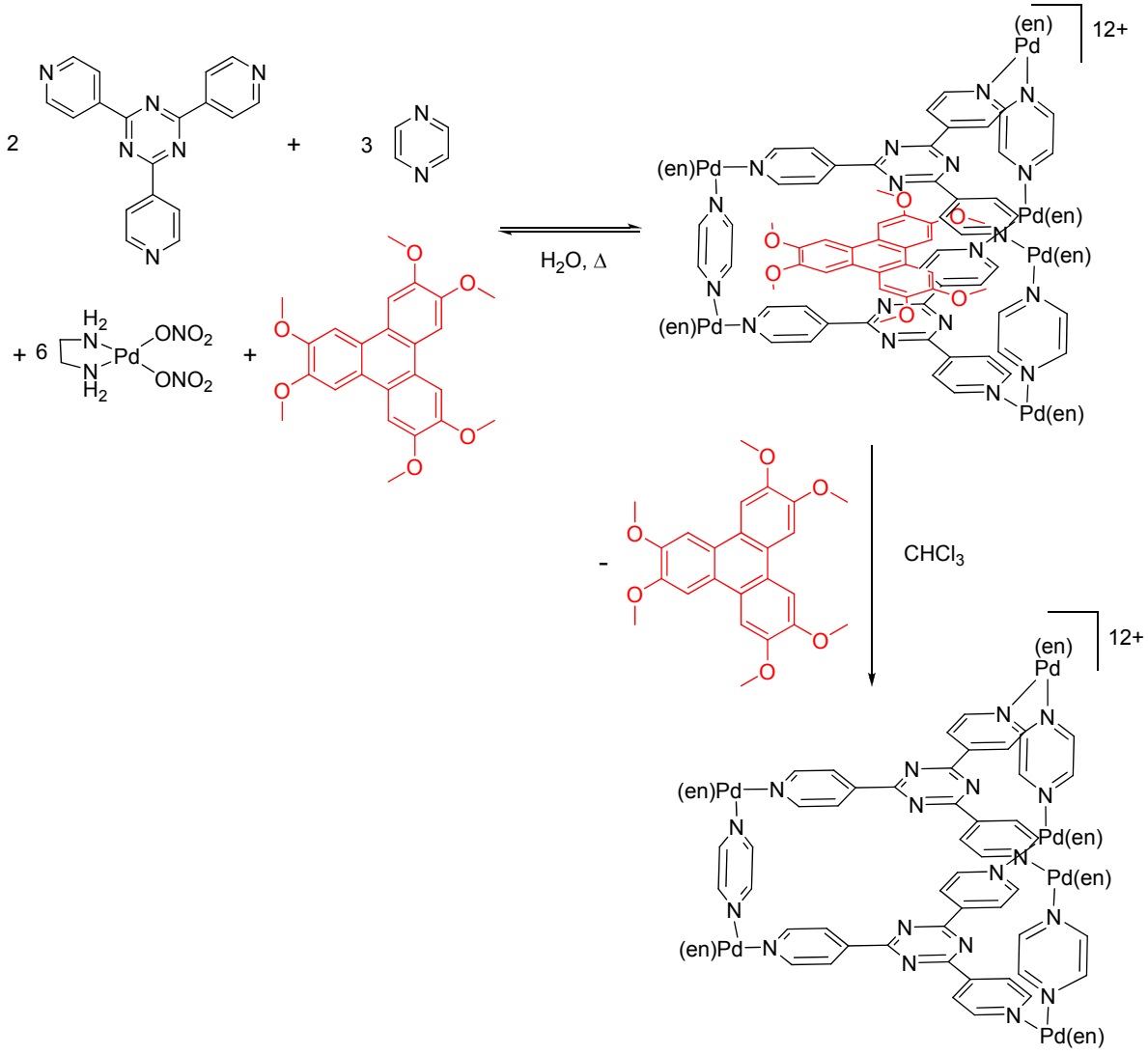

Figure 35. Templated synthesis of a molecular prism [132]

Templates not only help formation of certain assemblies but can also determine the final shape. An example of this is another structure by Fujita and co-workers where they examined the assembly of the tetradentate ligand 3,5-bis(3-pyridyl)-1-(3,5-pyrimidyl)-benzene and Pd corners. The presence of a large guest like dibenzoyl induced an open square pyramidal cone whereas a small guest like CBr_4 templated a closed tetrahedron structure (Figure 36) [133-134].

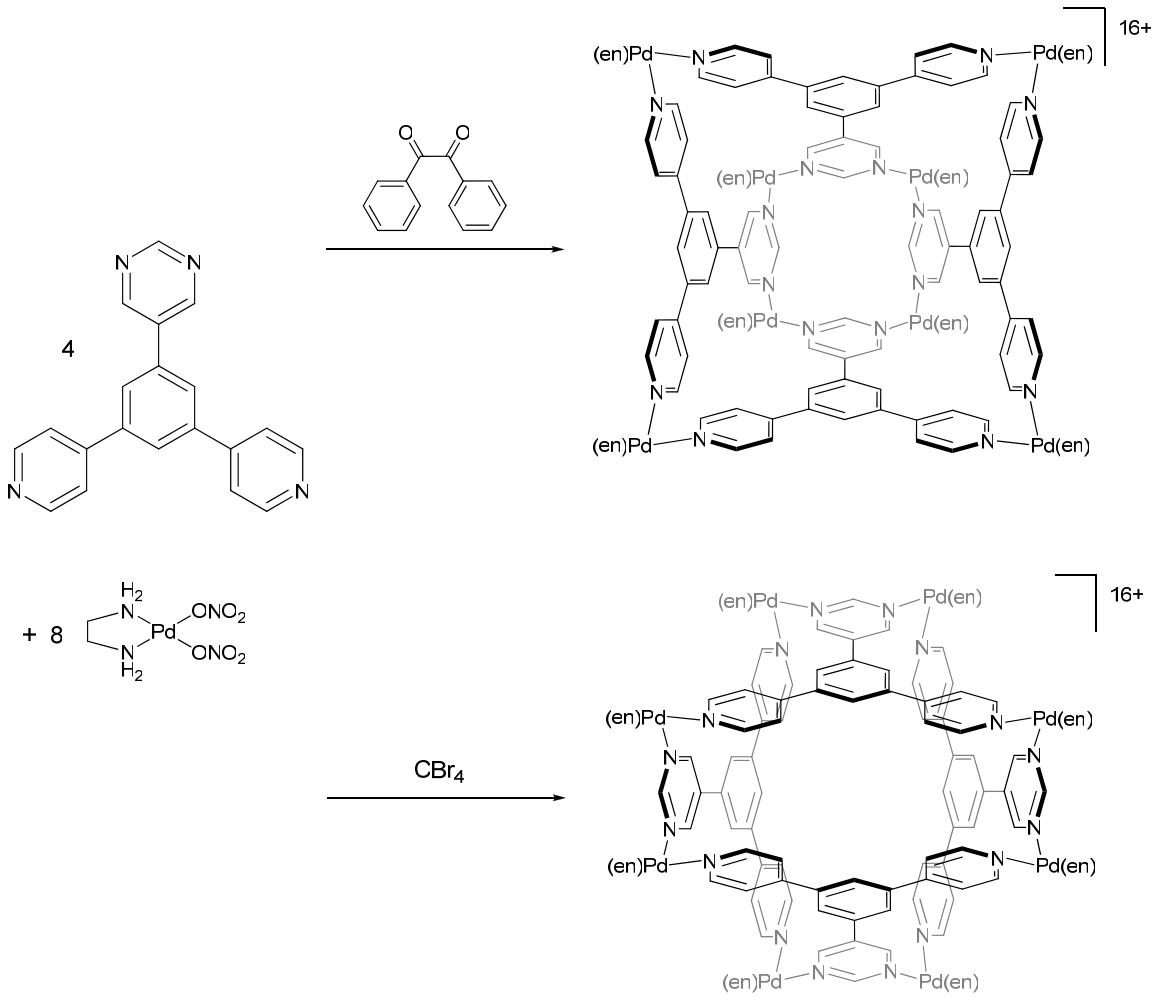

Figure 36. Structures of self-assembly based on template [133-134]

Supramolecular prisms can be obtained without using templates, this was investigated by Stang and co-workers. They managed to synthesize several prisms from the "molecular clip" strategy using both planar [135] and tetrahedral [136] tritopic units (Figure 37).

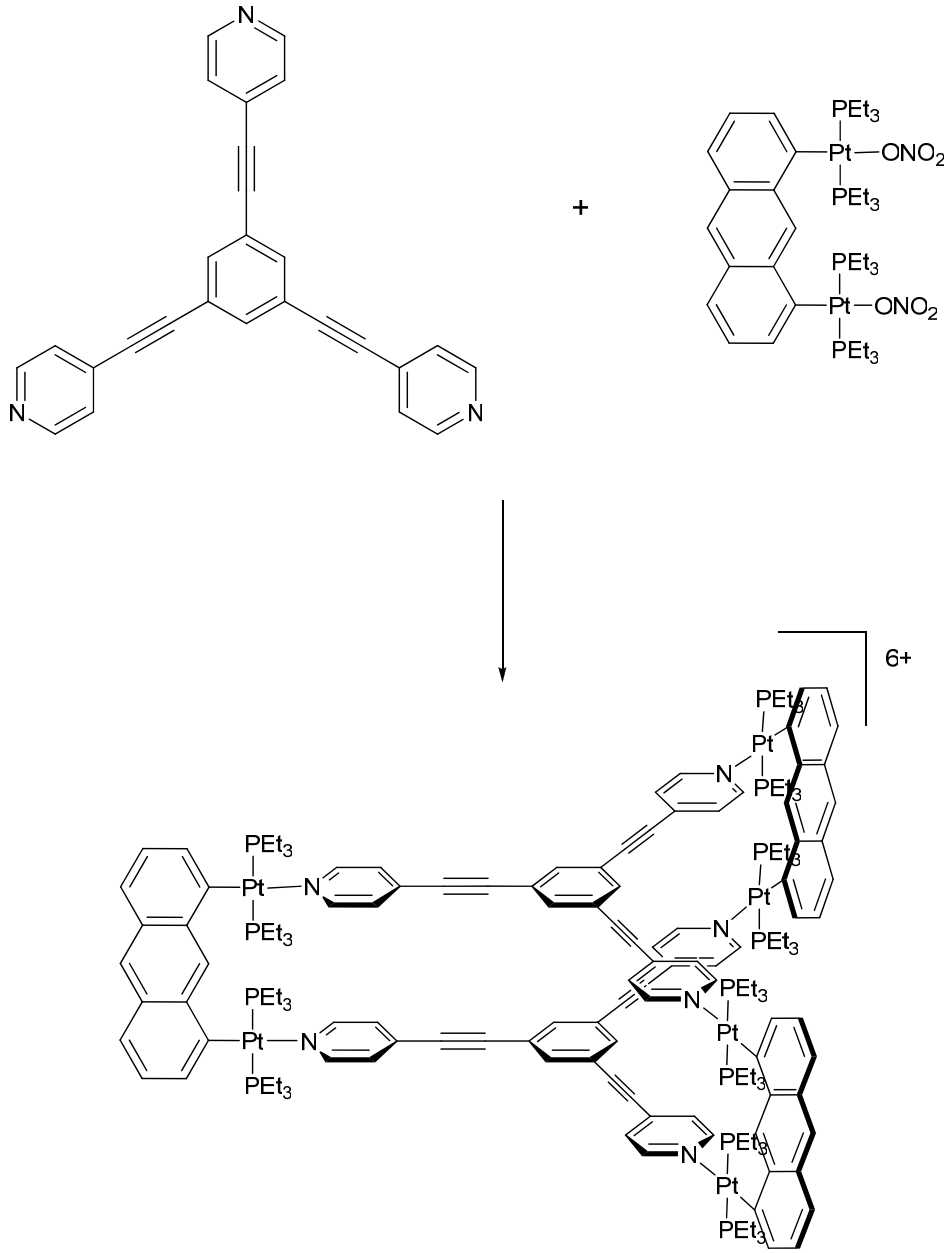

Figure 37. Molecular clip synthesis of a supramolecular prism

Using this strategy we rendered several prismatic structures based on arene ruthenium building blocks. Earlier results have proved that using arene ruthenium bimetallic complexes as molecular clips produces supramolecular rectangles. Having two 90° angular coordination sites the arene ruthenium complexes used as a bimetallic molecular clip could also produce prisms if mixed with tritopic ligands. The first arene ruthenium prisms to be synthesized were the chloro- and oxalato-bridged prisms. The

oxalato-bridged prism is synthesized by the metallic clip strategy (Figure 39), whereas for the chloro-bridged prism there are two possible methods. Either the chloro-bridged arene ruthenium dimer can be reacted with the tritopic panel ligand in water in the presence of silver triflate or the dimer directly reacted with the tritopic ligand which breaks the chloro-bridge forming a trinuclear ruthenium panel, 1 equivalent of silver triflate per ruthenium is then added to remove half of the chlorides which allows for the chloro-bridge to be reformed (Figure 38) [137-138].

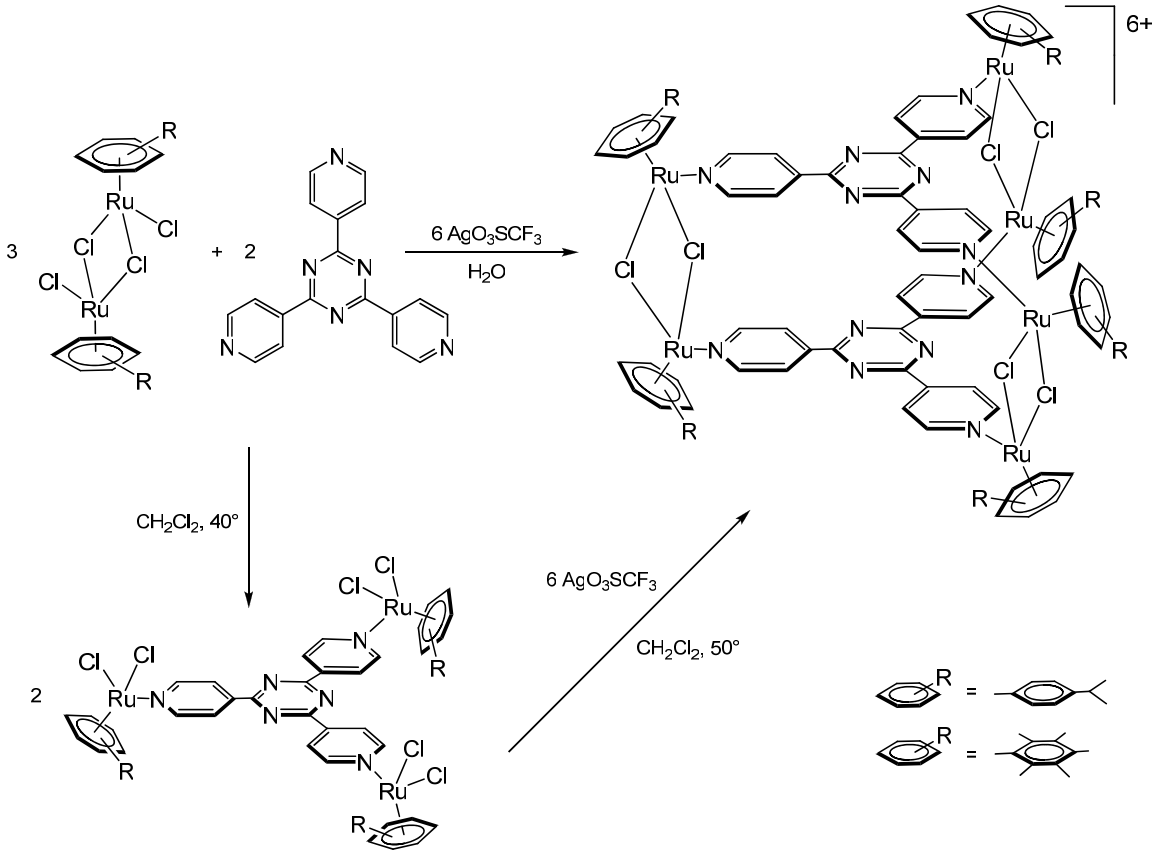

Figure 38. Two possible methods to obtain the chloro-bridged prism [137-138]

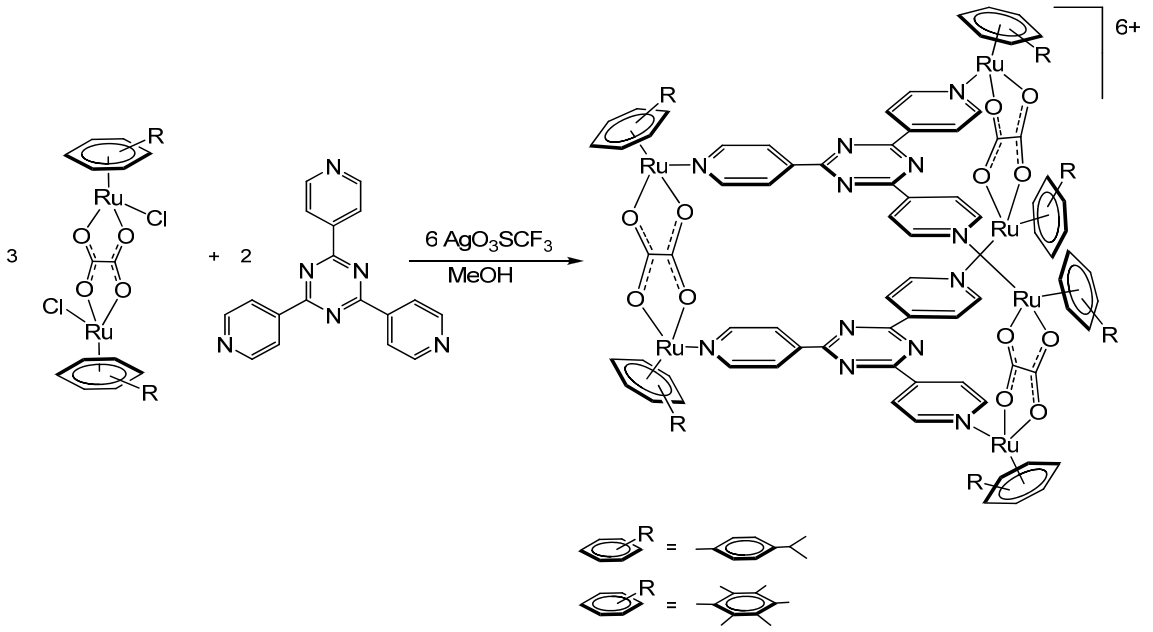

Figure 39. Molecular clip synthesis of oxalato bridged prism [137-138]

Although interesting 3D structures the distance between the two panels was too small to incorporate a guest molecule, a new larger molecular clip was therefore employed. Using dihydroxyquinone as bridging ligands to increase the Ru-Ru distance from 5.5 Å in the oxalato complex to 7.9 Å (Figure 40), introduction of guest molecules was possible.

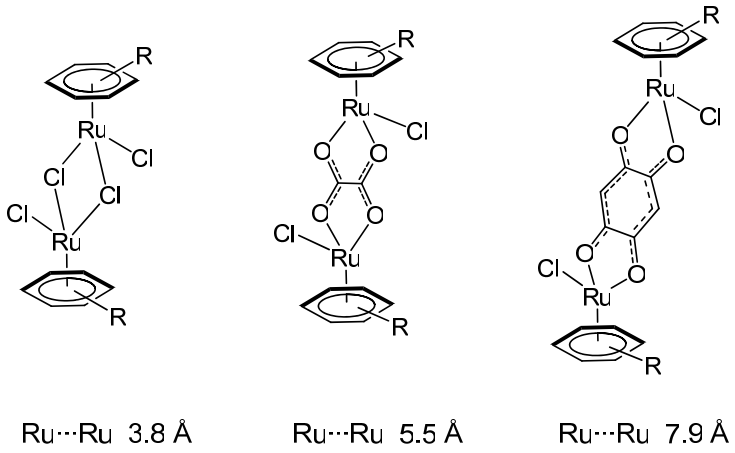

Figure 40. Molecular clips and their Ru–Ru distances

When using large aromatic molecules like hexamethoxytriphenylene as a template for the synthesis of the prism, it was realized that the guest cannot be removed afterwards. Instead a carceplex is produced i.e. the guest is trapped and cannot escape until breaking of the prism (Figure 41) [139]. The prisms are water soluble whereas the cavity is hydrophobic, they also contain arene ruthenium moieties which are biologically active. With this in mind the highly insoluble metal complexes $Pd(acac)_2$ and $Pt(acac)_2$ were encapsulated inside the prism solubilizing them (Figure 42). They were tested for biological activity and while the cage itself is active, the activity is increased in a synergistic fashion for the metal complex containing carceplex, especially the Pd complex. The $M(acac)_2$ complexes are not water soluble which is why their activity is difficult to test, but inside the prism they are hidden and like a Trojan horse the prism transport these complexes into the cell where they can be released [119].

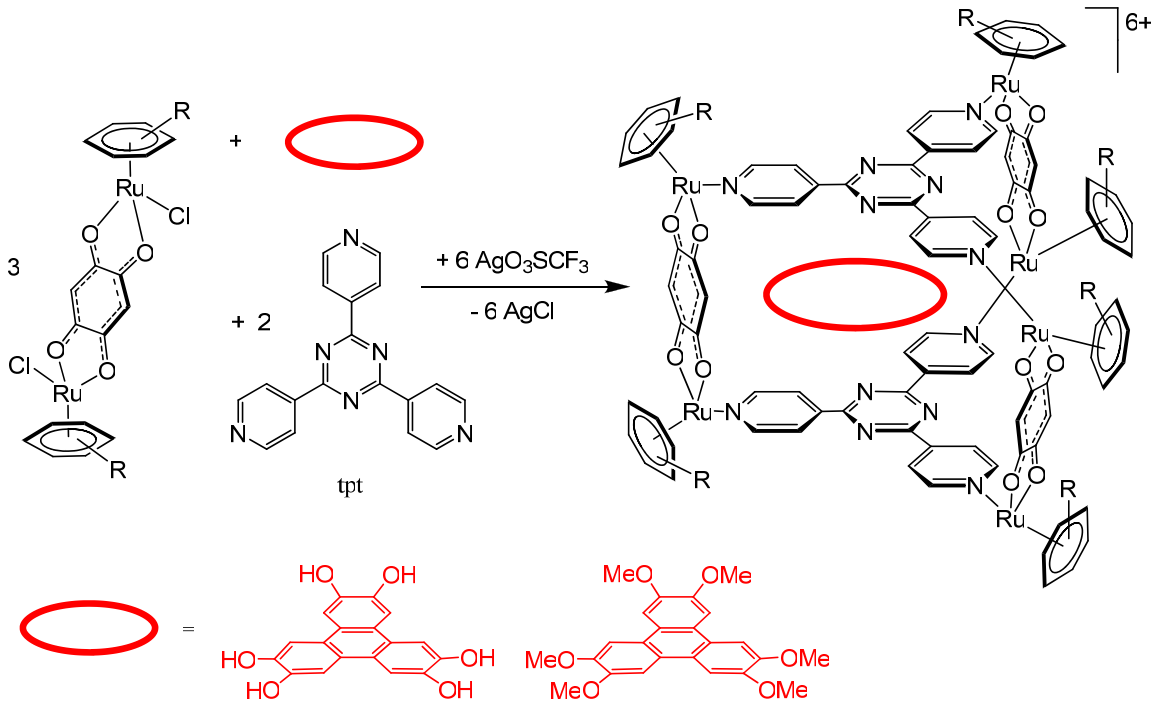

Figure 41. Synthesis of prismatic carceplexes [139]

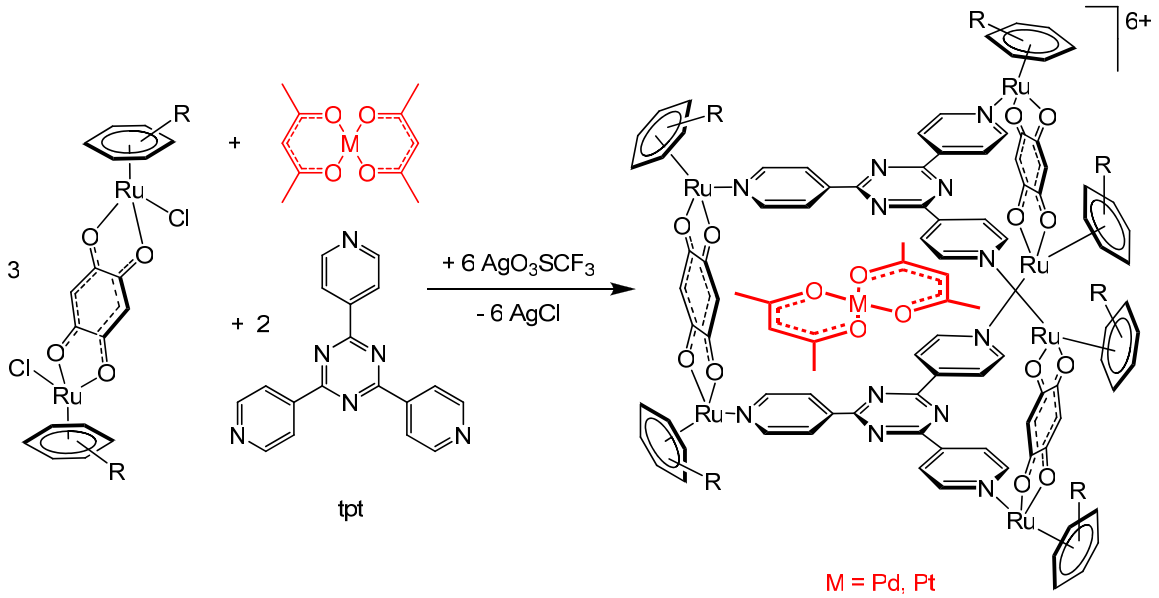

Figure 42. Synthesis of carceplex, $M(acac)_2$ incorporated into prism [119]

5.2 Supramolecular prisms with aromatic guests

With earlier studies in mind we wanted to further investigate the carceplex properties of this type of prism with different sized planar aromatic guests. The biological activity is also a very interesting subject and by testing aromatic systems varying their substituents, we can compare the effect on the activity, this work is presented in this chapter.

5.2.1 Synthesis

These types of prisms are synthesized by an analogous method to the rectangles. The bimetallic clips **7**-**10** are first reacted with silver triflate to produce the methanolate species, this then reacts with the tritopic panel tpt in methanol at room temperature overnight (Scheme 10). The prisms **23**-**26** are isolated in good yields as their triflate salts. They are soluble in most polar organic solvents and water.

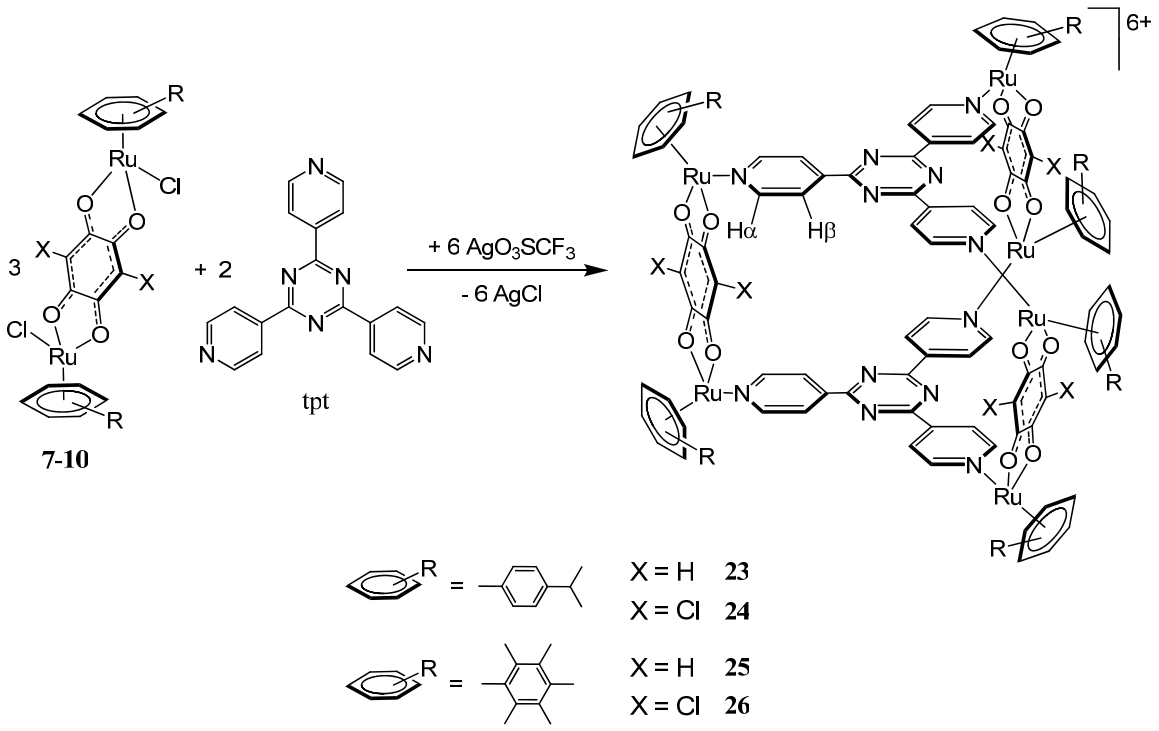

Scheme 10. Synthesis of supramolecular prisms **23-26**

Synthesis of the respective carceplexes follows the same procedure except that the bimetallic clip is added to tpt in methanol in the presence of the aromatic guest (pyrene, fluoranthene, benzo[*e*]pyrene, triphenylene and coronene) (Scheme 11), this reaction does not affect the yield or the solubility of the prism, moreover no traces of empty prism were observed.

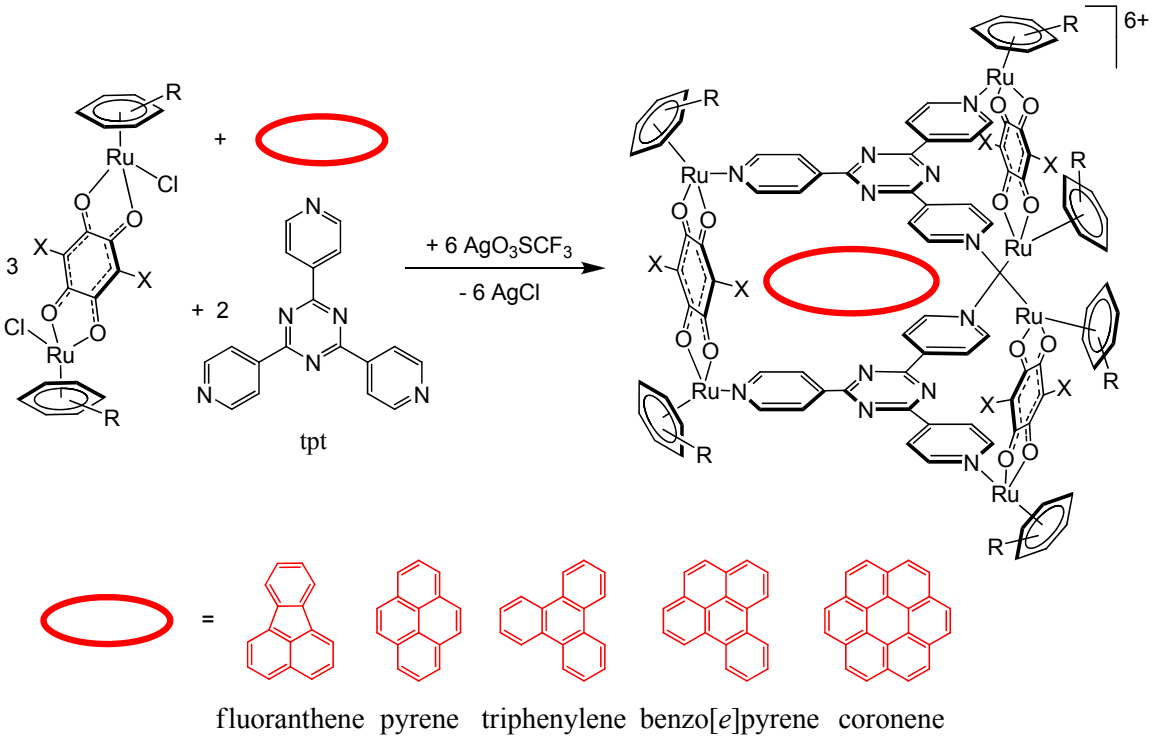

Scheme 11. Synthesis of carceplexes [guest⊂**23-26**]$^{6+}$

5.2.2 Studies by NMR spectroscopy

The preference of cage **23** for different aromatic molecules has also been studied. If a 1:1:1 mixture of coronene, triphenylene and pyrene is initially added, before the formation of cage **23**, only coronene is found encapsulated by the cage, [coronene⊂**23**][O_3SCF_3]$_6$ being exclusively isolated after workup. Similarly, just triphenylene is encapsulated if a 1:1 mixture of triphenylene and pyrene is used. Therefore, it is clear that cage **23** prefers aromatic molecules in the order coronene > triphenylene > pyrene. The formation of these inclusion systems can easily be monitored by ^{1}H NMR spectroscopy. As expected, the ^{1}H NMR spectrum of **23** shows a well organized structure with a quite simple set of signals. However, unlike the empty cage **23**, where the H_α and H_β of the pyridyl groups are found at expected positions (8.77 and 8.71 ppm in acetone-d_6) as compared to the uncoordinated tpt unit, upon encapsulation of

an aromatic molecule, the H_α and H_β signals are strongly shifted upfield (see Figure 43). Moreover, the protons (H_q) of the dhbq bridging ligands are shifted downfield, while the signals of the aromatic protons (H_{ar}) of the *p*-cymene ligand remain almost unchanged upon insertion of an aromatic molecule. Similarly, the protons of the methyl and isopropyl groups of the *p*-cymene ligand are not chemically affected by the presence of the large aromatic guest within the cavity of **23**.

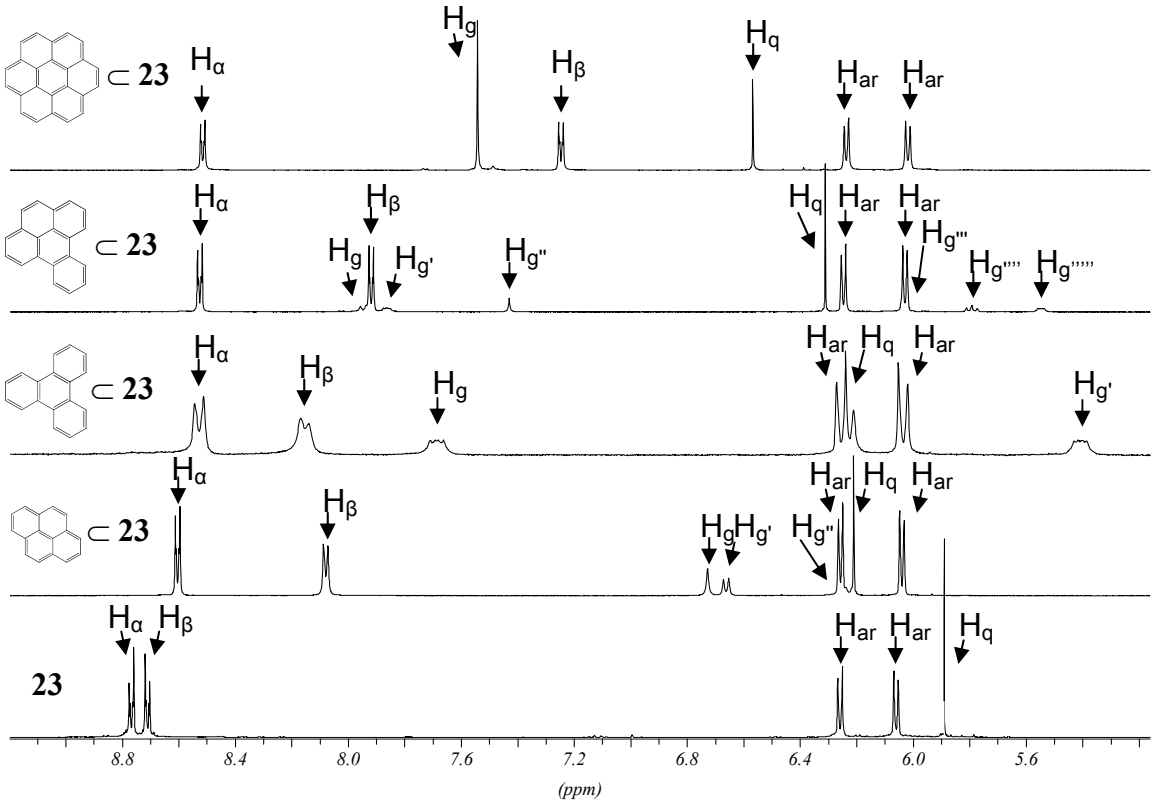

Figure 43. Aromatic region of ^{1}H NMR spectrum of **23**, pyrene⊂**23**, triphenylene⊂**23**, benzo[*e*]pyrene⊂**23** and coronene⊂**23**

For comparison, triphenylene as well as fluoranthene were encapsulated in the different cages **23**-**26**. The carceplex properties of the four cages are all the same, and the encapsulation of triphenylene by **23**-**26** is clearly demonstrated by ^{1}H NMR spectroscopy (see Figure 44). The two signals associated with the protons of the encapsulated triphenylene molecule (H_g and $H_{g'}$) are well separated and shifted upfield due to the special environment provided by the hydrophobic cavity of the cages. Indeed, H_g is shifted by 1.2 ppm, while $H_{g'}$ is shifted by as much as 3.6 ppm, suggesting a strong

interaction between triphenylene and the components of the cage, especially the tpt units. Similarly, the protons (H_g) of encapsulated fluoranthene molecules in cages **23**-**26** are strongly shifted upfield as compared to free fluoranthene (see Figure 45).

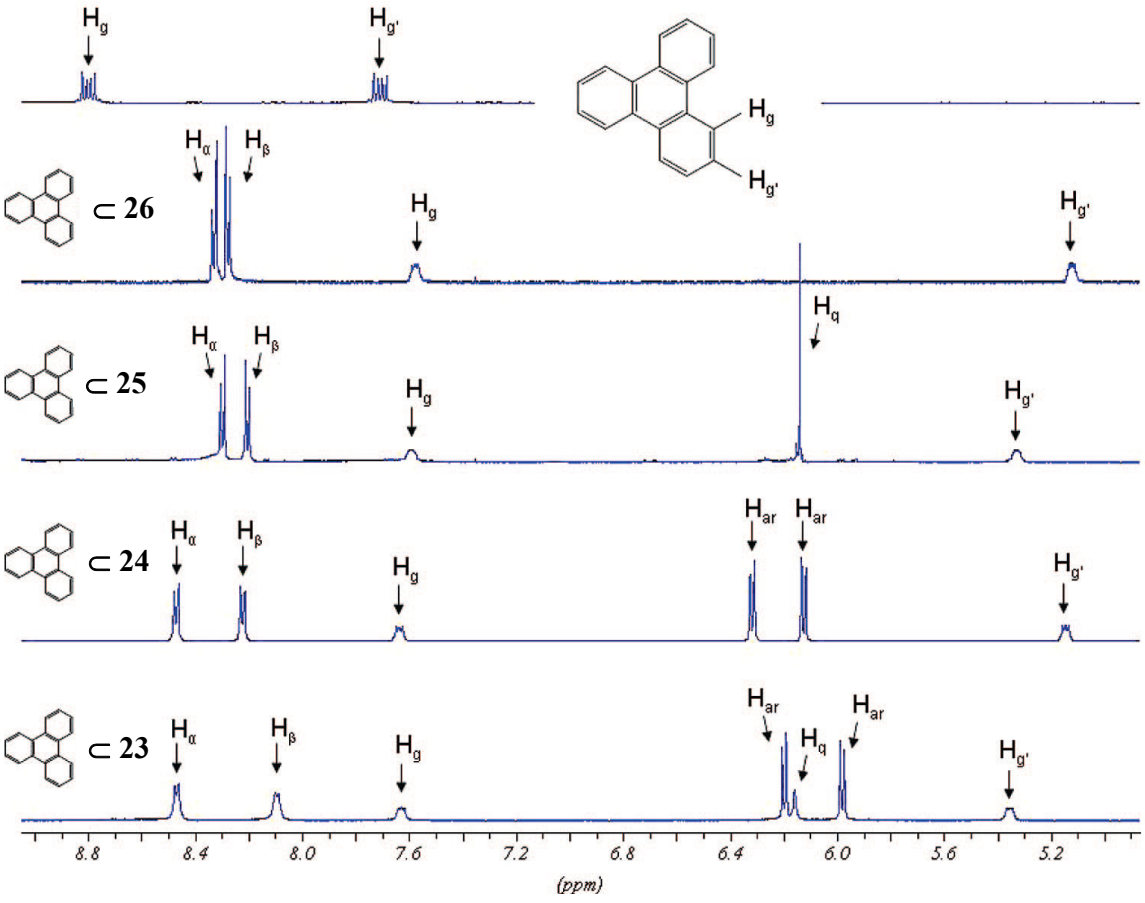

Figure 44. Aromatic region of the ^{1}H NMR spectrum of triphenylene⊂**23**-**26** and free triphenylene

Interestingly, in the pyrene⊂**23**, fluoranthene⊂**23**, and benzo[*e*]pyrene⊂**23** systems, in which the cage symmetry (D_{3h}) does not match the encapsulated molecule symmetry (D_{2h}), only the minimal numbers of signals are observed for **23**, even at low temperature (-50 °C). This suggests that in solution an unrestricted rotation of the large aromatic molecule within the hydrophobic cavity of **23** takes place. One-dimensional ROESY ^{1}H NMR experiments confirm the spatial proximity of the different components of the empty cages **23**-**26**. Indeed, in **23**, a strong interaction between the proton (H_q) of

the dihydroxybenzoquinone and the H_α of the tpt units is observed. Moreover, but only for the filled cage triphenylene⊂**23**, intense cross-peaks are observed between the protons of the encapsulated molecule (H_g and $H_{g'}$) and the protons of the different connecting components of the cage molecule (H_q, H_α, and H_β) (see Figure 46).

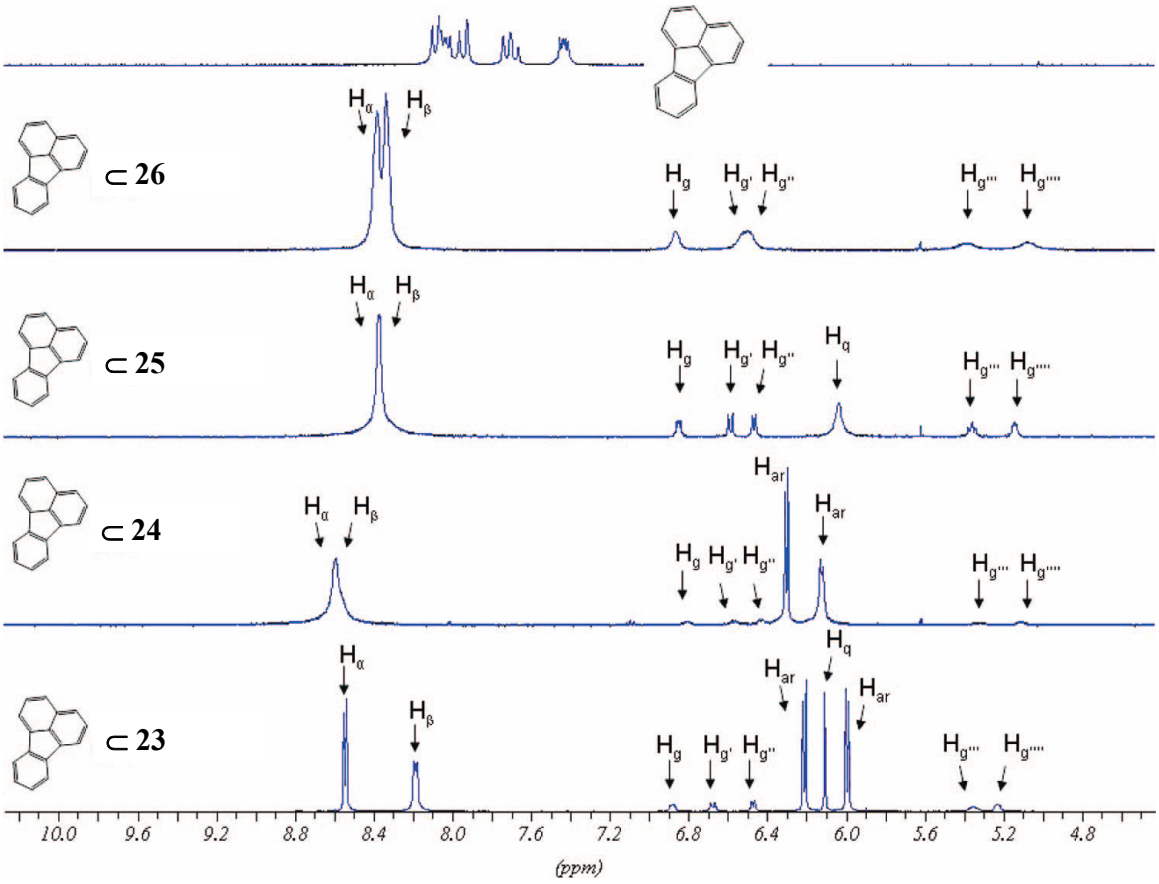

Figure 45. Aromatic region of the ^{1}H NMR spectrum of fluoranthene⊂**23**-**26** and free fluoranthene

This strong interaction between the encapsulated molecule and the cationic cage **23** suggests an eclipsed conformation of the tpt-triphenylene-tpt π-stacking arrangement. This is in agreement with the conformation observed in $[C_{18}H_6(OMe)_6\subset\mathbf{23}]^{6+}$ [139] and in the prismatic cage $[Pt_6(NH_2CH_2CH_2NH_2)_6(tpt)_2(C_4H_4N_2)_3]^{12+}$ encapsulating also a hexamethoxytriphenylene molecule [132]. However, the other systems show no cross-

peaks between the protons of the aromatic molecule and the protons of the components of **23**, as expected for rotationally unrestricted encapsulated molecules.

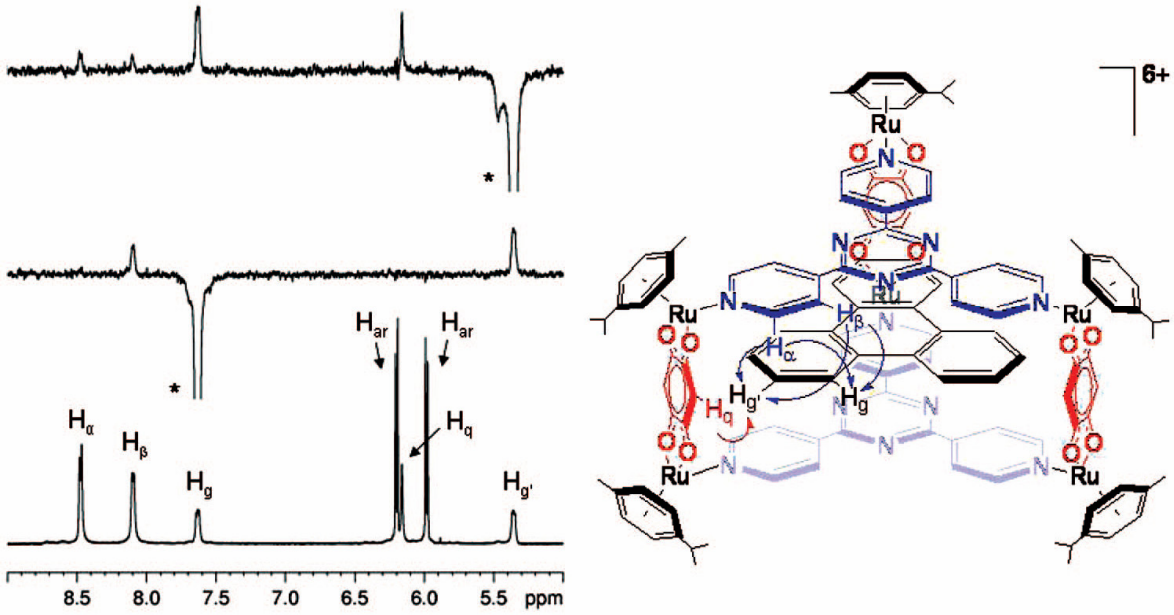

Figure 46. 1-D ROESY spectrum (400 MHz, acetone-d_6) and schematic representation of the corresponding cross-peaks observed in the system triphenylene⊂**23**

5.2.3 Analysis by mass spectroscopy

The stability of cage **23** is remarkable, and the encapsulation of the large aromatic molecule is definitive, even under mass spectrometry conditions. The ESI-MS spectra of triphenylene⊂**23**, benzo[*e*]pyrene⊂**23**, and coronene⊂**23** show peaks corresponding to [aromatic⊂**23** + $(O_3SCF_3)_4]^{2+}$ at *m*/*z* 1637.6, 1649.6, and 1673.6, respectively. These peaks have been assigned unambiguously on the basis of their characteristic Ru_6 isotope pattern. Furthermore, in the ESI-MS spectra of pyrene⊂**23**, triphenylene⊂**23**, benzo[*e*]pyrene⊂**23**, and coronene⊂**23**, major peaks corresponding to [**23**+$(O_3SCF_3)_4]^{2+}$ at *m*/*z*1523.6,[{$(\eta^6$-*p*-^{i}PrC_6H_4Me$)_4Ru_4$(tpt)$_2(C_6H_2O_4)_2$}+ $(O_3SCF_3)_2]^{2+}$ at *m*/*z* 1070.1, and [**23** +$(O_3SCF_3)_3]^{3+}$ at *m*/*z* 966.1 are observed as well.

5.2.4 X-Ray crystallography

Single crystals of [pyrene⊂**23**][O_3SCF_3]$_6$ and [benzo[*e*]pyrene⊂**23**][O_3SCF_3]$_6$ suitable for X-ray structure analysis were obtained by the slow diffusion of benzene in an acetone solution of the salts. The two molecular structures show parallel π-stacking interactions between the aromatic rings of the tpt subunits and the large aromatic molecule (see Figures 47, 48).

The single-crystal X-ray structure analyses of [pyrene⊂**23**][O_3SCF_3]$_6$ and [benzo[e]pyrene⊂**23**][O_3SCF_3]$_6$ reveal an average Ru-Ru separation of 7.93 Å for the 2,5-dihydroxy-1,4-benzoquinonato-bridged units and an average Ru-Ru separation of 13.2 Å in the plane of the tpt units: The volume of these hexanuclear metalla-prisms being on the order of 700 Å^3. It is clear from the van der Waals representations of the carceplex systems pyrene⊂**23** and benzo[*e*]pyrene⊂**23** that the pyrene and benzo[*e*]pyrene are permanently encapsulated in **23** (Figure 49).

The interplanar separation observed between the aromatic moieties (~3.42 Å) is shorter than the theoretical value calculated for this stacking mode [140], but comparable to the 3.46 Å separation observed between the triazine rings of two independent tpt units in the crystal packing of [$Ir_3(C_5Me_5)_3$(tpt){$S_2C_2(B_{10}H_{10})$}$_3$] [141]. The pyrene and benzo[*e*]pyrene molecules are slightly disordered within the cavity of **23**, thus supporting the observation that these aromatic molecules are rotationally unrestricted in solution. In the crystal packing of [pyrene⊂**23**][O_3SCF_3]$_6$ and [benzo[*e*]pyrene⊂**23**][O_3SCF_3]$_6$, no π-stacking interacting systems are observed between independent molecules.

The empty spaces left between the cationic hexanuclear cations are filled with O_3SCF_3 anions. In order to examine the stability of cage **23** in solution, we recorded the ^{1}H NMR spectra in various deuterated solvents (D_2O, CD_2Cl_2, CD_3CN, $(CD_3)_2CO$, $(CD_3)_2SO$) with different coordinating ability. At room temperature and even elevated temperature, ^{1}H NMR experiments for **23** in D_2O, CD_2Cl_2, CD_3CN, and $(CD_3)_2CO$ showed no signal changes, indicating the destruction of the cage or the presence of free

tpt units. However, in deuterated DMSO, cage **23** shows additional signals attributed to species generated by coordination of $(CD_3)_2SO$ ligands in line with decomplexation of the different building blocks.

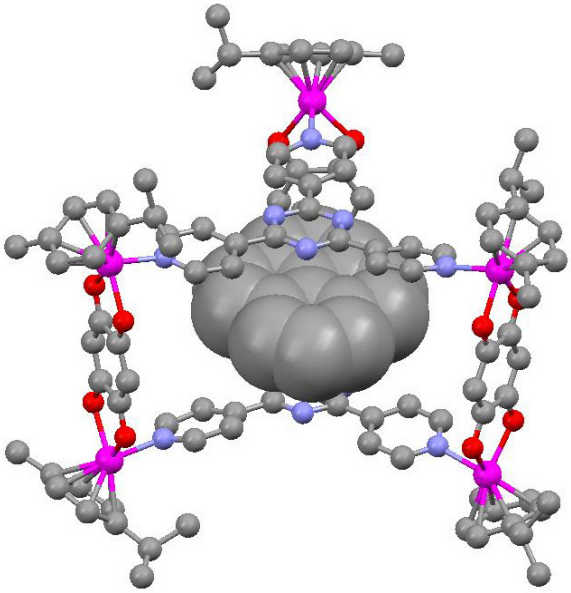

Figure 47. Mixed representation of pyrene⊂**23** (pyrene as space-filling model). Hydrogen atoms and O_3SCF_3 anions omitted for clarity

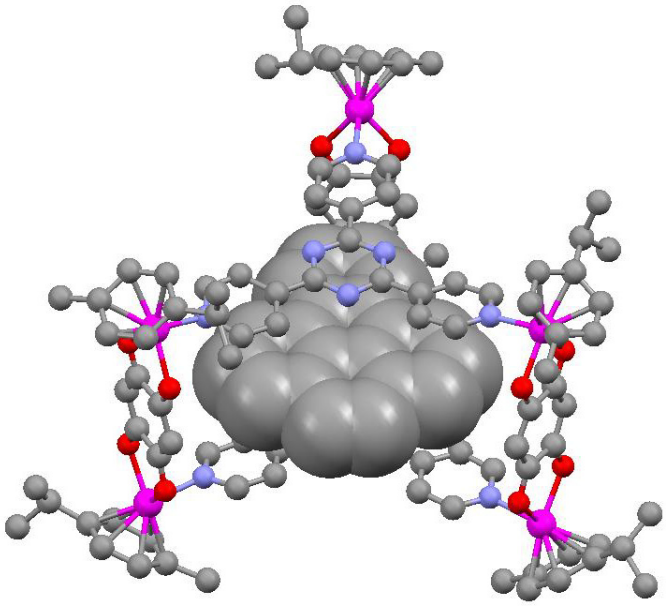

Figure 48. Mixed representation of benzo[*e*]pyrene⊂**23** (benzoepyrene as space-filling model). Hydrogen atoms and O_3SCF_3 anions omitted for clarity

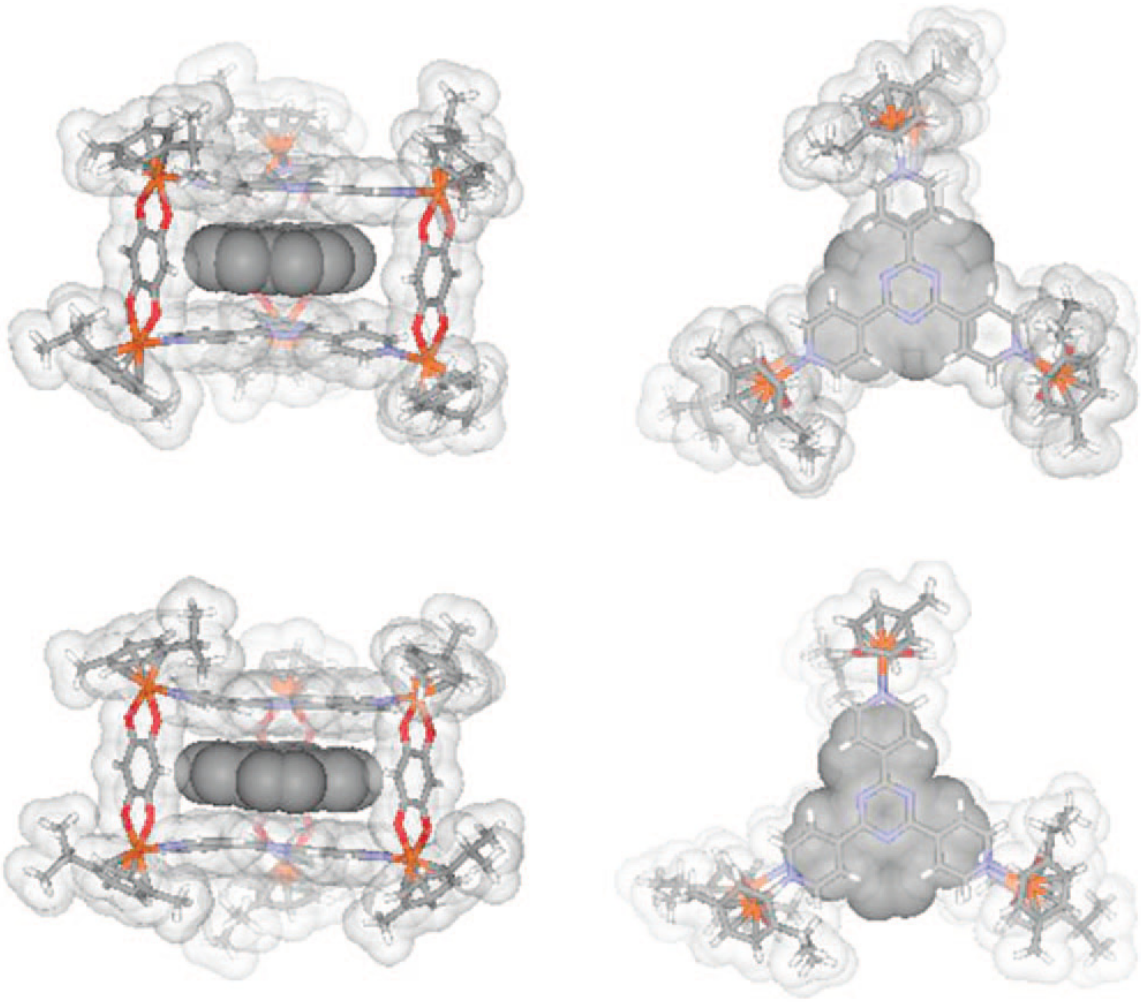

Figure 49. Top and side view representations of pyrene⊂**23** (top) and benzo[*e*]pyrene⊂**23** (bottom). Anions and hydrogen atoms of the aromatic molecules are omitted for clarity

5.3 Encapsulation of functionalized pyrenes

To investigate the effect on the prism and also to potentially increase the biological activity of these systems a number of functionalized pyrenes has been encapsulated. They possess one or two arms hanging out of the carceplex. The dangling

arm has an active group at the end on which reactions may be performed. Some of these pyrenes are commercially available and some have been synthesized.

Pyrenes are known to be biologically active and especially as DNA intercalators. They are as well fluorescent which helps binding studies in cells. A recent study showed that adding a charge and DNA binding substituent on a pyrene renders them biologically active, as well a compound with 2+ charges was more selective towards certain cancer cell lines than compounds of only 1+ [142]. Incorporating pyrenes into prismatic cages can therefore be used to deliver these hydrophobic DNA intercalating compounds into cells.

The pyrene derivatives were only encapsulated in prism **23** due to its solubility, easy accessibility as starting material and for easy monitoring of encapsulation.

5.3.1 Synthesis of pyrenes with bioactive functional groups

Two functionalized pyrenes were obtained from the reaction of 1-pyrenemethylamine and the corresponding acid chloride of ethacrynic acid and aspirin, respectively, which in turn are prepared *in situ* from oxalyl chloride according to a literature method (Scheme 12) [143].

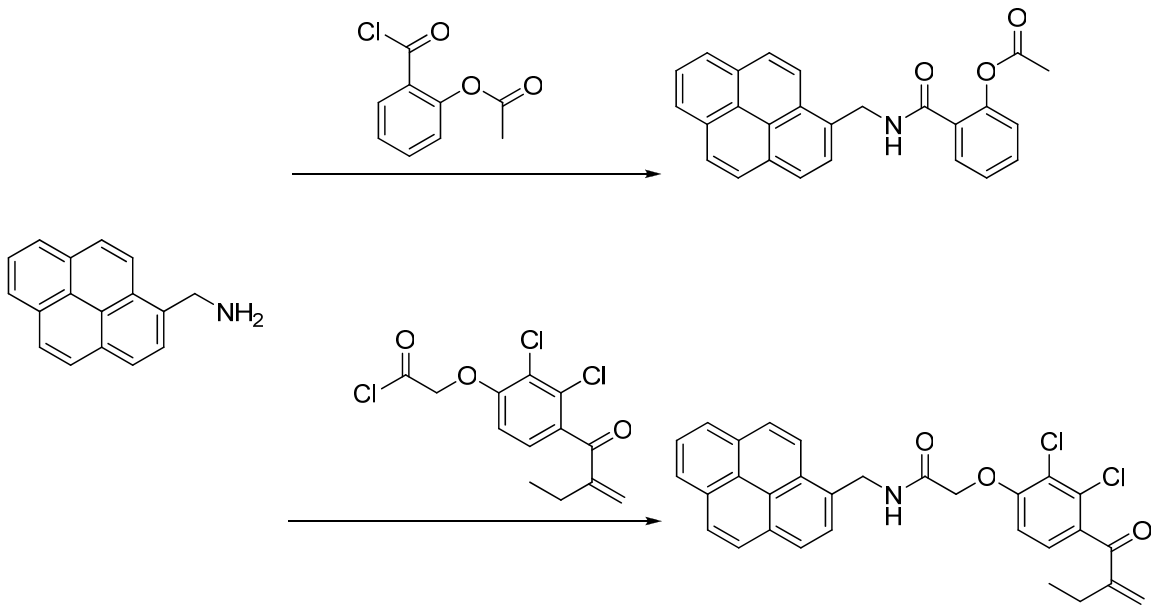

Scheme 12. Synthesis of functionalized pyrene derivatives with aspirin (top) and ethacrynic acid (bottom)

Moreover, a series of commercially available functionalized pyrenyl compounds, i.e. **a** = 1-pyrenebutyric acid, **b** = 1-pyrenebutanol, **c** = 1-pyrenemethylamine, **d** = 1-pyrenemethylbutanoate, **e** = 1-(4,6-dichloro-1,3,5-triazin-2-yl)pyrene, **f** = *N*-hexadecylpyrene-1-sulfonamide) and the two previously prepared (**g** = pyrenyl ethacrynic amide, **h** = 2-(pyren-1-ylmethylcarbamoyl) phenyl acetate), were encapsulated in the metalla-prism **23**.

The synthesis of the prismatic carceplexes with a dangling arm follows the same procedure as for the encapsulation of aromatic guests. Molecular clip **7** is first reacted with silver triflate in methanol which is then added to a mixture of tpt and the guest (**a**-**h**) in methanol (Scheme 13). The carceplexes [**a**-**h**⊂**23**][O_3SCF_3]$_6$ are obtained as red solids in good yields and are soluble in most polar organic solvents and water.

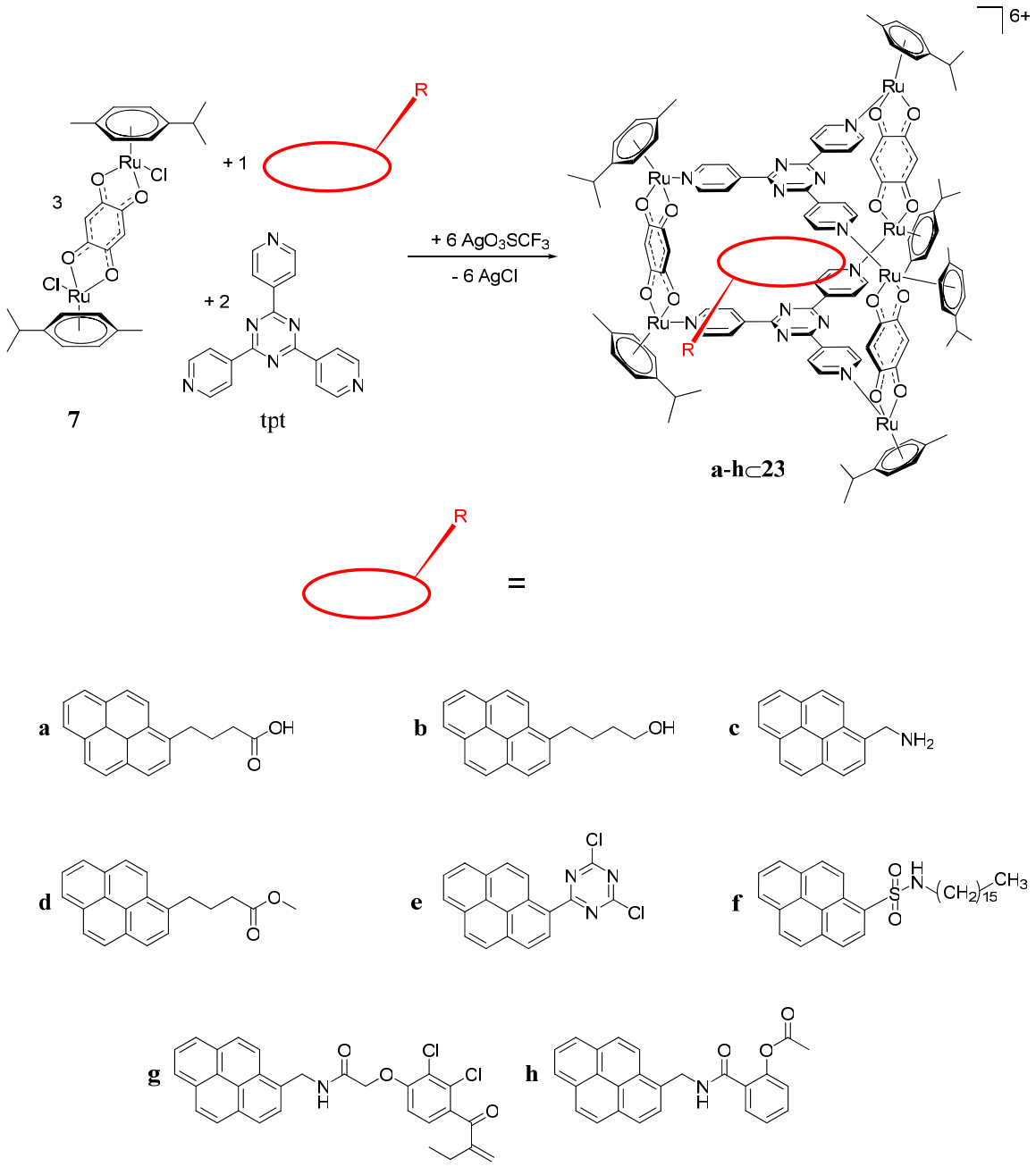

Scheme 13. Synthesis of dangling arm carceplexes

A two armed pyrene, 1,8-bis(3-methyl-butyn-1-yl-3-ol)pyrene, was synthesized from a two step synthesis starting with an iodization of pyrene followed by a Sonogashira coupling reaction (Scheme 14). The two isomers were separated after coupling by chromatography [144], thus affording the major product, 1,8-bis(3-methyl-butyn-1-yl-3-

ol)pyrene, in good yield. This bi-functionalized pyrene derivative was encapsulated following the same procedure (Scheme 15).

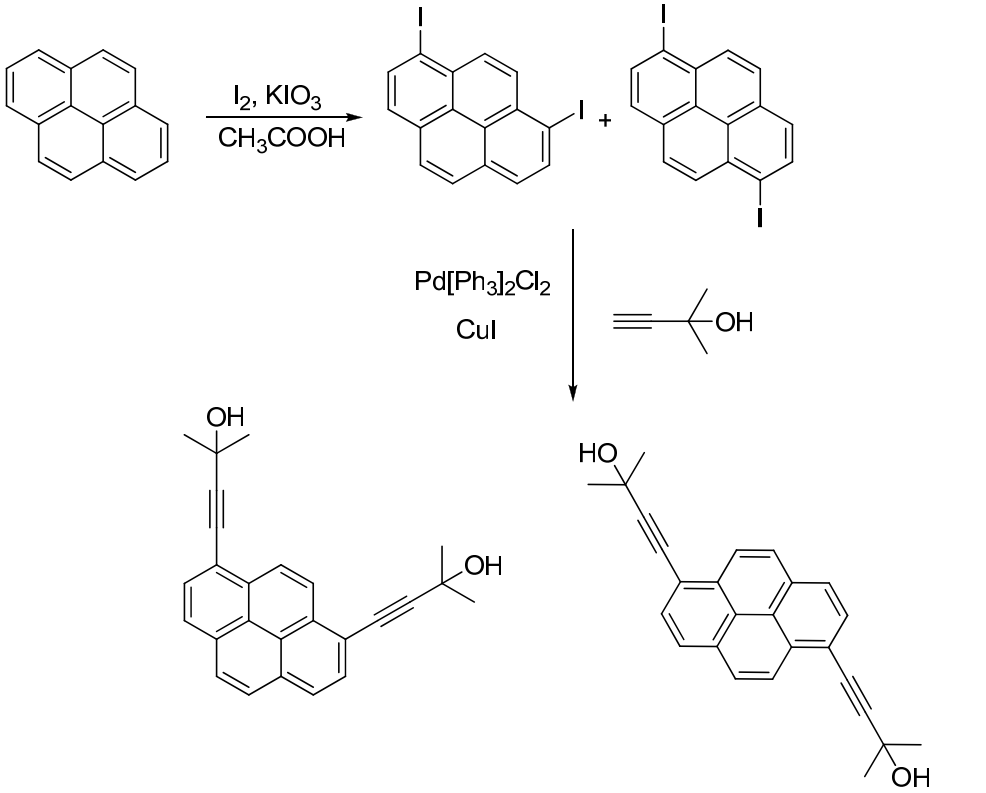

Scheme 14. Synthesis of two armed pyrene (**i**)

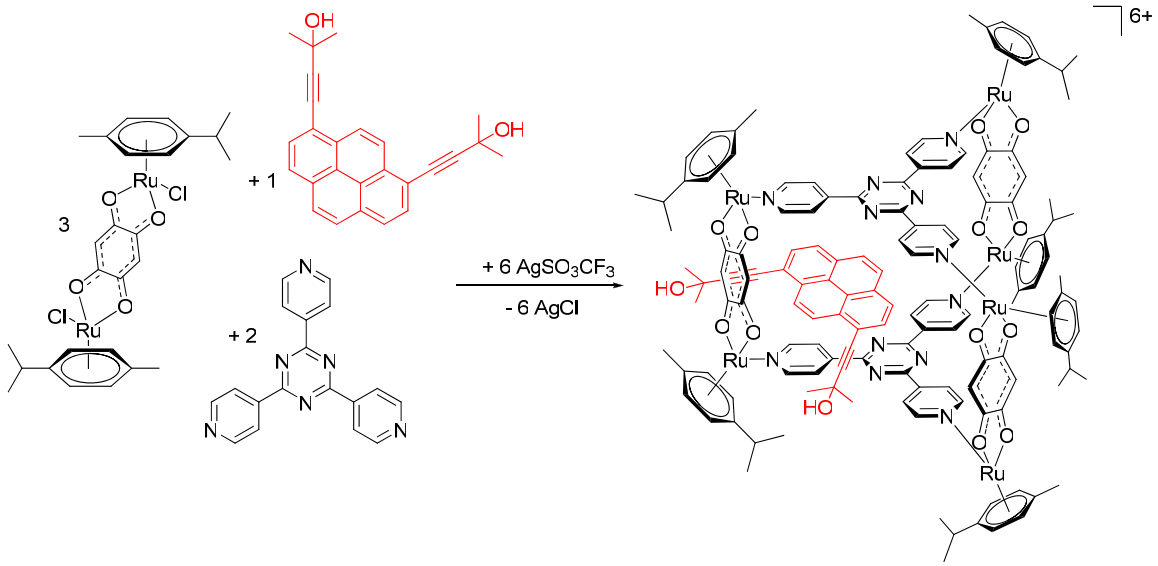

Scheme 15. Synthesis of carceplex with two armed guest **i⊂23**

5.3.2 Characterization by NMR spectroscopy

Encapsulation of pyrene-R (**a**-**h**) in **23** can be confirmed by ^{1}H NMR spectroscopy. In acetone-d_6 a doublet corresponding to the H_β protons of the tpt panels appear at 8.71 ppm in the empty cage **23**, this signal both broadens and shifts upfield by ca. 0.6 ppm upon encapsulation of the functionalized pyrenyl derivative. As the pyrene is no longer symmetric and free rotation is blocked by the dangling arm, the pyrenyl moiety gives rise to nine individual signals, all shifted upfield, which is as expected since the pyrenyl derivative is sandwiched between two tpt panels and involved in a π-stacking arrangement (Figure 50).

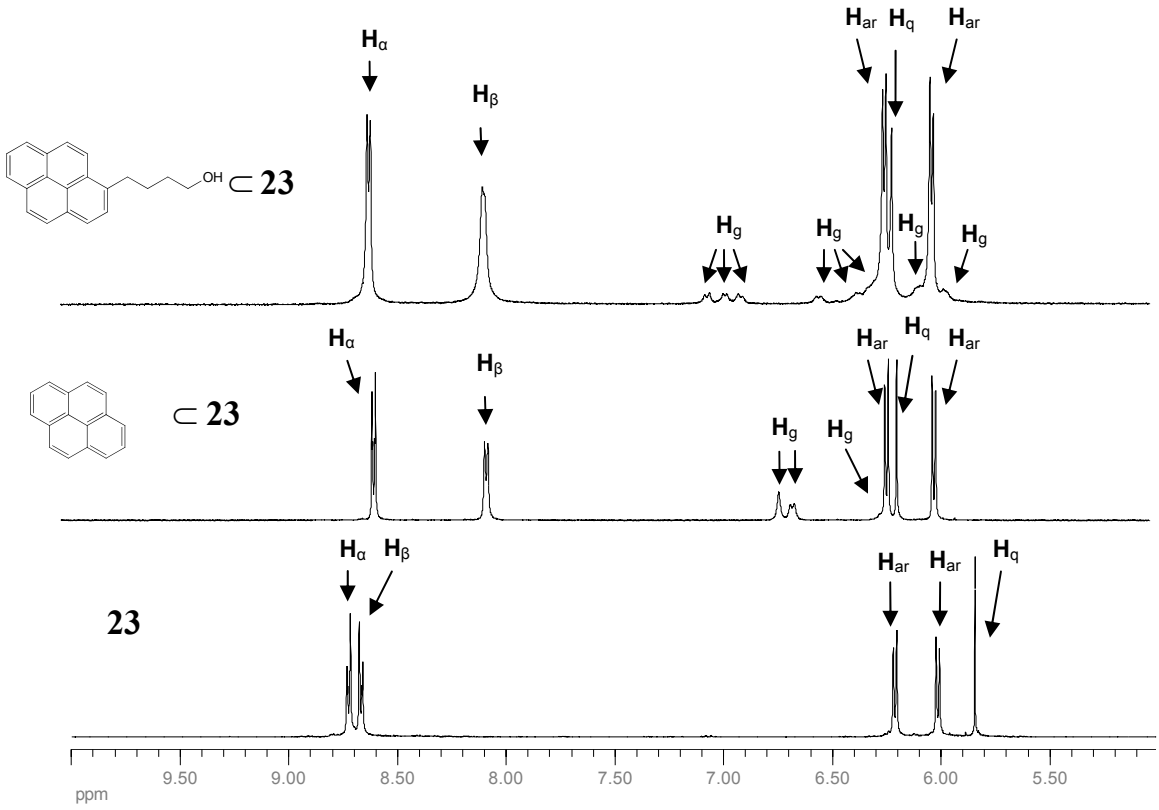

Figure 50. Aromatic region of ^{1}H NMR spectrum in acetone-d_6 of **23**, pyrene⊂**23** and **b**⊂**23**

In contrast, the signals of the dhbq protons are shifted downfield in all systems and by as much as 0.4 ppm in the case of **a**⊂**23**. In general, the signals of the adjacent

methylene group of the pyrenyl side-chain are shifted downfield, whereas the rest of the signals associated to the side-chain remain virtually unchanged.

To further confirm the encapsulation of the functionalized pyrenyl derivatives in the cavity of **23**, a series of diffusion-ordered (DOSY) NMR spectra were recorded. DOSY is a powerful tool for studying host-guest associations in solution [145-149]. The diffusion coefficient depends on the shape and size of the molecules. Therefore, in a carceplex system in which the guest is perfectly trapped in the cavity of the host, without significantly affecting the size and shape of the host, the diffusion coefficient of the guest⊂host adduct should be almost identical to the diffusion coefficient of the host alone. DOSY measurements of pyrenyl derivative **g**, the empty cage **23**, and the inclusion system [**g**⊂**23**][O_3SCF_3]$_6$, are presented in Figure 51.

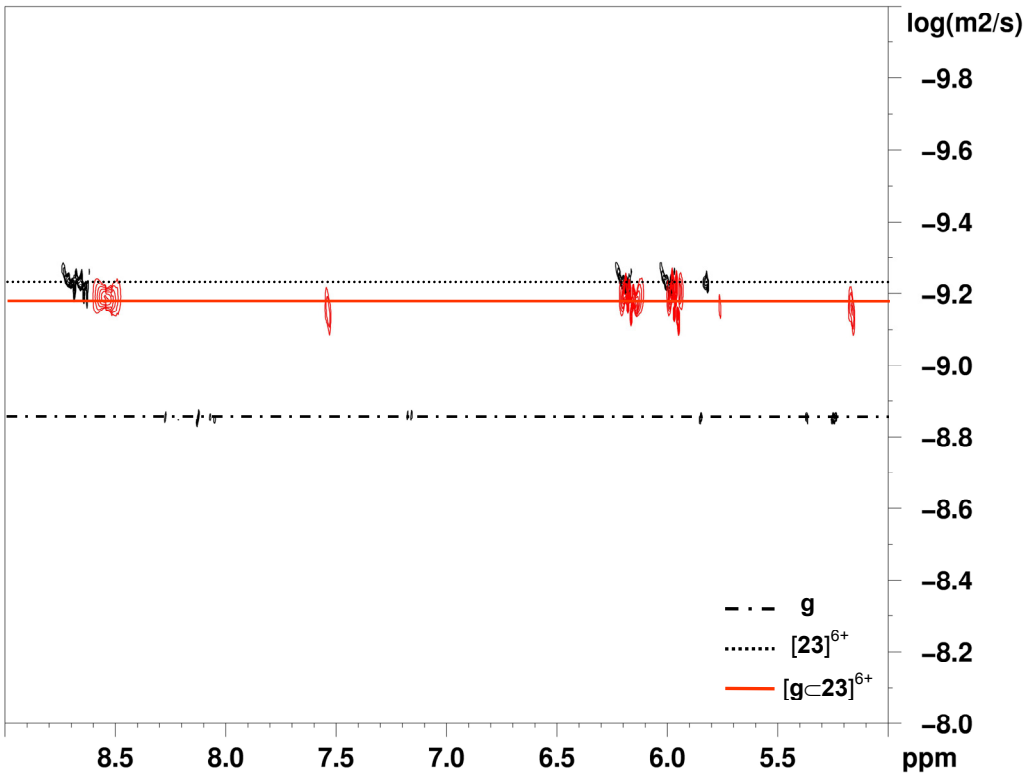

Figure 51. DOSY NMR spectra of **g**, **23** and **g**⊂**23** in acetone-d_6

These experiments show that in **g⊂23**, both components possess the same diffusion coefficient, which is almost identical to the diffusion coefficient of the empty cage **23**, thus confirming the encapsulation of **g** in **23**.

For the carceplex **i⊂23** the structure is confirmed by ^{1}H NMR in which the characteristic broadening and shift of the H protons of the tpt panels is observed. For **i⊂23**, however, two independent signals are now observed for the dhbq protons, which is in accordance with the symmetry and the deshielding effect produced by the proximity of the alkynyl bonds on four dhbq protons (6.38 ppm), with the other two dhbq protons appearing at 6.21 ppm.

5.3.3 Characterization by mass spectroscopy

The carceplex systems are remarkably stable and can be characterized by ESI-MS with loss of only 2, 3 or 4 counter ions. The characterization by ESI-MS was done in collaboration with Yoshihisa Sei and Kentaro Yamaguchi at Tokushima Bunri University (Japan). ESI-MS of all the carceplex systems corroborates their proposed structures, see Figure 52 for selected examples. The ESI mass spectra of [**a**-**g**⊂**23**][O_3SCF_3]$_6$ and **i⊂23** show peaks corresponding to the cationic carceplex system with loss of 2, 3 or 4 triflate counter ions. In the case of **h⊂23** the acetyl group of the aspirin moiety is cleaved. These peaks were assigned unambiguously on the basis of their characteristic isotope patterns.

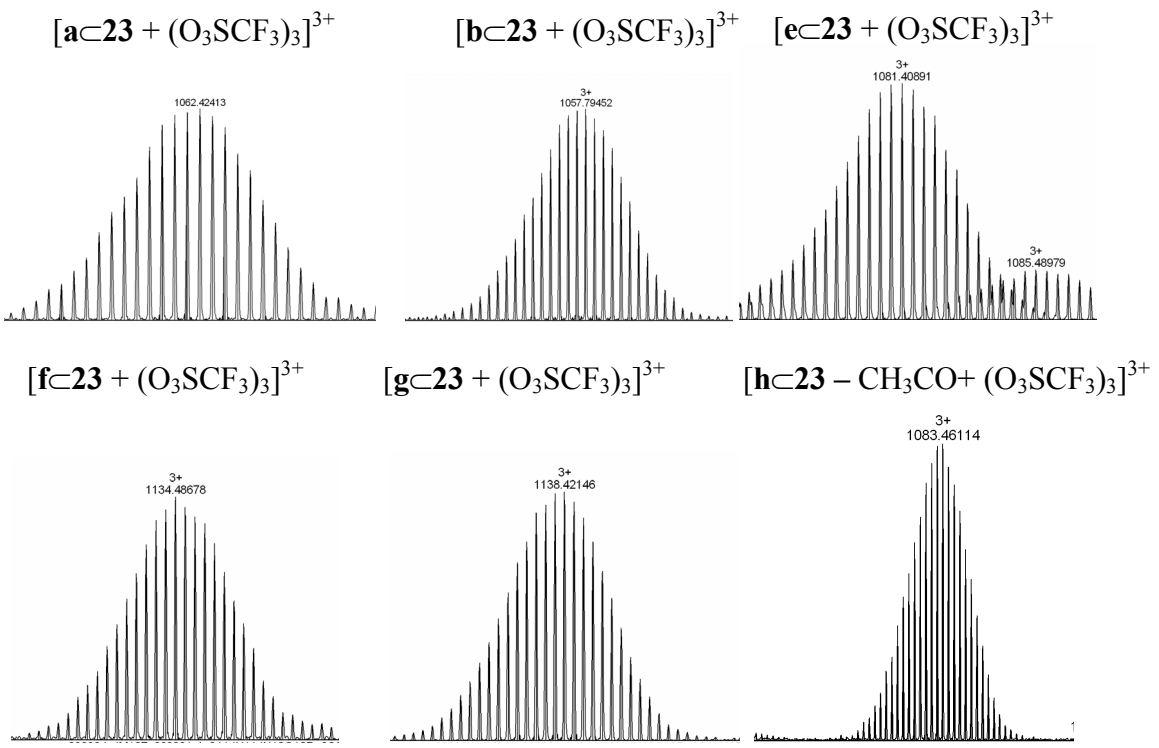

Figure 52. ESI-MS spectrum of selected carceplexes

5.4 Biological activity

5.4.1 Evaluation of cytotoxicity

The biological activity was tested in collaboration with Prof. Paul Dyson and co-workers at the EPFL (Switzerland). The anti-proliferative activity of **23** and all the inclusion systems [**a-i⊂23**][O_3SCF_3]$_6$ was evaluated against the human ovarian A2780 cancer cell line using the MTT assay which measures mitochondrial dehydrogenase activity as an indication of cell viability. The IC_{50} values are listed in Table 5 and are reported together with that of cisplatin for comparison purposes.

As mentioned before, there is considerable on-going interest in the anti-cancer properties of arene ruthenium complexes [150-153]. It should be noted that some pyrenyl derivatives have recently been shown to interact with various DNA and RNA polynucleotides and have been tentatively proposed to have potential applications in the treatment of certain types of tumors [142]. However, pyrene containing compounds are usually used as a probe in cells due to their favorable fluorescence properties [154]. Here, however, due to the encapsulation of the pyrene moiety into the water soluble metalla-prism the cytotoxic effect of even very hydrophobic derivatives was assessed.

Table 5. IC_{50} values measured on A2780 human ovarian cancer cell line

Complex	IC_{50} (μM)	Complex	IC_{50} (μM)
23	23 ± 2	**e⊂23**	6 ± 1.5
pyrene⊂**23**	9 ± 2	**f⊂23**	2 ± 0.6
a⊂23	18 ± 1.5	**g⊂23**	3 ± 1.1
b⊂23	21 ± 2	**h⊂23**	5 ± 0.4
c⊂23	14 ± 2	**i⊂23**	5 ± 0.8
d⊂23	17 ± 1	cisplatin	1.6 ± 0.6

The empty cage, **23**, exhibits a moderate cytotoxicity of 23 μM which is comparable to that of related molecular arene ruthenium and arene osmium cages carrying relatively high charges [119, 125, 155-156]. It should be noted that highly charged complexes cross cell membranes equally well as neutral complexes, and in some case, their ability of entering cells is superior to that of neutral compounds or compounds in a low charge state [157-159].

Encapsulation of the pyrenyl systems into the hexaruthenium cage has either a negligible effect on the cytotoxicity (pyrenes **a** to **d**) or significantly increases the cytotoxicity (pyrenes **e** to **i**), with **f⊂23** and **g⊂23** being an order of magnitude more cytotoxic than the empty cage **23**. Indeed, the cytotoxicity of **f⊂23** and **g⊂23** is comparable to cisplatin. These differences could be due to the intrinsic cytotoxicities of the different pyrenyl derivatives, which due to the poor water solubility of these

compounds could not be evaluated, or to differences in the uptake and/or further intracellular release of these molecules. Nevertheless, the greater activity of the inclusion compounds suggests a synergistic effect between the cage and its cargo.

The substituent tethered to the pyrenyl ring in **f⊂23**, the most active compound of the series, contains a group that is not too dissimilar from an extensive range of sulfonamide-containing inhibitors of carbonic anhydrase [160]. Carbonic anhydrases are potential targets for anti-cancer drugs [161] and therefore it is conceivable that the high cytotoxicity of **f⊂23** corresponds, at least in part, to the inhibition of this enzyme class.

The substituent tethered to the pyrenyl ring in **g⊂23**, which is also a very cytotoxic compound, is ethacrynic acid, which is an excellent inhibitor of glutathione transferase and has even been investigated as a potential anti-cancer drug [162]. Indeed, arene ruthenium compounds with tethered ethacrynic acid moieties are also good glutathione transferase inhibitors and are moderately cytotoxic [163].

The crystal structure of an arene ruthenium compounds containing ethacrynic acid embedded in the active site of the human glutathione transferase P1-1 has been reported [143]. Glutathione transferase catalyzes the nucleophilic attack by reduced glutathione (GSH) on non-polar nucleophiles, acting on a range of exogenous compounds including anti-cancer agents, forming part of a coordinated defense strategy to remove GSH conjugates from the cell [164].

Consequently, inhibition of this enzyme means that an anti-cancer drug can function more effectively and it is possible that **g⊂23** exerts its cytotoxicity by the ethacrynic acid derivative inhibiting glutathione transferase within the cell resulting in a sensitized cell that is more responsive to the empty cage, **23**. Indeed, a similar increase in cytotoxicity, of ca. one order of magnitude, was observed for the arene ruthenium compound and its ethacrynic acid derivative reported previously [163].

5.4.2 Uptake studies with fluorescence spectroscopy

The pyrene-R compound **e** (1-(4,6-dichloro-1,3,5-triazin-2-yl)pyrene) was encapsulated because it can be used as a fluorescent probe (Figure 53). Experiments proved that **e** as expected had no measurable cytotoxicity at concentrations of 20 μM due to low solubility but when encapsulated in the prism **23** the carceplex has a higher cytotoxicity than the prismatic cage on its own.

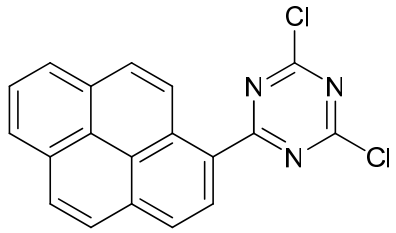

1-(4,6-dichloro-1,3,5-triazin-2-yl)pyrene, **e**

Figure 53. Fluorescent pyrene-R, **e**

Based on these results, we studied the uptake of pyrene-R (**e**) and pyrene-R⊂**23**, taking advantage of the natural fluorescence of pyrene-R. Interestingly, as shown in Figure 54 the pyrene-R inside the cage does not show fluorescence at pH 2 or pH 7, but at pH 12 it exhibits the typical fluorescence of pyrene-R alone.

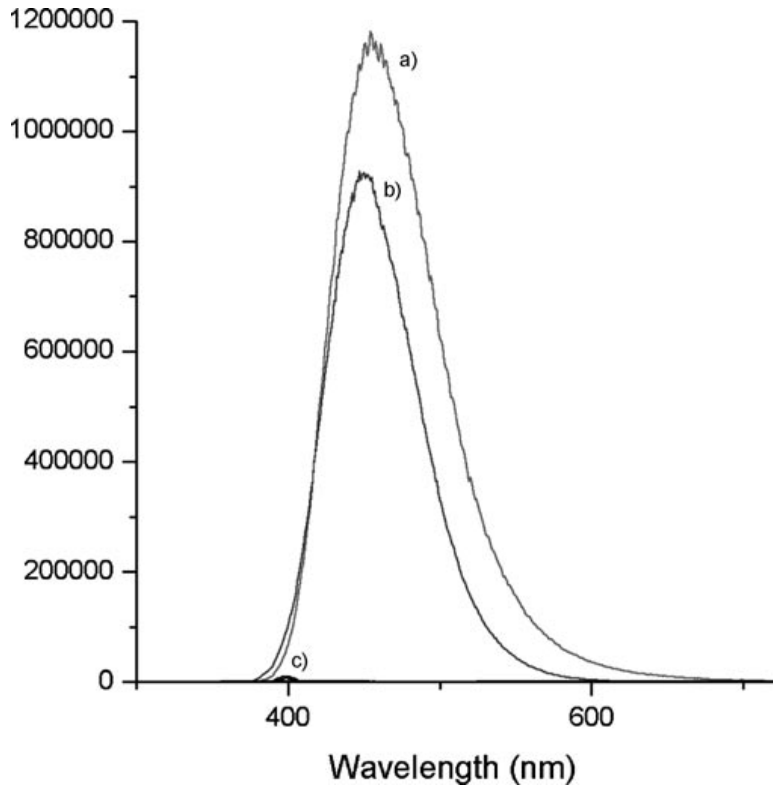

Figure 54. Fluorescence spectra of **e** and **e⊂23** at various pH, from 2 to 12. a) Fluorescence spectrum of **e** at pH 12; b) fluorescence spectrum of **e⊂23** at pH 12; c) fluorescence spectra of **e⊂23** at pH 2 and 7 which do not show significant fluorescence

The cage compound **23** does not show any fluorescence when excited at 350 nm (data not shown). This would suggest that once trapped inside the cage the fluorescence of the pyrene-R guest molecule is quenched and upon destruction of the cage complex at pH 12, the fluorescence due to free pyrene-R is regained.

Consequently, the free pyrene-R was tracked by fluorescence microscopy following incubation with A2780 cells (Figure 55). An increase of fluorescence is observed inside the cells following treatment with pyrene-R⊂**23**, whereas treatment with pyrene-R at the same concentration only shows a modest effect. It is also noteworthy that for pyrene-R⊂**23** accumulation in cytoplasmic organelles is observed.

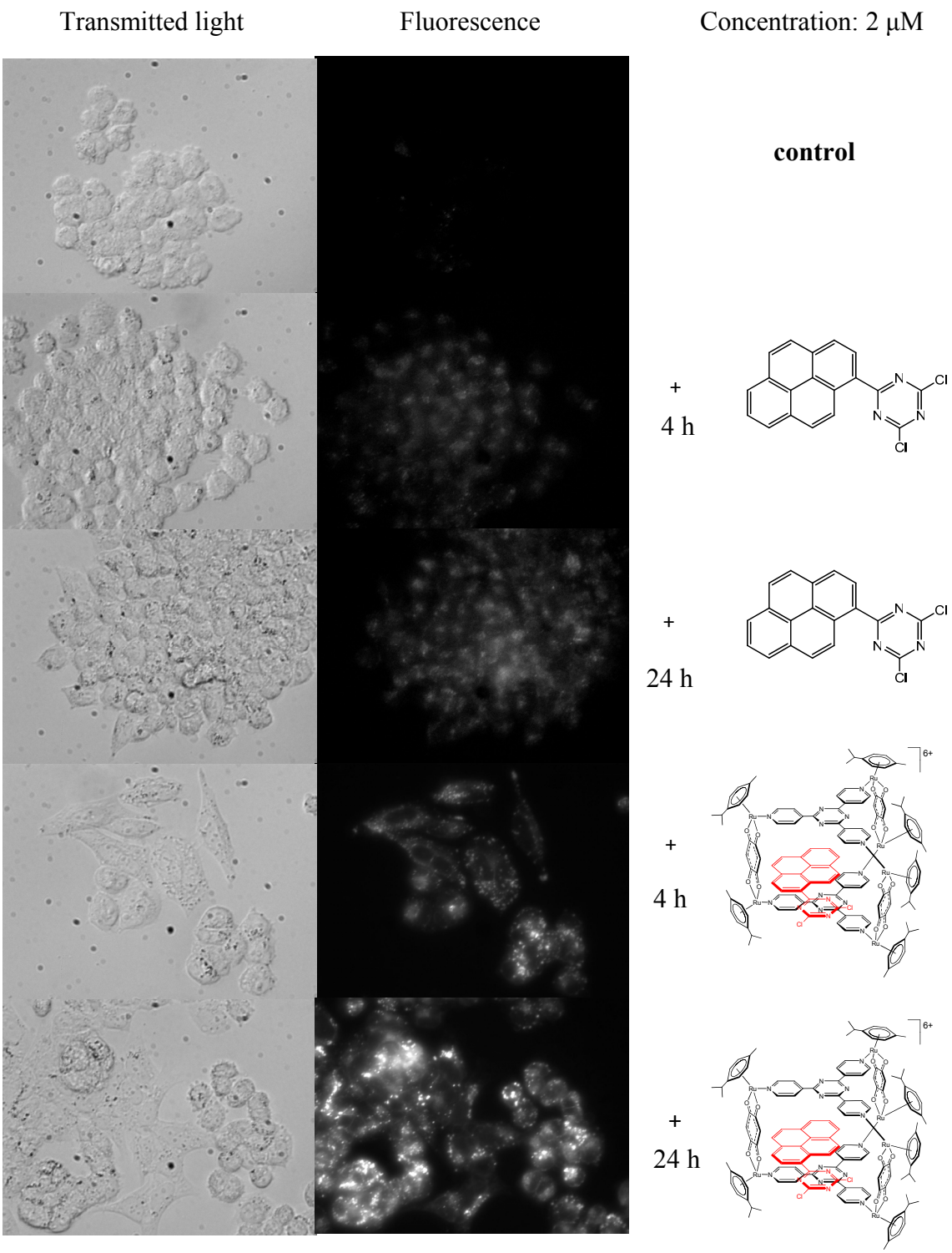

Figure 55. Microscopy images of cells incubated with **e** and **e**⊂**23** at 2 μM concentration

Recently, Puckett et al. used flow cytometry to quantify the uptake of a fluorescent polypyridyl ruthenium compound [165]. We exploited their technique to confirm the data obtained by microscopy and provide a more quantitative picture. Figure 56 shows typical histograms obtained from the fluorescence of cells treated with pyrene-R and **e**⊂**23**. These data confirm the higher fluorescence of cells treated with the encapsulated pyrene-R in **23** and allowed the uptake of the fluorophore to be quantitatively assessed.

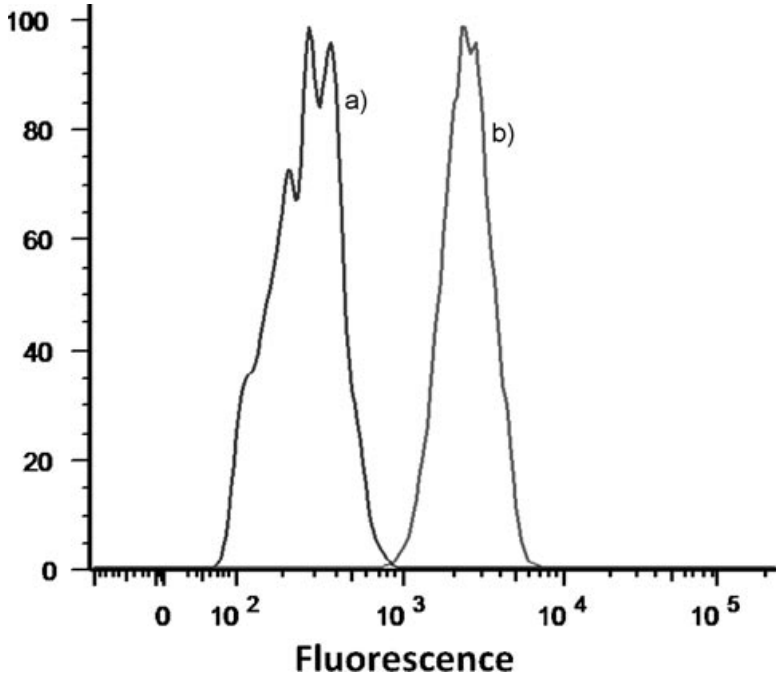

Figure 56. Flow cytometry analysis of the fluorescence of the A2780 cells treated with **e**⊂**23** (a) and **e** alone (b)

Small molecules can enter cells in multiple ways, including active, that is, energy-dependent (endocytosis or pumps), or energy-independent phenomena (passive diffusion or assisted diffusion) [165-167]. To provide insights into the uptake mechanism, the mean fluorescence, and accordingly the uptake/release of pyrene-R, as a function of concentration and time was monitored during incubation with **e**⊂**23** and during chase (Figure 57). Figure 57 (top left) shows that the uptake of the cage does not increase linearly with incubation time. This observation implies that, at least in part, the cellular machinery is involved, for example, membrane transporters or receptors that limited the

rate of uptake. This inference is confirmed by the fact that the fluorescence of the cell does not follow linearly with the concentration of **e⊂23** (Figure 57, top right).

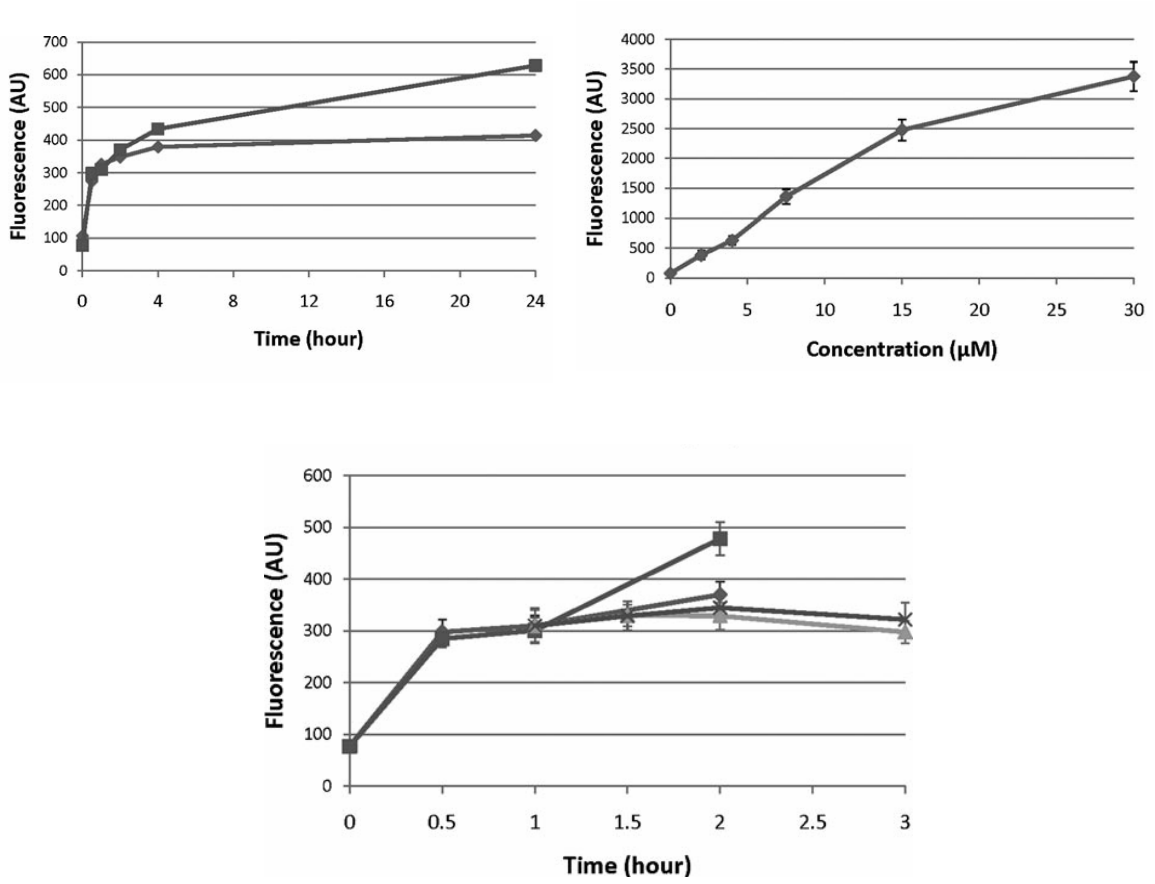

Figure 57. Influence of various treatments on the fluorescence of cells treated with **e⊂23**. The mean fluorescence of the cells was quantified by flow cytometry. Top left: Time course of release of **e** in cells treated with 2 μM (■) or 4 μM (◆) of **e⊂23**. Top right: Concentration dependency of the release of **e** in cells treated with **e⊂23**. Bottom: Monitoring of pyrene-R fluorescence during uptake at either 37°C (◆) or 4°C (■) and during chase after 1 hour incubation with 4 mm of **e⊂23** at 37°C (▲) or 4°C (×)

Nevertheless, at the concentrations tested it is not possible to determine if the uptake reaches a plateau or increases linearly at higher concentrations. Thus we cannot completely exclude a passive component in the mechanism of uptake, although an assisted diffusion pathway fits best with the obtained data. It is worth noting that at 4°C

neither uptake nor chase of pyrene-R seems to be significantly altered compared to the values obtained at 37 °C (Figure 57, bottom). Hence endocytosis may be disqualified as uptake does not require thermal energy.

5.5 Conclusions

We have investigated a number of prismatic cages proving that with large aromatic compounds they form carceplexes that will not release the guest unless the cage is broken. This makes them very attractive for drug transportation as many anti-cancer drugs are cytotoxic and could benefit from selective transportation to cancer cells. As these systems are water soluble and keep their water solubility even after encapsulation, they are good candidates to transport hydrophobic drugs. Like a Trojan horse they can bring drugs into cancer cells before release. We have shown that a functionalized aromatic molecule with one or two dangling arms can be encapsulated and that there is a synergistic effect on biological activity between the cage and the pyrene-R encapsulated. We have also proven by fluorescence studies the release of the encapsulated species inside the cell. This motivates further investigation to encapsulate species with higher activity to investigate the synergic effect, possibly the active DNA binding pyrenes of Schmuck and co-workers [142] or tether platinum complexes to a pyrene moiety, but there are many highly active compounds whose water solubility is too low to be utilized *in vivo*. If these compounds target the EPR effect is still uncertain however we proved it is not transported into the cell by endocytosis. *In vivo* tests are still needed to confirm the selectivity of these compounds.

6. General Conclusions and Perspectives

This thesis work deals with bio-organometallic chemistry to achieve large compounds with the possibility to target the EPR effect. Targeting the EPR effect is a recent and attractive fashion to gain selectivity for anti-cancer drugs. Moreover using ruthenium might reduce the general toxicity and side effect that platinum compounds often exhibit. A number of large arene ruthenium containing compounds has been synthesized and their biological activity has been evaluated.

6.1 Dendritic systems

The first part of this thesis deals with metalla-dendrimers. A number of different generation metalla-dendrimers were produced. Generations 1 and 2 were easily obtained from the commercial DAB dendrimer which is then reacted through a Schiff base condensation to produce the pyridyl end group dendrimer. These dendrimers can then be easily reacted with a ruthenium dimer to give the metalla-dendrimer in high yields. Four different metalla-dendrimers were synthesized and two mononuclear compounds for comparison.

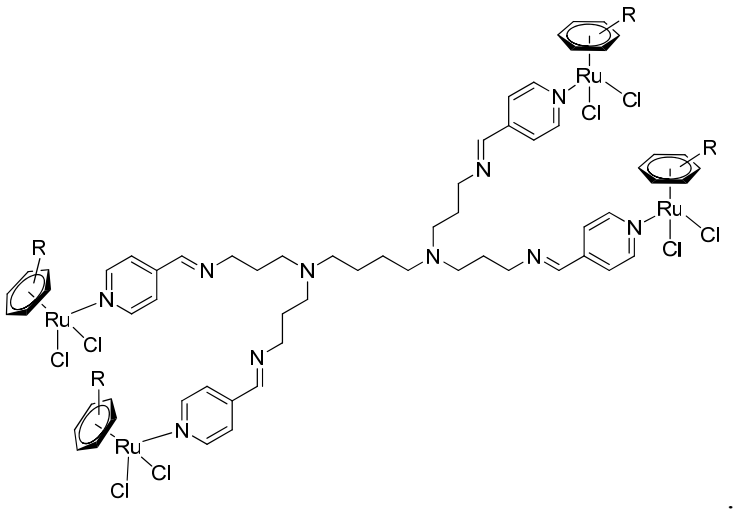

Their cytotoxicities were evaluated on A2780 human ovarian cancer cell line. The metalla-dendrimers exhibit moderate cytotoxicity but only as a function of the number of arene ruthenium complexes connected to the dendrimer. There is hence no synergistic effect of the dendrimer. However the results suggest that these metalla-dendrimers are taken up by the cells no matter the size. To test even larger systems like the 3rd and 4th generation would be interesting, as they might target the EPR effect more effectively. Introducing a charge onto these systems could also be an interesting approach as we have seen with the hexacationic prisms that such hexacationic systems are easily taken up by cancer cells, this could be done by introducing a 2,2'-bipyridyl moiety instead of the 4-pyridyl. In addition, bidentate ligands generate in general more active ruthenium species.

6.2 Supramolecular rectangles

The second part deals with supramolecular rectangles containing arene ruthenium corners. These are interesting not only for their structural properties but also their biological potential. A straightforward and simple synthesis using the molecular clip strategy affords these rectangles in good yields and high purity.

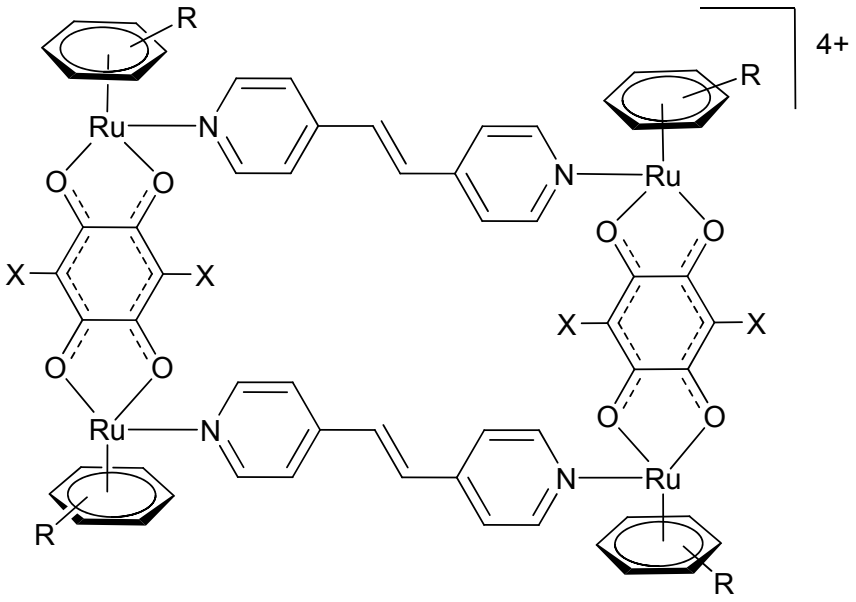

The biological activity was evaluated on A2780 human ovarian cancer cell line. However the smallest pyrazine bridged rectangles were not stable enough to be tested. The ones tested show moderate to high cytotoxicity, judging from the differences in their IC_{50} values the activity seems to increase with lipophilicity as the hexamethylbenzene complexes are in general more cytotoxic and with flexibility as the 1,2-di(4-pyridyl)ethylene complexes seem more active than the 4,4'-bipyridine derivatives.

The rectangular systems activity is interesting, however more studies needs to be done concerning their biological mechanism. A larger series of more diverse rectangles needs to be done comparing activity of; more or less flexible *N*∩*N* bridging ligands; the impact of the charge of the complex; possibility of these complexes to bind quadruplex DNA. There is also a possibility that the cavity in these systems can be exploited as host for transportation of hydrophobic drugs. Some of these aspects are currently under investigation within the group.

6.3 Supramolecular prisms

The third part deals with supramolecular prism with encapsulated aromatic molecules. They are easily synthesized by the same procedure as an empty prism but with the addition of a guest molecule. The large aromatic molecule encapsulated cannot be removed, thus a carceplex is formed, the only way to remove the guest is the breaking of the prismatic cage. Because of this property, and the fact that arene ruthenium compounds are biologically active, a number of functionalized pyrene species were encapsulated in the prismatic cage.

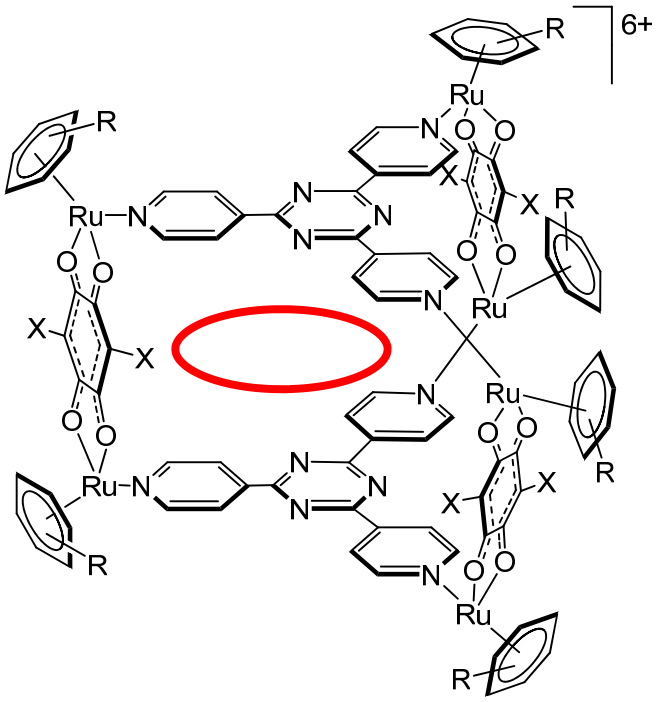

Biological tests on the A2780 human ovarian cancer cell line showed that the activity increased for some carceplexes as compared to the empty cage **23** and free pyrene. The activity of the pyrenes alone cannot be tested due to their poor water solubility. The effect of the pyrenes with simple active groups such as acid, alcohol and amine is negligible as IC_{50} values are almost the same as for **23** alone. Some

functionalized species however increase the activity of the carceplex and the most active possesses cytotoxicity comparable to that of cisplatin.

To shed some light on the mode of action of these carceplexes a fluorescence study of the carceplex **e⊂23** was done (**e** = 1-(4,6-dichloro-1,3,5-triazin-2-yl)pyrene). As the fluorescence of the pyrene-R is quenched when encapsulated the release of pyrene-R from the cage could be studied. Fluorescent microscopy on cells treated with free pyrene-R and **e⊂23** revealed stronger fluorescence from cells treated with the carceplex suggesting that the cage aids the uptake and then releases the pyrene by breaking. Further tests were done to investigate the mode of uptake where an active mode of uptake was excluded. There is a possibility that these complexes travels across the membrane through passive diffusion.

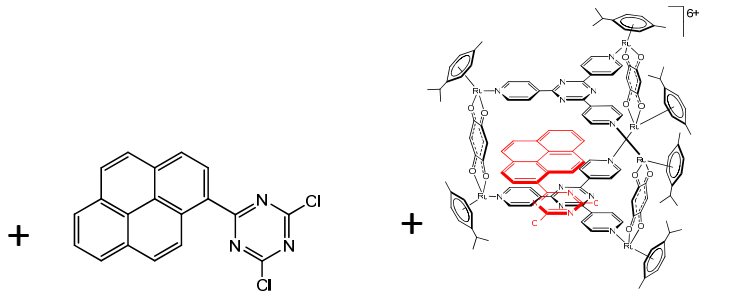

2 µM, 24 hours 2 µM, 24 hours

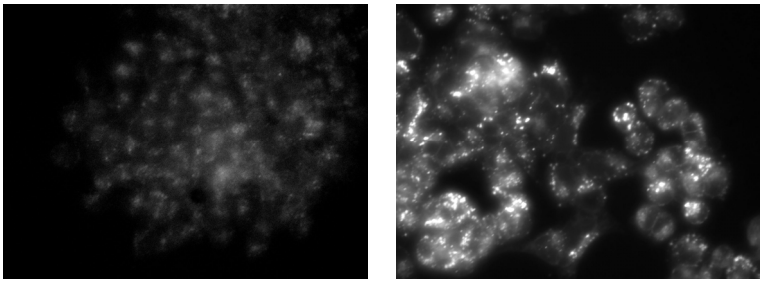

The prismatic cages are large and could benefit from the EPR effect, although this has yet to be proven, there are arguments that they are not large enough for this effect. However we have proven that cancer cells take up these complexes but an *in vivo* test has to be done to prove selectivity.

Biological *in vivo* tests would answer some of the questions raised for these compounds. For instance indication of the complexes selectivity and general toxicity could be evaluated with *in vivo* tests, which in extension would guide how to orientate future research.

Otherwise measures to increase activity can be taken. For example other types of compounds could be encapsulated. There are many drugs that are highly cytotoxic but disqualified from clinical use because of low water solubility. These prismatic cages could be a solution to transport such compounds into cancer cells and their high activity can be exploited.

The encapsulation of functionalized pyrenes can also be further developed. As biologically active groups increased their cytotoxicity adding more active groups or using the DNA/RNA binding pyrenes of Schmuck et al. [142] would be interesting. For example tethering platinum compounds to the pyrene might be interesting, something which is ongoing in the laboratory. Furthermore attaching two bioactive groups to the two armed pyrene would be interesting for comparison with the single armed, to see the impact of the bioactive groups.

Finally as the arene ruthenium complexes are versatile the arene may be derivatized. Attaching various bioactive groups to the arene could be of interest; this would transport one bioactive group per ruthenium into the cell increasing the activity sixfold as compared to an encapsulated group. However such an addition might change the solubility of the complex and thereby change its uptake and activity. PEG (poly ethylene glycol) chains could also be attached to the arene moiety making the complex larger and thereby increasing the possibility to target the EPR effect.

6.4 General conclusions

We have shown that arene ruthenium complexes incorporated in large systems or supramolecular assemblies are of biological relevance. Almost all compounds exhibit moderate to high cytotoxicity when tested on the A2780 human ovarian cancer cell line. Tests performed by Navarro and Barea [125] suggests that at least the rectangles are not generally toxic, something which encourages further exploration of this field. Moreover we have proven activity regardless of the size of the compound, however if selectivity can be gained through the benefit of the EPR effect has yet to be investigated.

7. Experimental section

7.1 General remarks

7.1.1 Solvents and gases

Solvents of analytical grade purchased from Acros organics or VWR International S.A.S were used for synthesis and unless otherwise stated degassed prior to use. The silica used for column chromatography (32-63, 60Å) was purchased from Brunshwig AG. The gas (N_2) when utilized was supplied by Carbagas and was used directly from cylinder without further purification.

7.1.2 Starting materials

All organic starting materials were purchased from Acros organics, Sigma-Aldrich, Fluka or TCI-Europe and used as received. The dimeric complexes $[(\eta^6\text{-}p\text{-}^{i}PrC_6H_4Me)RuCl_2]_2$ and $[(\eta^6\text{-}C_6Me_6)RuCl_2]_2$ [168], 2,4,6-tris(4-pyridyl)-1,3,5-triazine (tpt) [169] and diiodopyrene [144] were synthesized according to published methods. $RuCl_3$ hydrate was a generous loan from Johnson-Matthey.

7.1.3 Analytical instruments

The ^{1}H, $^{13}C\{^{1}H\}$ ROESY and DOSY NMR spectra were recorded on a Bruker AvanceII 400 spectrometer using the residual protonated solvent as internal standard.

Infrared spectra were, if not otherwise stated, recorded as KBr pellets on a Perkin-Elmer FTIR 1720-X spectrometer.

Electrospray ionization mass spectrometry conditions were recorded on a Bruker APEX II 9.4-tesra FT-ICR-MS equipped with an Apollo II electrospray ion source: sample condition 10-50 μmol/l in methanol at 30ºC, end plate voltage 3500 V, and capillary voltage.

Elemental analyses were done by Laboratoire de chimie pharmaceutique de l'Université de Genève (Switzerland) or by Mikroelementar-analytisches Laboratorium de ETH Zürich (Switzerland).

7.1.4 Electrochemistry

Electrochemical measurements were carried out with a computer-controlled multipurpose potentiostat μAUTOLAB III (Eco Chemie) at room temperature using a standard Metrohm three-electrode cell with platinum disk electrode (AUTOLAB RDE; 3 mm diameter) as the working electrode, platinum sheet auxiliary electrode, and calomel reference electrode (3 M KCl). The analyzed compounds were dissolved in dichloromethane (Fluka, absolute, declared H_2O content ≤ 0.005%) to give a solution containing 5×10^{-4} M of the analyte and 0.1 M Bu_4NPF_6 (Fluka, purissimum for electrochemistry). In the case of poorly soluble compounds, saturated solutions were used. The solutions were deaerated with argon prior to the measurement and then kept under an argon blanket. The redox potentials are given relative to the ferrocene/ferrocenium reference and are reproducible within ca. ± 5 mV.

7.1.5 X-ray structure analysis

The crystallographic analyses were done by Dr Bruno Therrien. In general the crystals were mounted on a Stoe Image Plate Diffraction system equipped with a ϕ circle goniometer, using Mo Kα graphite-monochromated radiation (λ=0.71073 Å) with ϕ range 0-200°, increment of 1.2° and 1.0°, respectively, 2θ range from 4.0° to 52°, D_{max} - D_{min}= 12.45 - 0.81 Å. The structures were solved by direct methods using the program SHELXS-97 [170]. Refinement and all further calculations were carried out using SHELXL-97 [170]. In all compounds the H atoms were included in calculated positions and treated as riding atoms using the SHELXL default parameters. All non H atoms were refined anisotropically, using weighted fullmatrix least-squares on F^2. Crystallographic details can be found through each compounds CCDC number listed in appendix. Molecular representations were drawn with ORTEP [171] or MERCURY [172].

7.2 Synthesis

7.2.1 Imine pyridine dendrimers G1 and G2

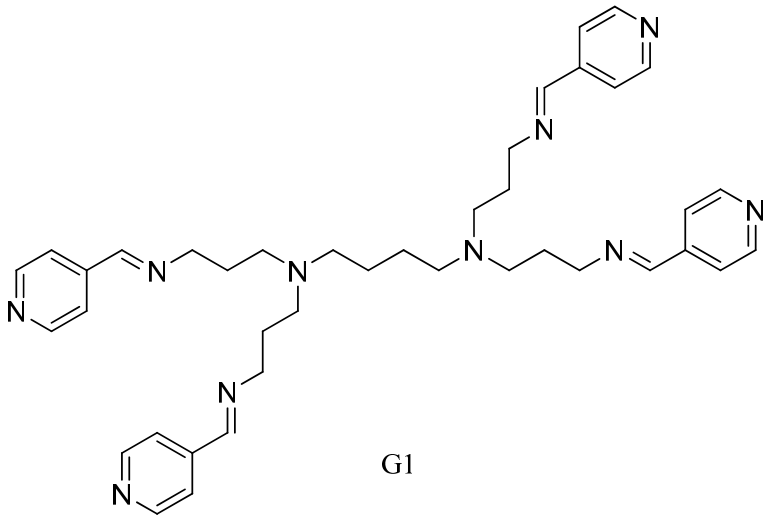

G1

General synthesis of iminopyridyl dendrimers

A solution of 4-pyridinecarboxaldehyde (1.23 mL, 12.9 mmol for G1, 2.46 mL, 15.8 mmol for G2) in dry toluene (5 mL) was added dropwise to an ice-cooled solution of DAB-$(NH_2)_4$ (1.006 g, 3.18 mmol) in dry toluene (50 mL). The reaction mixture was stirred at room temperature in the presence of anhydrous $MgSO_4$ (~10 g) for 24 h. The slurry was filtered and the solvent removed by rotary evaporation yielding an orange residue. The residue was dissolved in CH_2Cl_2 (20 mL), and washed with H_2O (6× 20 mL). The organic layer was collected and dried over anhydrous $MgSO_4$. The solvent was then removed by rotary evaporation to yield the product as an oil, which was dried *in vacuo*.

Dendritic iminopyridyl ligand G1. Yield 1.48 g (67.9%). ^{1}H NMR (400 MHz, $CDCl_3$): δ (ppm) = 8.63 (d, 8H, $^3J_{H\text{-}H}$ = 6.02 Hz, H_{ar}), 8.23 (s, 4H, imine), 7.52 (d, 8H, $^3J_{H\text{-}H}$ = 6.04 Hz, H_{ar}), 3.63 (t, 8H, $^3J_{H\text{-}H}$ = 7.53 Hz, CH_2), 2.52 (m, 8H, CH_2), 2.38 (br t, 4H, CH_2), 1.83 (qn, 8H, CH_2), 1.42 (m, 4H, CH_2). $^{13}C\{^1H\}$ NMR (100 MHz, $CDCl_3$): δ

(ppm) = 159.0 (CH, imine), 150.4 (CH, Ar_{pyr}), 143.0 (C, Ar_{pyr}), 159.0 (CH, imine), 150.4 (CH, Ar_{pyr}), 143.0 (C, Ar_{pyr}), 121.8, 59.8 (CH_2), 54.1, 51.7, 28.3, 25.3. IR (NaCl cells, CH_2Cl_2, cm^{-1}): $\nu_{(imine\ C=N)}$ 1648 (s), $\nu_{(aromatic\ C=N)}$ 1599 (s). Anal. Calc. for $C_{40}H_{52}N_{10}\cdot {}^1/_2CH_2Cl_2$: C, 68.00; H, 7.47; N, 19.58. Found: C, 68.42; H, 7.50; N, 20.02%.

Dendritic iminopyridyl ligand G2. Yield 1.47g (75.4%). ^{1}H NMR (300 MHz, $CDCl_3$): δ (ppm) = 8.57 (d, 16H, $^3J_{H-H}$ = 5.99 Hz, H_{ar}), 8.17 (s, 8H, imine), 7.48 (d, 16H, $^3J_{H-H}$ = 6.03 Hz, H_{ar}), 3.56 (br t, 16H, $^3J_{H-H}$ = 6,49 Hz, CH_2), 1.94-2.44 (overlapping m, 36H, CH_2), 1.72 (m, 16H, CH_2), 1.47 (br m, 8H, CH_2), 1.39 (br m, 4H, CH_2). $^{13}C\{^1H\}$ NMR (75 MHz, $CDCl_3$): δ (ppm) = 159.0 (CH, imine), 150.4 (CH, Ar_{pyr}), 142.9 (C, Ar_{pyr}), 121.8, 59.8 (CH_2), 54.3, 52.3, 52.2, 51.7, 28.3, 25.2, 24.8. IR (NaCl cells, CH_2Cl_2, cm^{-1}): $\nu_{(imine\ C=N)}$ 1648 (s), $\nu_{(aromatic\ C=N)}$ 1599 (s). Anal. Calc. for $C_{88}H_{120}N_{22}\cdot {}^1/_2CH_2Cl_2$: C, 69.54; H, 7.98; N, 20.16. Found: C, 69.24; H, 8.18; N, 20.49%.

7.2.2 Metalla-dendrimers, compounds **1-4**

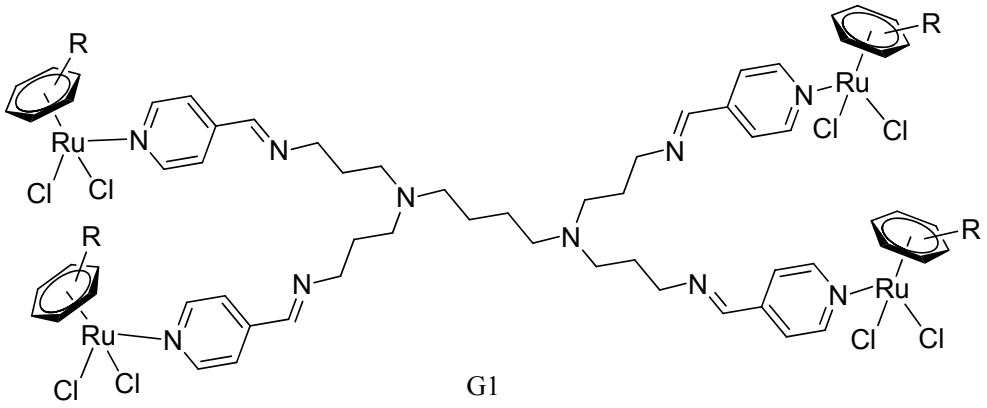

G1

General synthesis for metalla-dendrimers

The dimer ($[(\eta^6\text{-}p\text{-}^iPrC_6H_4Me))RuCl_2]_2$ (0.35 mmol, 0.213 g) for **1,** (0.307 mmol, 0.187 g) for **3** and $[(\eta^6\text{-}C_6Me_6))RuCl_2]_2$ (0.081 mmol, 0.054 g) for **2**, (0.248 mmol, 0.165 g) for **4**) was dissolved in dry CH_2Cl_2 (30 mL). To this was added a solution of the dendritic ligand in CH_2Cl_2 (5 mL) (G1 (0.17 mmol, 0.117 g) for **1**, (0.041 mmol, 0.027 g)

for **2**, and G2 (0.077 mmol, 0.114 g) for **3** and (0.062 mmol, 0.092 g) for **4**). The reaction mixture was stirred at room temperature for 5 h. The solvent was then reduced to 3 mL, and the product was precipitated with petroleum ether. The resulting yellow–orange precipitate was filtered, washed with petroleum ether and dried *in vacuo*.

[{(η^6-*p*-^{i}PrC$_6$H$_4$Me)RuCl$_2$}$_4$G1)] (**1**). Yield 0.26 g (79.1%). M.p.: 165 °C (decompose, without melting). ^{1}H NMR (300 MHz, $CDCl_3$): δ (ppm) = 9.06 (d, 8H, $^3J_{H\text{-}H}$ = 5.42 Hz, H_{ar}), 8.20 (s, 4H, imine), 7.49 (d, 8H, $^3J_{H\text{-}H}$ = 6.15 Hz, H_{ar}), 5.70 (d, 8H, $^3J_{H\text{-}H}$ = 5.70 Hz, H_{ar}), 5.28 (d, 8H, $^3J_{H\text{-}H}$ = 6.09 Hz, H_{ar}), 3.67 (m, 8H, H_5), 2.97 (m, 4H, $CHMe_2$), 2.44–2.97 (overlapping m, 12H, H_2, H_3), 2.09 (s, 12H, CH_3), 1.83 (br m, 8H, CH_2), 1.47 (br m, 4H, CH_2), 1.30 (d, 24H, $^3J_{H\text{-}H}$ = 6.87 Hz, $CHMe_2$). ^{13}C{^{1}H} NMR (100 MHz, $CDCl_3$): δ (ppm) = 158.4 (CH, imine), 139.8 (C, pyr), 155.3 (CH, pyr), 122.5, 103.3 (C, *p*-cym), 97.5, 83.3 (CH, *p*-cym), 82.1, 58.8 (CH_2), 53.7, 51.2, 31.5, 30.7, 27.1, 22.3 (CH_3, *p*-cym), 18.3. IR (NaCl cells, CH_2Cl_2, cm^{-1}): $\nu_{(imine,\ C=N)}$ 1646 (s), $\nu_{(pyr,\ C=N)}$ 1615 (s). Anal. Calc. for $C_{80}H_{108}Ru_4Cl_8N_{10}\cdot 1^1/_2CH_2Cl_2$: C, 48.34; H, 5.52; N, 6.92. Found: C, 48.22; H, 5.15; N, 6.74%. MS (ESI, m/z): 565.0 $[M + 4H + 4CH_2Cl_2 + H_2O]^{4+}$.

[{(η^6-C$_6$Me$_6$)RuCl$_2$}$_4$G1] (**2**). Yield 0.050 g (86.5%). M.p.: 188 °C (decompose, without melting). ^{1}H NMR (300 MHz, $CDCl_3$): δ (ppm) = 8.78 (d, 8H, $^3J_{H\text{-}H}$ = 6.3 Hz, H_{ar}), 8.23 (s, 4H, imine), 7.51 (d, 8H, $^3J_{H\text{-}H}$ = 6.4 Hz, H_{ar}), 3.67 (m, 8H, CH_2), 2.49–2.58 (overlapping m, 12H, CH_2), 1.97 (s, 72H, CH_3), 1.85 (br m, 8H, CH_2), 1.44 (br m, 4H, CH_2). ^{13}C{^{1}H} NMR (75 MHz, $CDCl_3$): δ (ppm) = 158.9 (CH, imine), 155.0 (CH, pyr), 143.9 (C, pyr), 122.5, 91.4 (C, HMB), 58.2 (CH_2), 53.4, 51.0, 26.2, 24.2, 15.4 (CH_3, HMB). IR (NaCl cells, CH_2Cl_2, cm^{-1}): $\nu_{(imine,\ C=N)}$ 1646 (s), $\nu_{(pyr,\ C=N)}$ 1614 (s). Anal. Calc. for $C_{88}H_{124}Ru_4Cl_8N_{10}\cdot CH_2Cl_2$: C, 51.03; H, 6.06; N, 6.69. Found: C, 51.01; H, 5.85; N, 6.39%. MS (ESI, m/z): 635.0 $[M\text{-}3Cl]^{3+}$

[{(η^6-*p*-^{i}PrC$_6$H$_4$Me)RuCl$_2$}$_8$G2] (**3**). Yield 0.30 g (98.1%). M.p.: 214 °C (decompose, without melting). ^{1}H NMR (300 MHz, $CDCl_3$): δ (ppm) = 9.05 (d, 16H, $^3J_{H\text{-}H}$ = 6.53 Hz, H_{ar}), 8.19 (s, 8H, imine), 7.49 (d, 16H, $^3J_{H\text{-}H}$ = 6.61 Hz, H_{ar}), 5.49 (d, 16H, $^3J_{H\text{-}H}$ = 6.01 Hz, H_{ar}), 5.28 (d, 16H, $^3J_{H\text{-}H}$ = 6.02 Hz, H_{ar}), 3.67 (m, 16H, CH_2), 2.97 (m, 8H, $CHMe_2$), 2.30–2.53 (overlapping m, 36H, CH_2), 2.09 (s, 24H, CH_3), 1.78 (m, 16H, CH_2), 1.35–1.48 (overlapping m, 12H, CH_2), 1.32 (d, 48H, $^3J_{H\text{-}H}$ = 6.92 Hz, $CHMe_2$). $^{13}C\{^1H\}$ NMR (75 MHz, $CDCl_3$): δ (ppm) = 158.3 (CH, imine), 155.3 (CH, pyr), 144.2 (C, pyr), 122.5, 103.2 (C, *p*-cym), 97.4, 83.0 (CH, *p*-cym), 82.0, 58.8 (CH_2), 55.2, 51.4, 38.8, 30.6, 27.1, 22.2 (CH_3, *p*-cym), 18.2. IR (NaCl cells, CH_2Cl_2, cm^{-1}): $\nu_{(imine,\ C=N)}$ 1646 (s), $\nu_{(pyr,\ C=N)}$ 1614 (s). Anal. Calc. for $C_{168}H_{232}Ru_8Cl_{16}N_{22}\cdot 4CH_2Cl_2$: C, 48.32; H, 5.66; N, 7.21. Found: C, 48.37; H, 6.03; N, 6.61%. MS (ESI, m/z): 569.0 $[M\text{-}7Cl + 3CH_2Cl_2 + CH_3CN]^{7+}$.

[{(η^6-C$_6$Me$_6$)RuCl$_2$}$_8$G2] (**4**). Yield 0.23 g (91.7%). M.p.: 194 °C (decompose, without melting). ^{1}H NMR (400 MHz, $CDCl_3$): δ (ppm) = 8.78 (d, 16H, $^3J_{H\text{-}H}$ = 5.6 Hz, H_{ar}), 8.23 (s, 8H, imine), 7.54 (d, 16H, $^3J_{H\text{-}H}$ = 6.0 Hz, H_{ar}), 3.69 (m, 16H, CH_2), 2.60 (m, 16H, CH_2), 2.50 (m, 4H, CH_2,), 2.15–2.38 (overlapping m, 24H, CH_2), 1.99 (s, 144H, CH_3), 1.87 (m, 8H, CH_2), 1.63 (br m, 8H, CH_2), 1.31 (br m, 4H, CH_2). $^{13}C\{^1H\}$ NMR (100 MHz, $CDCl_3$): δ (ppm) = 158.9 (C, imine), 155.0 (CH, pyr), 144.1 (C, pyr), 122.5, 91.4 (C, HMB), 25.3–58.9 (CH_2), 15.4 (CH_3, HMB). IR (NaCl cells, CH_2Cl_2, cm^{-1}): $\nu_{(imine,\ C=N)}$ 1646 (s), $\nu_{(pyr,\ C=N)}$ 1613 (s). Anal. Calc. for $C_{184}H_{264}Ru_8Cl_{16}N_{22}\cdot 2CH_2Cl_2$: C, 51.60; H, 6.24; N, 7.12. Found: C, 51.69; H, 6.43; N, 6.82%. MS (ESI, m/z): 631.0 $[M\text{-}7Cl + 5CH_2Cl_2 + 2CH_3CN]^{7+}$.

7.2.3 Mononuclear compounds **5-6**

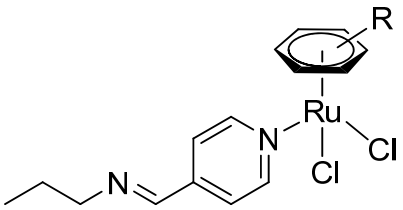

General synthesis of mononuclear reference compounds

The N-(pyridin-4-ylmethylene)propan-1-amine (L), was prepared by the reaction of 4-pyridinecarboxaldehyde (0.107 g, 0.723 mmol for **5**; 0.030 g, 0.200 mmol for **6**) with n-propylamine in Et_2O. The dimer ($[(\eta^6\text{-}p\text{-}^{i}PrC_6H_4Me)RuCl_2]_2$ (0.223 g, 0.362 mmol) for **5** and $[(\eta^6\text{-}C_6Me_6)RuCl_2]_2$ (0.068 g, 0.100 mmol) for **6**) was dissolved in dry CH_2Cl_2 (30 mL). A solution of the N-(pyridin-4-ylmethylene)propan-1-amine (0.107 g, 0.723 mmol) in dry CH_2Cl_2 (5 mL) was added dropwise and the reaction mixture was stirred for 5 hours. The solvent was then reduced to 3 mL and the product was precipitated with petroleum ether. The orange-yellow precipitate was filtered, washed with petroleum ether and dried *in vacuo*.

$[(\eta^6\text{-}p\text{-}^{i}PrC_6H_4Me)RuCl_2(L)]$ (**5**). Yield 0.15 g (91.1%). M.p.: 163-166 °C. ^{1}H NMR (400 MHz, $CDCl_3$): δ (ppm) = 9.10 (d, 2H, $^3J_{H\text{-}H}$ = 6.43 Hz, H_{ar}). 8.27 (s, 1H, imine), 7.60 (d, 2H, $^3J_{H\text{-}H}$ = 6.53 Hz, H_{ar}), 5.45 (d, 2H, $^3J_{H\text{-}H}$ = 5.92 Hz, H_{ar}), 5.23 (d, 2H, $^3J_{H\text{-}H}$ = 5.93 Hz, H_{ar}), 3.66 (t, 2H, $^3J_{H\text{-}H}$ = 6.47 Hz, CH_2), 3.00 (m, 1H, $CHMe_2$), 2.11 (s, 3H, CH_3), 1.75 (m, 2H, CH_2), 1.32 (d, 6H, $^3J_{H\text{-}H}$ = 6.93 Hz, $CHMe_2$), 0.97 (t, 3H, $^3J_{H\text{-}H}$ = 7.39 Hz, CH_3). $^{13}C\{^1H\}$ NMR (100 MHz, $CDCl_3$): δ (ppm) = 157.3 (CH, imine), 155.3 (CH, pyr), 144.6 (C, pyr), 122.5, 103.6 (C, *p*-cym), 97.3, 83.1 (CH, *p*-cym), 82.2, 63.6 (CH_2), 30.7, 23.8, 22.3 (CH_3, *p*-cym), 18.2, 11.8 (CH_3). IR (NaCl cells, CH_2Cl_2, cm^{-1}): $\nu_{(imine,\ C=N)}$ 1647 (s), $\nu_{(pyr,\ C=N)}$ 1615 (s). Anal. Calc. for $C_{19}H_{26}RuCl_2N_2$: C, 50.22; H, 5.77; N, 6.16. Found: C, 49.96; H, 5.38; N, 5.99%. MS (ESI, m/z): 419.1 $[M\text{-}Cl]^+$.

[(η^6-C_6Me_6)$RuCl_2$(L)] (**6**). Yield 0.15 g (91.1%). M.p.: 139 °C (decompose, without melting). ^{1}H NMR (400 MHz, $CDCl_3$): δ (ppm) = 8.86 (d, 2H, $^3J_{H-H}$ = 6.2 Hz, H_{ar}), 8.26 (s, 1H, imine), 7.57 (d, 2H, $^3J_{H-H}$ = 6.4 Hz, H_{ar}), 3.66 (t, 2H, $^3J_{H-H}$ = 6.9 Hz, CH_2), 2.03 (s, 18H, CH_3), 1.74 (m, 2H, CH_2), 0.96 (t, 3H, $^3J_{H-H}$ = 7.4 Hz, CH_3). $^{13}C\{^1H\}$ NMR (100 MHz, $CDCl_3$): δ (ppm) = 157.5 (CH, imine), 155.1 (CH, pyr), 144.2 (C, pyr), 122.5, 91.4 (C, HMB), 63.6 (CH_2), 23.8, 15.4 (CH_3, HMB), 11.8 (CH_3). IR (NaCl cells, CH_2Cl_2, cm^{-1}): $\nu_{(imine,\ C=N)}$ 1646 (s), $\nu_{(pyr,\ C=N)}$ 1614 (s). Anal. Calc. for $C_{21}H_{30}RuCl_2N_2$: C, 52.28; H, 6.27; N, 5.81. Found: C, 51.84; H, 5.94; N, 5.47%. MS (ESI, m/z): 447.1 $[M\text{-}Cl]^+$.

Cytotoxicity study on metalla-dendrimers

While imine bonds are susceptible to hydrolysis, the presence of the aromatic substituent together with a possible dendrimer effect reduces the rate of hydrolysis, and for the compounds studied herein only a slow decomposition is observed. The human A2780 ovarian cancer cell line was obtained from the European Collection of Cell Cultures (Salisbury, UK). Cells were grown routinely in RPMI medium containing glucose, 5% foetal calf serum (FCS) and antibiotics at 37 °C and 5% CO_2. Cytotoxicity was determined using the MTT assay (MTT = 3-(4,5-dimethyl-2-thiazolyl)-2,5-diphenyl-2*H*-tetrazolium bromide). Cells were seeded in 96-well plates as monolayers with 100 μL of cell solution (approximately 20,000 cells) per well and pre-incubated for 24 hours in medium supplemented with 10% FCS. Compounds were prepared as DMSO solution then dissolved in the culture medium and serially diluted to the appropriate concentration, to give a final DMSO concentration of 0.5%. One hundred micro liter of drug solution was added to each well and the plates were incubated for another 72 h. Subsequently, MTT (5 mg/mL solution) was added to the cells and the plates were incubated for a further 2 h. The culture medium was aspirated, and the purple formazan crystals formed by the mitochondrial dehydrogenase activity of vital cells were dissolved in DMSO. The optical density, directly proportional to the number of surviving cells, was quantified at 540 nm using a multiwell plate reader and the fraction of surviving cells was calculated

from the absorbance of untreated control cells. Evaluation is based on means from two independent experiments, each comprising 3 microcultures per concentration level.

7.2.4 Bimetallic molecular clip, compounds **7**-**10**

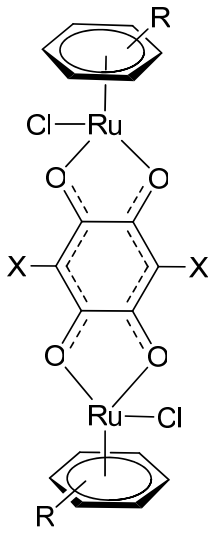

General synthesis of bimetallic molecular clips

A mixture of $[(\eta^6\text{-arene})RuCl_2]_2$ ($[(\eta^6\text{-}p\text{-}^{i}PrC_6H_4Me)RuCl_2]_2$ (184 mg, 0.3 mmol) for **7** and **8** and $[(\eta^6\text{-}C_6Me_6)RuCl_2]_2$ (201 mg, 0.3 mmol) for **9** and **10**) and the quinone (2,5-dihydroxy-1,4-benzoquinone (dhbq-H_2) (42 mg, 0.3 mmol) for **7** and **9** and chloranillic acid (dchq-H_2) (63 mg, 0.3 mmol) for **8** and **10**) was suspended in MeOH (30 mL) and stirred for 2 h at room temperature. The precipitate was filtered, washed with Et_2O, and dried *in vacuo*.

$[(\eta^6\text{-}p\text{-}^{i}PrC_6H_4Me)_2Ru_2(dhbq)Cl_2]$ (**7**). Yield: 165 mg (81%). ^{1}H NMR (400 MHz, $CDCl_3$): δ (ppm) = 5.82 (s, 2H, H_q), 5.66 (d, 4H, $^3J_{H\text{-}H}$ = 6.12 Hz, H_{ar}), 5.41 (d, 4H, H_{ar}), 2.97 (sept, 2H, $^3J_{H\text{-}H}$ = 6.72 Hz, CH), 2.32 (s, 6H, CH_3), 1.35 (d, 12H, CH_3). $^{13}C\{^1H\}$ NMR (100 MHz, $CDCl_3$): δ (ppm) = 184.45, 139.12, 119.46, 102.29, 97.03, 81.55, 79.60, 31.70, 22.87, 19.09. IR (cm^{-1}): 1528(s), 1377(s), 1257(s). Anal. Calc. for $C_{26}H_{30}Cl_2O_4Ru_2$: C, 45.90; H, 4.45. Found: C, 45.72; H, 4.60%.

[(η^6-*p*-^{i}PrC$_6$H$_4$Me)$_2$Ru$_2$(dchq)Cl$_2$] (**8**). Yield: 165 mg (74%). ^{1}H NMR (400 MHz, $CDCl_3$): δ (ppm) = 5.74 (d, 4H, $^3J_{H\text{-}H}$ = 6.20 Hz, H_{ar}), 5.48 (d, 4H, H_{ar}), 2.98 (sept, 2H, $^3J_{H\text{-}H}$ = 7.00 Hz, CH), 2.34 (s, 6H, CH_3), 1.36 (d, 12H, CH_3). $^{13}C\{^1H\}$ NMR (100 MHz, $CDCl_3$): δ (ppm) = 184.72, 137.45, 118.41, 102.36, 98.62, 82.07, 76.44, 31.72, 21.53, 18.59. IR (cm^{-1}): 1639(s), 1496(s), 1370(s). Anal. Calc. for $C_{26}H_{28}O_4Cl_4Ru_2$: C, 41.70; H, 3.77. Found: C, 41.61; H, 3.82%.

[(η^6-C$_6$Me$_6$)Ru$_2$(dhbq)Cl$_2$] (**9**). Yield: 170 mg (77%). ^{1}H NMR (400 MHz, $CDCl_3$): δ (ppm) = 5.90 (s, 2H, H_q), 2.17 (s, 36H, CH_3). $^{13}C\{^1H\}$ NMR (100 MHz, $CDCl_3$): δ (ppm) = 182.96, 114.62, 105.88, 90.55, 16.24. IR (cm^{-1}): 1638(s), 1617(s), 1551(s), 1532(m), 1374(m), 1255(s), 620(s). Anal. Calc. for $C_{30}H_{38}O_4Cl_2Ru_2$: C, 48.98; H, 5.20. Found: C, 48.77; H, 5.94%.

[(η^6-C$_6$Me$_6$)Ru$_2$(dchq)Cl$_2$] (**10**). Yield: 185 mg (77%). ^{1}H NMR (200 MHz, $CDCl_3$): δ (ppm) = 2.02 (s, 36H, CH_3). $^{13}C\{^1H\}$ NMR (100 MHz, $CDCl_3$): δ (ppm) = 184.53, 126.27, 107.36, 92.64, 15.18. IR (cm^{-1}): 1638(s), 1617(s), 1499(m), 1363(m), 1111(m), 620(s). Anal. Calc. for $C_{30}H_{36}O_4Cl_4Ru_2$: C, 44.79; H, 4.51. Found: C, 44.89; H, 4.73%.

7.2.5 Supramolecular rectangles, compounds **11-22**

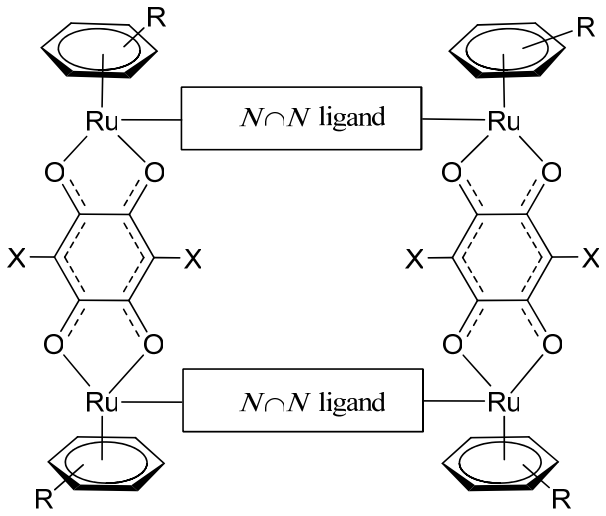

General synthetic method for supramolecular rectangles [11-22][O_3SCF_3]$_4$

A mixture of **7**-**10** (0.1 mmol) and 2 equiv of AgO_3SCF_3 (0.2 mmol) in MeOH (20 mL) was stirred at room temperature for 2 h and then filtered to remove AgCl. To the red filtrate, the corresponding *N*∩*N* ligand (0.1 mmol) was added. The mixture was stirred at room temperature for 24 h, the solvent was then removed under vacuum. The residue was taken up in CH_2Cl_2 (20 mL), the extract was then filtered and concentrated (3 mL), Et_2O was slowly added to precipitate the product as a dark orange or red solid.

[(η^6-*p*-^{i}PrC$_6$H$_4$Me)$_4$Ru$_4$(pyrazine)$_2$(dhbq)$_2$][O_3SCF_3]$_4$ ([**11**][O_3SCF_3]$_4$). Yield: 71 mg (72%). ^{1}H NMR(400 MHz, acetone-d_6): δ (ppm) = 8.70 (s, 8H, CH_{pyz}), 6.21 (d, 8H, $^3J_{H\text{-}H}$ = 6.4 Hz, H_{ar}), 6.05 (d, 8H, $^3J_{H\text{-}H}$ = 6.4 Hz, H_{ar}), 5.64 (s, 4H, H_q), 2.96 (sep, 4H, $^3J_{H\text{-}H}$ = 7.0 Hz, CH), 2.35 (s, 12H, CH_3), 1.39 (d, 24H, $^3J_{H\text{-}H}$ = 7.0 Hz, CH_3). ^{13}C{^{1}H} NMR (100 MHz, acetone-d_6): δ (ppm) = 184.8 (C=O), 149.9 (CH_{pyz}), 104.8 ($C_{p\text{-cym}}$), 102.1 (CH_q), 98.5 ($C_{p\text{-cym}}$), 83.8 ($CH_{p\text{-cym}}$), 83.2 ($CH_{p\text{-cym}}$), 31.1 ($CH(CH_3)_2$), 21.1 (CH_3), 16.5 ($CH(CH_3)_2$). IR (cm^{-1}): 1637(w), 1529(s), 1377(m), 1259(s), 1227(w), 1162(m), 1030(m),

635(w). Anal. Calc. for $C_{64}H_{68}N_4O_{20}F_{12}S_4Ru_4$: C, 38.95; H, 3.47; N, 2.84. Found: C, 38.73; H, 3.44; N, 2.78%.

[(η^6-*p*-^{i}PrC$_6$H$_4$Me)$_4$Ru$_4$(pyrazine)$_2$(dchq)$_2$][O$_3$SCF$_3$]$_4$ ([**12**][O_3SCF_3]$_4$). Yield: 71 mg (68%). ^{1}H NMR (400 MHz, acetone-d_6): δ (ppm) = 8.75 (s, 8H, CH_{pyz}), 6.30 (d, 8H, $^3J_{H\text{-}H}$ = 6.4 Hz, H_{ar}), 6.14 (d, 8H, $^3J_{H\text{-}H}$ = 6.4 Hz, H_{ar}), 3.06 (sep, 4H, $^3J_{H\text{-}H}$ = 6.9 Hz, CH), 2.44 (s, 12H, CH_3), 1.46 (d, 24H, $^3J_{H\text{-}H}$ = 6.9 Hz, CH_3). ^{13}C{^{1}H} NMR (100 MHz, acetone-d_6): δ (ppm) = 177.9 (C=O), 150.3 (CH_{pyz}), 106.1 ($C_{p\text{-cym}}$), 104.5 (CCl_q), 98.8 ($C_{p\text{-cym}}$), 84.1 ($CH_{p\text{-cym}}$), 83.9 ($CH_{p\text{-cym}}$), 31.3 ($CH(CH_3)_2$), 21.4 (CH_3), 17.3 ($CH(CH_3)_2$). IR (cm^{-1}): 1627(w), 1504(s), 1373(s), 1266(s), 1225(w), 1163(m), 1029(m), 637(m). Anal. Calc. for $C_{64}H_{64}Cl_4N_4O_{20}F_{12}S_4Ru_4{\cdot}3CH_2Cl_2$: C, 35.54; H, 3.03; N, 2.55. Found: C, 35.08; H, 3.17; N, 2.69%.

[(η^6-C$_6$Me$_6$)$_4$Ru$_4$(pyrazine)$_2$(dhbq)$_2$][O$_3$SCF$_3$]$_4$ ([**13**][O_3SCF_3]$_4$). Yield: 88 mg (83%). ^{1}H NMR (400 MHz, acetone-d_6): δ (ppm) = 8.70 (s, 8H, CH_{pyz}), 5.72 (s, 4H, H_q), 2.20 (s, 72H, CH_3). ^{13}C{^{1}H} NMR (100 MHz, acetone-d_6): δ (ppm) = 183.9 (C=O), 148.0 (CH_{pyz}), 101.7 (CH_q), 93.7 (C_{hmb}), 14.6 (CH_3). IR (cm^{-1}): 1628(w), 1527(s), 1374(s), 1257(s), 1224(w), 1156(m), 1031(m), 638(m). Anal. Calc. for $C_{72}H_{84}N_4O_{20}F_{12}S_4Ru_4$ ·$3CH_2Cl_2$: C, 40.39; H, 3.99; N, 2.58. Found: C, 39.85; H, 4.01; N, 2.70%.

[(η^6-C$_6$Me$_6$)$_4$Ru$_4$(pyrazine)$_2$(dchq)$_2$][O$_3$SCF$_3$]$_4$ ([**14**][O_3SCF_3]$_4$). Yield: 82 mg (75%). ^{1}H NMR (400 MHz, acetone-d_6): δ (ppm) = 8.71 (s, 8H, CH_{pyz}), 2.21 (s, 72H, CH_3). ^{13}C{^{1}H} NMR (100 MHz, acetone-d_6): δ (ppm) = 183.8 (C=O), 148.0 (CH_{pyz}), 105.3 (CCl_q), 93.7 (C_{hmb}), 14.6 (CH_3). IR (cm^{-1}): 1626(w), 1504(s), 1372(m), 1260 (m) 1158(w), 1031(m), 638(w). Anal. Calc. for $C_{72}H_{80}Cl_4N_4O_{20}F_{12}S_4Ru_4$: C, 38.89; H, 3.63; N, 2.52. Found: C, 38.63; H, 3.77; N, 2.45%.

[(η^6-p-^{i}PrC$_6$H$_4$Me)$_4$Ru$_4$(4,4'-bipyridine)$_2$(dhbq)$_2$][O$_3$SCF$_3$]$_4$ ([**15**][O$_3$SCF$_3$]$_4$). Yield: 79 mg (74%). ^{1}H NMR (400 MHz, acetone-d_6): δ (ppm) = 8.54 (d, 8H, $^3J_{H-H}$ = 4.4 Hz, CH_{bpy}), 8.02 (d, 8H, $^3J_{H-H}$ = 4.4 Hz, CH_{bpy}), 6.20 (d, 8H, $^3J_{H-H}$ = 8.0 Hz, H_{ar}), 5.99 (d, 8H, $^3J_{H-H}$ = 8.0 Hz, H_{ar}), 5.79 (s, 4H, H_q), 2.95 (sep, 4H, $^3J_{H-H}$ = 8.0 Hz, CH), 2.21 (s, 12H, CH_3), 1.38 (d, 24H, $^3J_{H-H}$ = 8.0 Hz, CH_3). ^{13}C{^{1}H} NMR (100 MHz, acetone-d_6): δ (ppm) = 174.3 (C=O), 154.0 (CH_{bpy}), 144.7 (C_{bpy}), 123.6 (CH_{bpy}), 103.7 ($C_{p\text{-cym}}$), 101.7 (CH_q), 99.3 ($C_{p\text{-cym}}$), 83.9 ($CH_{p\text{-cym}}$), 82.1 ($CH_{p\text{-cym}}$), 31.2 ($CH(CH_3)_2$), 21.6 (CH_3), 17.2 ($CH(CH_3)_2$). IR (cm^{-1}): 1637(s), 1616(s), 1526(m), 1378(s), 1259(m), 1159(s), 1030(s), 636(s). Anal. Calc. for $C_{76}H_{76}N_4O_{20}F_{12}S_4Ru_4$: C, 42.94; H, 3.60; N, 2.64. Found: C, 42.91; H, 3.87; N, 2.61%.

[(η^6-*p*-^{i}PrC$_6$H$_4$Me)$_4$Ru$_4$(4,4'-bipyridine)$_2$(dchq)$_2$][O$_3$SCF$_3$]$_4$ ([**16**][O$_3$SCF$_3$]$_4$). Yield: 86 mg (75%). ^{1}H NMR (400 MHz, acetone-d_6): δ (ppm) = 8.54 (d, 8H, $^3J_{H-H}$ = 6.4 Hz, CH_{bpy}), 8.06 (d, 8H, $^3J_{H-H}$ = 6.4 Hz, CH_{bpy}), 6.28 (d, 8H, $^3J_{H-H}$ = 6.4 Hz, H_{ar}), 6.11 (d, 8H, $^3J_{H-H}$ = 6.4 Hz, H_{ar}), 2.99 (sep, 4H, $^3J_{H-H}$ = 6.8Hz, CH), 2.34 (s, 12H, CH_3), 1.42 (d, 24H, $^3J_{H-H}$ = 6.8 Hz, CH_3). ^{13}C{^{1}H} NMR (100 MHz, acetone-d_6): δ (ppm) = 178.5 (C=O), 154.8 (CH_{bpy}), 145.6 (C_{bpy}), 124.6 (CH_{bpy}), 107.0 ($C_{p\text{-cym}}$), 104.8 (CCl_q), 100.1 ($C_{p\text{-cym}}$), 84.9 ($CH_{p\text{-cym}}$), 83.8 ($CH_{p\text{-cym}}$), 32.2 ($CH(CH_3)_2$), 22.5 (CH_3), 18.2 ($CH(CH_3)_2$). IR (cm^{-1}): 1637(s), 1617(s), 1502(m), 1374(m), 1259(s), 1163(m), 1031(s), 638(s). Anal. Calc. for $C_{76}H_{72}N_4O_{20}F_{12}S_4Cl_4Ru_4$: C, 40.32; H, 3.21; N, 2.47. Found: C, 40.85; H, 3.32; N, 2.36%.

[(η^6-C$_6$Me$_6$)$_4$Ru$_4$(4,4'-bipyridine)$_2$(dhbq)$_2$][O$_3$SCF$_3$]$_4$ ([**17**][O$_3$SCF$_3$]$_4$). Yield: 60 mg (54%). ^{1}H NMR (400 MHz, acetone-d_6): δ (ppm) = 8.39 (d, 8H, $^3J_{H-H}$ = 5.3 Hz, CH_{bpy}), 8.08 (d, 8H, $^3J_{H-H}$ = 5.3 Hz, CH_{bpy}), 5.76 (s, 4H, H_q), 2.16 (s, 72H, CH_3). ^{13}C{^{1}H} NMR (100 MHz, acetone-d_6): δ (ppm) = 175.2 (C=O), 153.4 (CH_{bpy}), 144.1 (C_{bpy}), 123.6 (CH_{bpy}), 101.7 (CH_q), 93.6 (C_{hmb}), 14.7 (CH_3). IR (cm^{-1}): 1638(s), 1617(s), 1525(s), 1375(m), 1258(s), 1162(m), 1032(s), 622(s). Anal. Calc. for $C_{84}H_{92}N_4O_{20}F_{12}S_4Ru_4$: C, 45.08; H, 4.14; N, 2.50. Found: C, 45.01; H, 4.14; N, 2.32%. Crystals suitable for X-ray

diffraction analysis were obtained by slow diffusion of Et_2O in an acetone solution of [**17**][O_3SCF_3]$_4$.

[(η^6-C_6Me_6)$_4$$Ru_4$(4,4'-bipyridine)$_2$(dchq)$_2$][$O_3SCF_3$]$_4$ ([**18**][O_3SCF_3]$_4$). Yield: 86 mg (73%). ^{1}H NMR (400 MHz, acetone-d_6): δ (ppm) = 8.40 (dd, 8H, $^3J_{H\text{-}H}$ = 5.4 Hz, $^4J_{H\text{-}H}$ = 1.5 Hz, CH_{bpy}), 8.13 (dd, 8H, $^3J_{H\text{-}H}$ = 5.4 Hz, $^4J_{H\text{-}H}$ = 1.5 Hz, CH_{bpy}), 2.18 (s, 72H, CH_3). ^{13}C{^{1}H} NMR (100 MHz, acetone-d_6): δ (ppm) = 177.5 (C=O), 153.8 (CH_{bpy}), 144.6 (C_{bpy}), 126.7 (CH_{bpy}), 106.4 (CCl_q), 94.4 (C_{hmb}), 15.2 (CH_3). IR (cm^{-1}): 1637(s), 1617(s), 1499(s), 1369(m), 1259(s), 1161(m), 1032(s), 638(s). Anal. Calc. for $C_{84}H_{88}N_4O_{20}F_{12}S_4Cl_4Ru_4$: C, 42.46; H, 3.73; N, 2.36. Found: C, 42.44; H, 3.23; N, 2.32%.

[(η^6-*p*-^{i}PrC$_6$H$_4$Me)$_4$$Ru_4$(1,2-bis(4-pyridyl)ethylene)$_2$(dhbq)$_2$][O_3SCF_3]$_4$
([**19**][O_3SCF_3]$_4$). Yield: 87 mg (80%). ^{1}H NMR (400 MHz, acetone-d_6): δ (ppm) = 8.35 (d, 8H, $^3J_{H\text{-}H}$ = 6.6 Hz, CH_{bpe}), 7.74 (d, 8H, $^3J_{H\text{-}H}$ = 6.6 Hz, CH_{bpe}), 7.63 (s, 4H, CH_{bpe}), 6.17 (d, 8H, $^3J_{H\text{-}H}$ = 6.4Hz, H_{ar}), 5.98 (d, 8H, $^3J_{H\text{-}H}$ = 6.4 Hz, H_{ar}), 5.78 (s, 4H, H_q), 2.96 (sep, 4H, $^3J_{H\text{-}H}$ = 7.1 Hz, CH), 2.23 (s, 12H, CH_3), 1.36 (d, 24H, $^3J_{H\text{-}H}$ = 7.1 Hz, CH_3). ^{13}C{^{1}H} NMR (100 MHz, acetone-d_6): δ (ppm) = 184.2 (C=O), 153.2 (CH_{bpe}), 146.1 (C_{bpe}), 131.7 (CH_{bpe}), 123.9 (CH_{bpe}), 103.7 ($C_{p\text{-}cym}$), 101.7 (CH_q), 99.0 ($C_{p\text{-}cym}$), 83.7 ($CH_{p\text{-}cym}$), 82.1 ($CH_{p\text{-}cym}$), 31.2 ($CH(CH_3)_2$), 21.6 (CH_3), 17.2 ($CH(CH_3)_2$). IR (cm^{-1}): 1638(s), 1616 (s), 1525(s), 1378(m), 1259(m), 1161(m), 1031(m), 636(s). Anal. Calc. for $C_{80}H_{80}N_4O_{20}F_{12}S_4Ru_4$: C, 44.12; H, 3.70; N, 2.57. Found: C, 44.06; H, 3.86; N, 2.55%.

[(η^6-*p*-^{i}PrC$_6$H$_4$Me)$_4$$Ru_4$(1,2-bis(4-pyridyl)ethylene)$_2$(dchq)$_2$][O_3SCF_3]$_4$
([**20**][O_3SCF_3]$_4$). Yield: 85 mg (74%). ^{1}H NMR (400 MHz, acetone-d_6): δ (ppm) = 8.32 (dd, 8H, $^3J_{H\text{-}H}$ = 5.4 Hz, $^4J_{H\text{-}H}$ = 1.4 Hz, CH_{bpe}), 7.77 (dd, 8H, $^3J_{H\text{-}H}$ = 5.4 Hz, $^4J_{H\text{-}H}$ = 1.4 Hz, CH_{bpe}), 7.69 (s, 4H, CH_{bpe}), 6.25 (d, 8H, $^3J_{H\text{-}H}$ = 6.4 Hz, H_{ar}), 6.08 (d, 8H, $^3J_{H\text{-}H}$ = 6.4 Hz, H_{ar}), 3.03 (sep, 4H, $^3J_{H\text{-}H}$ = 7.0 Hz, CH), 2.32 (s, 12H, CH_3), 1.42 (d, 24H, $^3J_{H\text{-}H}$ = 7.0

Hz, CH_3). $^{13}C\{^1H\}$ NMR (100 MHz, acetone-d_6): δ (ppm) = 178.0 (C=O), 153.3 (CH_{bpe}), 146.4 (C_{bpe}), 132.0 (CH_{bpe}), 124.2 (CH_{bpe}), 106.2 ($C_{p\text{-cym}}$), 104.0 (CCl_q), 99.0 ($C_{p\text{-cym}}$), 83.9 ($CH_{p\text{-cym}}$), 82.9 ($CH_{p\text{-cym}}$), 31.4 ($CH(CH_3)_2$), 21.7 (CH_3), 17.4 ($CH(CH_3)_2$). IR (cm^{-1}): 1638(s), 1619(s), 1501(s), 1373(m), 1258(s), 1163(m), 1031(m), 638(s). Anal. Calc. for $C_{80}H_{76}N_4O_{20}F_{12}S_4Cl_4Ru_4$: C,41.49; H, 3.31; N, 2.42. Found: C, 41.43; H, 3.49; N, 2.26%.

$[(\eta^6\text{-}C_6Me_6)_4Ru_4\{1,2\text{-bis(4-pyridyl)ethylene}\}_2(dhbq)_2][O_3SCF_3]_4$ ([**21**][O_3SCF_3]$_4$). Yield: 93 mg (83%). ^1H NMR (400 MHz, acetone-d_6): δ (ppm) = 8.20 (dd, 8H, $^3J_{H\text{-}H}$ = 5.4 Hz, $^4J_{H\text{-}H}$ = 1.4 Hz, CH_{bpe}), 7.76 (dd, 8H, $^3J_{H\text{-}H}$ = 5.4 Hz, $^4J_{H\text{-}H}$ = 1.4 Hz, CH_{bpe}), 7.59 (s, 4H, CH_{bpe}), 5.76 (s, 4H, H_q), 2.15 (s, 72H, CH_3). $^{13}C\{^1H\}$ NMR (100 MHz, acetone-d_6): δ (ppm) = 184.6 (C=O), 153.5 (CH_{bpe}), 146.9 (C_{bpe}), 132.6 (CH_{bpe}), 125.2 (CH_{bpe}), 102.7 (CH_q), 94.3 (C_{hmb}), 15.6 (CH_3). IR (cm^{-1}): 1638(s), 1617(s), 1524(m), 1374(m), 1257(m), 1112(m), 1031(m), 621(s). Anal. Calc. for $C_{88}H_{96}N_4O_{20}F_{12}S_4Ru_4$: C, 46.15; H, 4.22; N, 2.45. Found: C, 46.32; H, 4.46; N, 2.29%.

$[(\eta^6\text{-}C_6Me_6)_4Ru_4\{1,2\text{-bis(4-pyridyl)ethylene}\}_2(dchq)_2][O_3SCF_3]_4$ ([**22**][O_3SCF_3]$_4$). Yield: 80 mg (66%). ^1H NMR (400 MHz, acetone-d_6): δ (ppm) = 8.19 (dd, 8H, $^3J_{H\text{-}H}$ = 6.6 Hz, $^4J_{H\text{-}H}$ = 1.2 Hz, CH_{bpe}), 7.80 (dd, 8H, $^3J_{H\text{-}H}$ = 6.6 Hz, $^4J_{H\text{-}H}$ = 1.2 Hz, CH_{bpe}), 7.67 (s, 4H, CH_{bpe}), 2.18 (s, 72H, CH_3). $^{13}C\{^1H\}$ NMR (100 MHz, acetone-d_6): δ (ppm) = 177.5 (C=O), 152.6 (CH_{bpe}), 146.2 (C_{bpe}), 131.9 (CH_{bpe}), 124.4 (CH_{bpe}), 106.0 (CCl_q), 93.7 (C_{hmb}), 14.7 (CH_3). IR (cm^{-1}): 1638(s), 1617(s), 1498(s), 1370(m), 1164(m), 1031(m), 623(s). Anal. Calc. for $C_{88}H_{92}N_4O_{20}F_{12}S_4Cl_4Ru_4$: C, 43.53; H, 3.82; N, 2.31. Found: C, 43.92; H, 3.94; N, 2.25%. Crystals suitable for X-ray diffraction analysis were obtained by slow diffusion of Et_2O in an acetone solution of [**22**][O_3SCF_3]$_4$.

Cytotoxicity study of supramolecular rectangles

The human A2780 ovarian cancer cell line was obtained from the European Collection of Cell Cultures (Salisbury, UK). Cells were grown routinely in RPMI

medium containing glucose, 5% fetal calf serum (FCS), and antibiotics at 37 °C and 5% CO_2. Cytotoxicity was determined using the MTT assay (MTT = 3-(4,5-dimethyl-2-thiazolyl)-2,5-diphenyl-2*H*-tetrazolium bromide). Cells were seeded in 96-well plates as monolayers with 100 µL of cell solution (approximately 20 000 cells) per well and preincubated for 24 h in medium supplemented with 10% FCS. Compounds were predissolved in DMSO, then added to the culture medium (to give a final DMSO concentration of 0.5%) and serially diluted to the appropriate concentration; 100 µL of drug solution was added to each well, and the plates were incubated for another 72 h. Subsequently, MTT (5 mg/mL solution) was added to the cells, and the plates were incubated for a further 2 h. The culture medium was aspirated, and the purple formazan crystals formed by the mitochondrial dehydrogenase activity of vital cells were dissolved in DMSO. The optical density, directly proportional to the number of surviving cells, was quantified at 540 nm using a multiwell plate reader, and the fraction of surviving cells was calculated from the absorbance of untreated control cells. Evaluation is based on means from two independent experiments, each comprising 3 microcultures per concentration level.

7.2.5 Pyrenyl derivatives

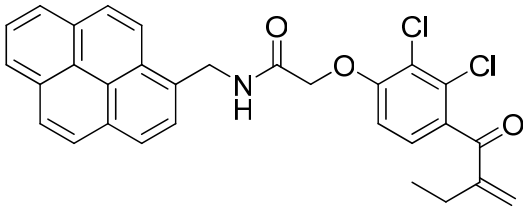

Synthesis of pyrenyl ethacrynic amide (g)

Ethacrynic acid (0.23 g, 0.756 mmol) was suspended in oxalyl chloride (5 mL) and refluxed for 1 h. The unreacted oxalyl chloride was removed by reduced pressure. A suspension of methylamine pyrene (0.202 g, 0.756 mmol) and Et_3N (0.75 mL, 5.3 mmol) in THF (50 mL) was added dropwise to the ethacrynic acid chloride. The mixture was

then stirred at 60°C for 18 h. The solvent was removed by reduced pressure and the product re-dissolved in $CHCl_3$. The solution was filtered and the filtrate was washed with $NaHCO_3$ solution and thereafter brine, dried over $MgSO_4$ and the solvent evaporated to give an oil which was purified on silica gel column, mobile phase CH_2Cl_2:acetone 3:1, to give the product as a pale yellow powder. Yield: 163 mg (39%).

Pyrenyl ethacrynic amide (g). ^{1}H NMR (400 MHz, CD_2Cl_2): δ (ppm) = 8.32 (d, 1H, $^3J_{H-H}$ = 9.24 Hz, H_{py}), 8.24 (m, 2H, H_{py}), 8.20 (d, 1H, $^3J_{H-H}$ = 2.24 Hz, H_{py}), 8.18 (s, 1H, H_{py}), 8.07 (m, 4H, H_{py}), 7.18 (s, 1H, NH), 7.12 (d, 1H, $^3J_{H-H}$ = 8.52 Hz, H_{ar}), 6.89 (d, 1H, $^3J_{H-H}$ = 8.55 Hz, H_{ar}), 5.85 (t, 1H, $^3J_{H-H}$ = 1.38 Hz, $H_{c=c}$), 5.42 (s, 1H, $H_{c=c}$), 5.28 (d, 2H, $^3J_{H-H}$ = 5.80 Hz, Py-*CH*$_2$-NH), 4.68 (s, 2H, CO-*CH*$_2$-O), 2.40 (q, 2H, $^3J_{H-H}$ = 7.41 Hz, C-*CH*$_2$-CH_3), 1.10 (t, 3H, $^3J_{H-H}$ = 7.44 Hz, CH_3). ^{13}C{^{1}H} NMR (100 MHz, CD_2Cl_2): δ (ppm) = 206.5, 195.4, 166.5, 154.7, 150.2, 134.2, 131.4, 131.3, 131.0, 130.8, 128.9, 128.7, 128.3, 127.6, 127.4, 127.3, 126.9, 126.3, 125.6, 125.5, 125.0, 125.0, 124.7, 122.7, 111.3, 68.7, 41.4, 30.7, 23.4, 12.3. IR (cm^{-1}): 3427(br), 3267(m), 1653(vs), 1586(m), 1564(m), 1466(m), 1382(w), 1251(m), 1124(w), 1089(m), 998(w), 849(s), 841(m), 827(w), 797(w), 714(w). MS (ESI, m/z): 553.6 [M(2× ^{35}Cl)+K]$^+$, 555.6 [M(^{35}Cl, ^{37}Cl)+K]$^+$, 557.6 [M(2× ^{37}Cl)+K]$^+$.

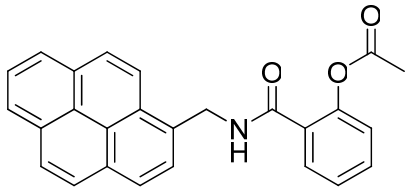

Synthesis of 2-(Pyren-1-ylmethylcarbamoyl) phenyl acetate (h)

Aspirin (150 mg, 0.83 mmol) was suspended in thionyl chloride (20 mL) and stirred for 4 h at room temperature. Thionyl chloride was removed by reduced pressure and then a mixture of 1-pyrenemethylamine (223 mg, 0.83 mmol) and Et_3N (0.12 mL,

0.85 mmol) in THF (50 mL) was slowly added. The mixture was stirred at 60°C for 18 h. The solvent was removed by reduced pressure and the product re-dissolved in $CHCl_3$. The solution was filtered and the filtrate washed with $NaHCO_3$ solution and thereafter brine, dried over $MgSO_4$ and then the solvent evaporated to give an oil which was purified on silica gel column, mobile phase CH_2Cl_2:acetone 3:1, to give the product as a pale yellow powder. Yield: 50 mg (15%).

2-(Pyren-1-ylmethylcarbamoyl) phenyl acetate (**h**). ^{1}H NMR (400 MHz, CD_2Cl_2): δ (ppm) = 8.33 (d, 1H, $^3J_{H-H}$ = 9.25 Hz, H_{py}), 8.21 (m, 4H, H_{py}), 8.06 (m, 4H, H_{py}), 7.38 (ddd, 1H, $^3J_{H-H}$ = 7.81 Hz, $^4J_{H-H}$ = 1.52 Hz, H_{ar}), 7.32 (dd, 1H, $^3J_{H-H}$ = 8.02 Hz, $^4J_{H-H}$ = 1.51 Hz, H_{ar}), 6.97 (dd, 1H, $^3J_{H-H}$ = 8.38 Hz, $^4J_{H-H}$ = 1.02 Hz, H_{ar}), 6.78 (ddd, 1H, $^3J_{H-H}$ = 7.62 Hz, $^4J_{H-H}$ = 1.17 Hz, H_{ar}), 6.75 (br, 1H, NH), 5.35 (d, 2H, $^3J_{H-H}$ = 5.37 Hz, Py-*CH*$_2$-NH), 1.27 (s, 3H, CH_3). ^{13}C{^{1}H} NMR (100 MHz, CD_2Cl_2): δ (ppm) = 169.8, 161.8, 134.4, 131.5, 131.4, 130.8, 130.5, 129.2, 128.5, 127.7, 127.421, 127.3, 126.3, 125.6, 125.5, 125.1, 124.9, 124.7, 122.7, 118.7, 118.5, 114.2, 42.0, 29.8. IR (cm^{-1}): 3332(w), 1635(m), 1583(s), 1537(s), 1493(m), 1443(w), 1356(s), 1300(m), 1246(m), 1229(m), 1216(s), 1033(w), 847(s), 817(w), 758(m), 721(w), 704(w). MS (ESI, m/z): 350.3 [(M-CH_2CO)-H]$^-$.

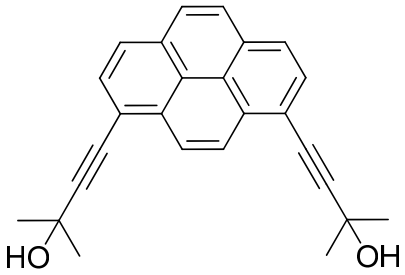

Synthesis of 1,8-Bis(3-methyl-butyn-1-yl-3-ol)pyrene (**i**)

This procedure follows a published method [144]. A Schlenk flask was charged with a solution of 2-methyl-but-3-yn-2-ol (1 mL, 10.3 mmol) in freshly distilled diethylamine (60 mL). The solution was freeze–pump–thaw degassed and transferred to a mixture of 1,6- and 1,8-diiodo pyrene (2.0 g, 4.4 mmol), $Pd[PPh_3]_2Cl_2$ (68 mg), and CuI (0.12 mmol) under nitrogen atmosphere. The reaction mixture was heated at 50 °C under

nitrogen for 20 h. The solvent was removed under vacuum and the product was dissolved in CH_2Cl_2 and filtered. The filtrate was then evaporated and the crude product was purified using column chromatography, eluted with CH_2Cl_2:MeOH (1% MeOH). The product obtained as a yellow solid. Yield 0.1 g (6 %). ^{1}H NMR (400 MHz $CDCl_3$): δ (ppm) = 8.60 (s, 2H), 8.10 (s 4H), 8.04 (s, 2H), 1.81 (s, 12H).

7.2.6 Supramolecular prismatic cages, compound **23-26**

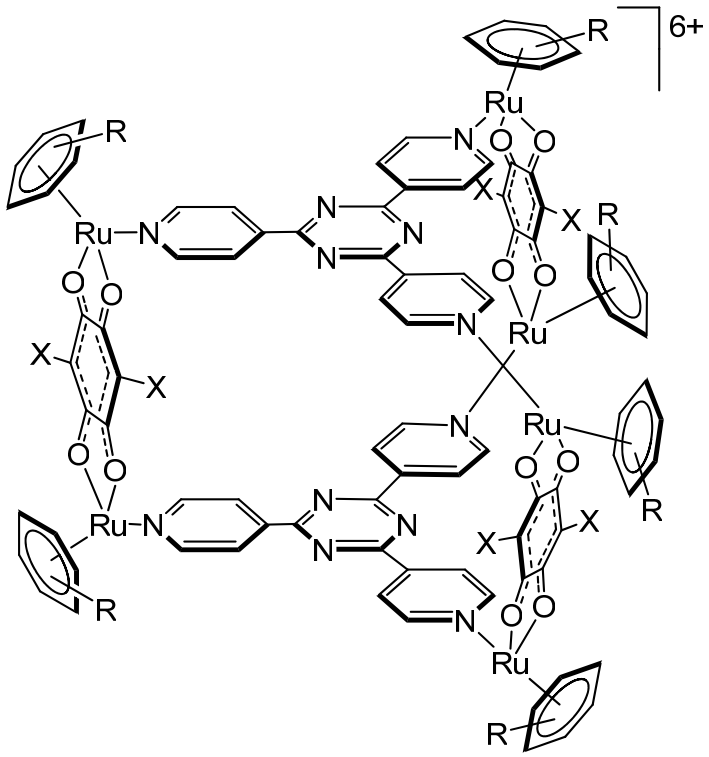

General synthesis of supramolecular prisms

A mixture of bimetallic clip $[(\eta^6\text{-}p\text{-}^i\text{PrC}_6\text{H}_4\text{Me})_2\text{Ru}_2(\text{dhbq})\text{Cl}_2]$ (60 mg, 0.09 mmol) for **23**, $[(\eta^6\text{-}p\text{-}^i\text{PrC}_6\text{H}_4\text{Me})_2\text{Ru}_2$ $(\text{dchq})\text{Cl}_2]$ (67.5 mg, 0.09 mmol) for **24,** $[(\eta^6\text{-}C_6\text{Me}_6)_2\text{Ru}_2(\text{dhbq})\text{Cl}_2]$ (66.7 mg, 0.09 mmol) for **25** and $[(\eta^6\text{-}C_6\text{Me}_6)_2\text{Ru}_2(\text{dchq})\text{Cl}_2]$ (72.4 mg, 0.09 mmol) for **26**) and AgO_3SCF_3 (46 mg, 0.18 mmol) in MeOH (20 mL) was stirred at room temperature for 2 h, then filtered. To the red filtrate was added tpt (18.4

mg, 0.06 mmol). The mixture was stirred at RT for 48 h, and the solvent removed under vacuum. The dark residue was taken up in CH_2Cl_2 (20 mL), and after filtration, the solution was concentrated (3 mL) and Et_2O was added to precipitate a red solid.

[(η^6-*p*-^{i}PrC$_6$H$_4$Me)$_6$Ru$_6$(tpt)$_2$(dhbq)$_3$][O$_3$SCF$_3$]$_6$ ([**23**][O_3SCF_3]$_6$). Yield: 75 mg (75%) ^{1}H NMR (400 MHz, acetone-d_6): δ (ppm) = 8.75 (dd, 12H, $^3J_{H\text{-}H}$ = 5.36 Hz, $^4J_{H\text{-}H}$ = 1.56 Hz, H_α), 8.68 (dd, 12H, H_β), 6.24 (d, 12H, $^3J_{H\text{-}H}$ = 6.32 Hz, H_{ar}), 6.03 (d, 12H, H_{ar}), 5.87 (s, 6H, H_q), 3.00 (sept, 6H, $^3J_{H\text{-}H}$ = 6.92 Hz, CH), 2.28 (s, 18H, CH_3), 1.41 (d, 36H, CH_3). $^{13}C\{^1H\}$ NMR (100 MHz, acetone-d_6): δ (ppm) = 170.0, 154.8, 144.6, 125.1, 123.2, 120.2, 104.4, 102.1, 99.5, 84.2, 82.7, 31.6, 22.0, 17.6. IR (cm^{-1}): 1635(s), 1524(s), 1377(m), 1259(s), 1161(m), 1031(m), 639(s). Anal. Calc. for $C_{120}H_{114}N_{12}O_{30}F_{18}S_6Ru_6$: C, 43.09; H, 3.44; N, 5.02. Found: C, 42.96; H, 3.33; N, 4.86%.

[(η^6-*p*-^{i}PrC$_6$H$_4$Me)$_6$Ru$_6$(tpt)$_2$(dchq)$_3$][O$_3$SCF$_3$]$_6$ ([**24**][O_3SCF_3]$_6$). Yield: 73 mg (68%). ^{1}H NMR (400 MHz, acetone-d_6): δ (ppm) = 8.72 (dd, 12H, $^3J_{H\text{-}H}$ = 5.28 Hz, $^4J_{H\text{-}H}$ = 1.56 Hz, H_α), 8.62 (dd, 12H, H_β), 6.29 (d, 12H, $^3J_{H\text{-}H}$ = 6.44 Hz, H_{ar}), 6.12 (d, 12H, H_{ar}), 3.04 (sept, 6H, $^3J_{H\text{-}H}$ = 6.84 Hz, CH), 2.36 (s, 18H, CH_3), 1.46 (d, 36H, CH_3). $^{13}C\{^1H\}$ NMR (100 MHz, acetone-d_6): δ (ppm) = 178.9, 170.5, 155.1, 145.6, 125.8, 120.6, 107.1, 105.0, 99.9, 84.8, 83.9, 32.2, 22.5, 18.18. IR (cm^{-1}): 1744(s), 1408(s), 1218(s), 1092(s), 1032(s), 904(s), 797(s). Anal. Calc. for $C_{120}H_{108}N_{12}Cl_6O_{30}F_{18}S_6Ru_6$: C, 40.60; H, 3.01; N, 4.73. Found: C, 40.36; H, 3.17; N, 4.52%.

[(η^6-C$_6$Me$_6$)$_6$Ru$_6$(tpt)$_2$(dhbq)$_3$][O$_3$SCF$_3$]$_6$ ([**25**][O_3SCF_3]$_6$). Yield: 50 mg (47%). ^{1}H NMR (400 MHz, acetone-d_6): δ (ppm) = 8.85 (dd, 12H, $^3J_{H\text{-}H}$ = 5.12 Hz, $^4J_{H\text{-}H}$ = 1.48 Hz, H_α), 8.46 (dd, 12H, H_β), 5.84 (s, 6H, H_q), 2.17 (s, 108H, CH_3). $^{13}C\{^1H\}$ NMR (100 MHz, acetone-d_6): δ (ppm) = 183.6, 169.4, 153.7, 144.1, 125.2, 105.3, 101.9, 93.7, 14.7. IR

(cm^{-1}): 1748(s), 1388(s), 1221(s), 1092(s), 781(s). Anal. Calc. for $C_{132}H_{138}N_{12}O_{30}F_{18}S_6Ru_6$: C, 45.12; H, 3.96; N, 4.78. Found: C, 45.54; H, 3.76; N, 4.59%.

[(η^6-C_6Me_6)$_6$$Ru_6(tpt)_2$(dchq)$_3$][$O_3SCF_3$]$_6$ ([**26**][O_3SCF_3]$_6$). Yield: 88 mg (79%). ^{1}H NMR (400 MHz, acetone-d_6): δ (ppm) = 8.89 (dd, 12H, $^3J_{H-H}$ = 6.60 Hz, $^4J_{H-H}$ = 1.44 Hz, H_α), 8.44 (dd, 12H, H_β), 2.20 (s, 108H, CH_3). $^{13}C\{^1H\}$ NMR (100 MHz, acetone-d_6): δ (ppm) = 177.4, 169.5, 153.6, 144.4, 125.5, 108.8, 106.1, 94.0, 14.8. IR (cm^{-1}): 1742(s), 1374(s), 1206(s), 1092(s), 849(s). Anal. Calc. for $C_{132}H_{132}N_{12}O_{30}F_{18}S_6Cl_6Ru_6$: C, 42.62; H, 3.58; N, 4.52. Found: C, 42.81; H, 3.25; N, 4.78%.

7.2.7 Prisms with aromatic guest molecule, aromatic⊂**23**-**26**

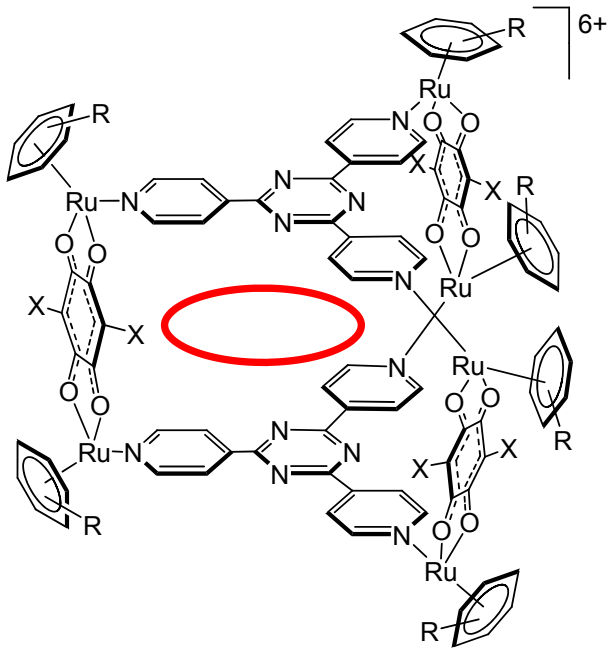

General synthesis of [aromatic⊂23][O_3SCF_3]$_6$

Synthesis of [aromatic⊂**23**][O_3SCF_3]$_6$. A mixture of [(η^6-*p*-^{i}PrC_6H_4Me)$_2$$Ru_2$(dhbq)$Cl_2$] (70 mg, 0.1 mmol) and AgO_3SCF_3 (54 mg, 0.2 mmol) in MeOH (20 mL) was stirred at room temperature for 2 h, then filtered. To the red filtrate was added tpt (21 mg, 0.07 mmol) and the aromatic molecule (pyrene 7.6 mg, 0.038 mmol; fluoranthene 7 mg, 0.035 mmol; triphenylene 9.0 mg, 0.037 mmol; benzo[*e*]pyrene 9.5 mg, 0.038 mmol; coronene 12 mg, 0.036 mmol). The mixture was stirred at room temperature for 24 h, and the solvent removed *in vacuo*. The dark residue was taken up in CH_2Cl_2 (20 mL), and after filtration, the solution was concentrated (3 mL) and Et_2O was added to precipitate a red solid.

[pyrene⊂23][O_3SCF_3]$_6$. Yield: 85 mg (82%). ^{1}H NMR (400 MHz, acetone-d_6): δ (ppm) = 8.56 (dd, 12H, $^3J_{H\text{-}H}$ = 5.04 Hz, $^4J_{H\text{-}H}$ = 1.36 Hz, H_α), 8.04 (dd, 12H H_β), 6.68 (s, 4H, H_g), 6.62 (d, 4H, $^3J_{H\text{-}H}$ = 7.44 Hz, H_g), 6.22 (d, 12H, $^3J_{H\text{-}H}$ = 6.24 Hz, H_{ar}), 6.20 (d, 2H, H_g), 6.17 (s, 6H, H_q), 6.00 (d, 12H, H_{ar}), 2.99 (sept, 6H, $^3J_{H\text{-}H}$ = 7.00 Hz, CH), 2.22 (s, 18H, CH_3), 1.39 (d, 36H, CH_3). ^{13}C{^{1}H} NMR (100 MHz, acetone-d_6): δ (ppm) = 185.1, 168.6, 144.3, 130.3, 127.9, 126.5, 125.1, 123.4, 104.9, 102.8, 100.2, 84.8, 83.1, 32.1, 22.5, 18.1. IR (cm^{-1}): 1638(s), 1617(s), 1524(s), 1377(m), 1259(s), 1159(m), 1030(m), 636(s). Anal. Calc. for $C_{136}H_{124}N_{12}O_{30}F_{18}S_6Ru_6$: C, 45.63; H, 3.49; N, 4.69. Found: C, 45.93; H, 3.77; N, 4.53%.

[fluoranthene⊂23][O_3SCF_3]$_6$. Yield: 85 mg (81%). ^{1}H NMR (400 MHz, acetone-d_6): δ (ppm) = 8.54 (dd, 12H, $^3J_{H\text{-}H}$ = 5.12 Hz, $^4J_{H\text{-}H}$ = 1.48 Hz, H_α), 8.18 (dd, 12H H_β), 6.88 (br, 2H, H_g), 6.67 (d, 2H, $^3J_{H\text{-}H}$ = 7.80 Hz, H_g), 6.47 (d, 2H, $^3J_{H\text{-}H}$ = 6.60 Hz, H_g), 6.21 (d, 12H, $^3J_{H\text{-}H}$ = 6.36 Hz, H_{ar}), 6.11 (s, 6H, H_q), 5.99 (d, 12H, H_{ar}), 5.35 (br, 2H, H_g), 5.23 (br, 2H, H_g), 2.98 (sept, 6H, $^3J_{H\text{-}H}$ = 7.08 Hz, CH), 2.22 (s, 18H, CH_3), 1.39 (d, 36H, CH_3). ^{13}C{^{1}H} NMR (100 MHz, acetone-d_6): δ (ppm) = 184.1, 168.2, 153.8, 143.5, 134.7, 128.3, 126.7, 124.5, 121.5, 120.1, 117.0, 113.2, 104.0, 101.9, 99.3, 83.9, 82.2, 31.2, 21.6, 17.2. IR (cm^{-1}): 1716(s), 1524(m), 1435(m), 1363(s), 1221(s), 1092(m),

1032(m), 850(s). Anal. Calc. for $C_{136}H_{124}N_{12}O_{30}F_{18}S_6Ru_6$: C, 46.05; H, 3.52; N, 4.74. Found: C, 46.21; H, 3.85; N, 4.63%.

[triphenylene⊂23][O_3SCF_3]$_6$. Yield: 95 mg (72%). ^{1}H NMR (400 MHz, acetone-d_6): δ (ppm) = 8.47 (d, 12H, $^3J_{H\text{-}H}$ = 6.08 Hz, H_α), 8.10 (d, 12H, H_β), 7.62 (dd, 6H, $^3J_{H\text{-}H}$ = 2.72 Hz, H_g), 6.20 (d, 12H, $^3J_{H\text{-}H}$ = 6.24 Hz, H_{ar}), 6.16 (s, 6H, H_q), 5.98 (d, 12H, H_{ar}), 5.35 (dd, 6H, H_g), 2.96 (sept, 6H, $^3J_{H\text{-}H}$ = 6.80 Hz, CH), 2.21 (s, 18H, CH_3), 1.38 (d, 36H, CH_3). $^{13}C\{^1H\}$ NMR (100 MHz, acetone-d_6): δ (ppm) = 184.6, 168.2, 153.9, 143.5, 128.6, 127.0, 125.0, 123.4, 104.5, 102.4, 99.7, 84.4, 82.7, 31.6, 22.1, 17.7. IR (cm^{-1}): 1638(s), 1617(s), 1524(s), 1377(s), 1259(s), 1162(m), 1031(s), 638(s). Anal. Calc. for $C_{138}H_{126}N_{12}O_{30}F_{18}S_6Ru_6$: C, 45.97; H, 3.52; N, 4.66. Found: C, 45.81; H, 3.88; N, 4.45%.

[benzo[*e*]pyrene⊂23][O_3SCF_3]$_6$. Yield: 90 mg (68%). ^{1}H NMR (400 MHz, acetone-d_6): δ (ppm) = 8.48 (d, 12H, $^3J_{H\text{-}H}$ = 5.20 Hz, H_α), 7.90 (d, 2H, $^3J_{H\text{-}H}$ = 8.00 Hz, H_g), 7.88 (d, 12H, H_β), 7.82 (dd, 4H, $^3J_{H\text{-}H}$ = 5.96 Hz, H_g), 7.39 (s, 2H, H_g), 6.27 (s, 6H, H_q), 6.20 (d, 12H, $^3J_{H\text{-}H}$ = 6.24 Hz, H_{ar}), 5.99 (d, 12H, H_{ar}), 5.75 (dd, 2H, $^3J_{H\text{-}H}$ = 7.48 Hz, H_g), 5.50 (dd, 2H, H_g), 2.97 (sept, 6H, $^3J_{H\text{-}H}$ = 6.92 Hz, CH), 2.21 (s, 18H, CH_3), 1.40 (d, 36H, CH_3). $^{13}C\{^1H\}$ NMR (100 MHz, acetone-d_6): δ (ppm) = 184.3, 167.4, 153.4, 142.7, 128.2, 126.3, 124.2, 122.4, 120.4, 119.7, 118.3, 113.4, 106.7, 104.1, 102.0, 99.2, 83.9, 82.3, 31.2, 21.6, 17.2. IR (cm^{-1}): 1634(s), 1619(s), 1524(s), 1375(s), 1225(m), 1160(m), 1031(s), 638(s). Anal. Calc. for $C_{140}H_{126}N_{12}O_{30}F_{18}S_6Ru_6$: C, 46.74; H, 3.53; N, 4.67. Found: C, 46.72; H, 3.80; N, 4.42%.

[coronene⊂23][O_3SCF_3]$_6$. Yield 95 mg (70%). ^{1}H NMR (200 MHz, acetone-d_6): δ (ppm) = 8.48 (dd, 12H, $^3J_{H\text{-}H}$ = 5.50 Hz, $^4J_{H\text{-}H}$ = 1.48 Hz, H_α), 7.50 (s, 12H, H_g), 7.20 (dd, 12H, H_β), 6.53 (s, 6H, H_q), 6.19 (d, 12H, $^3J_{H\text{-}H}$ = 6.60 Hz, H_{ar}), 5.97 (d, 12H, H_{ar}), 3.03 (sept, 6H, $^3J_{H\text{-}H}$ = 6.96 Hz, CH), 2.21 (s, 18H, CH_3), 1.40 (d, 36H, CH_3). $^{13}C\{^1H\}$ NMR (100 MHz, acetone-d_6): δ (ppm) = 184.5, 166.3, 153.5, 141.8, 127.6, 126.0, 123.5, 120.8,

104.1, 102.3, 99.1, 83.8, 82.4, 31.2, 21.6, 17.2. IR (cm^{-1}): 1638(s), 1617(s), 1522(s), 1377(s), 1259(s), 1225(m), 1161(s), 1030(s), 638(s). Anal. Calc. for $C_{144}H_{126}N_{12}O_{30}F_{18}S_6Ru_6$: C, 51.03; H, 3.74; N, 4.96. Found: C, 51.09; H, 3.83; N, 4.29%.

General synthesis of [aromatic⊂24][O_3SCF_3]$_6$

These carceplex systems are prepared in the same procedure as described above for [aromatic⊂**23**][O_3SCF_3]$_6$ using [(η^6-*p*-^{i}PrC_6H_4Me)$_2$$Ru_2$(dchq)$Cl_2$] (70mg, 0.09 mmol), AgO_3SCF_3 (49 mg, 0.19 mmol), tpt (20 mg, 0.06 mmol), and the aromatic molecule (fluoranthene 7 mg, 0.03 mmol; triphenylene 8 mg, 0.03 mmol).

[fluoranthene⊂24][O_3SCF_3]$_6$. Yield: 87 mg (75%). ^{1}H NMR (400 MHz, acetone-d_6): δ (ppm) = 8.59 (m, 24H, H_α, H_β), 6.81 (m, 2H, H_g), 6.57 (m, 2H, H_g), 6.43 (m, 2H, H_g), 6.30 (d, 8H, $^3J_{H\text{-}H}$ = 6.33 Hz, H_{ar}), 6.12 (d, 12H, $^3J_{H\text{-}H}$ = 5.49 Hz, H_{ar}), 5.32 (m, 2H, H_g), 5.12 (m, 2H, H_g), 3.05 (sept, 6H, $^3J_{H\text{-}H}$ = 6.94 Hz, CH), 2.35 (s, 18H, CH_3), 1.46 (d, 36H, $^3J_{H\text{-}H}$ = 6.92 Hz, CH_3). ^{13}C{^{1}H} NMR (100 MHz, acetone-d_6): δ (ppm) = 177.9, 153.9, 144.3, 135.8, 129.8, 127.5, 127.2, 125.9, 124.0, 122.5, 120.9, 120.8, 120.7, 106.5, 104.4, 99.3, 84.1, 83.1, 31.5, 21.7, 17.4. IR (cm^{-1}): 1618(w), 1574(w), 1500(vs), 1373(s), 1313(w), 1258(s), 1224(m), 1159(m), 1057(w), 1030(s), 867(w), 810(w), 638(s). Anal. Calc. for $C_{140}H_{126}N_{12}O_{30}F_{18}S_6Ru_6$: C, 43.51; H, 3.17; N, 4.48. Found: C, 36.46; H, 3.25; N, 4.49%.

[triphenylene⊂24][O_3SCF_3]$_6$. Yield: 80 mg (68%). ^{1}H NMR (400 MHz, acetone-d_6): δ (ppm) = 8.47 (d, 12H, $^3J_{H\text{-}H}$ = 6.60 Hz, H_α), 8.22 (d, 12H, H_β), 7.63 (dd, 6H, $^3J_{H\text{-}H}$ = 6.08 Hz, H_g), 6.31 (d, 12H, $^3J_{H\text{-}H}$ = 6.36 Hz, H_{ar}), 6.12 (d, 12H, H_{ar}), 5.14 (dd, 6H, H_g), 3.03 (sept, 6H, $^3J_{H\text{-}H}$ = 7.12 Hz, CH), 2.32 (s, 18H, CH_3), 1.46 (d, 36H, CH_3). ^{13}C{^{1}H} NMR (100 MHz, acetone-d_6): δ (ppm) = 177.7, 167.9, 153.3, 143.4, 128.4, 126.0, 125.0, 123.3, 120.5, 106.7, 104.4, 99.4, 84.1, 83.0, 31.5, 21.6, 17.3. IR (cm^{-1}): 1723(s), 1504(s), 1414(s), 1227(s), 1152(m), 1032(m), 1092(s), 901(s), 829(s). Anal. Calc. for

$C_{138}H_{120}N_{12}O_{30}F_{18}S_6Cl_6Ru_6$: C, 43.85; H, 3.20; N, 4.45. Found: C,43.45; H, 3.61; N, 4.25%.

General synthesis of [aromatic⊂25][O_3SCF_3]$_6$

These carceplex systems are prepared in the same procedure as described above for [aromatic⊂**23**][O_3SCF_3]$_6$ using [(η^6-C_6Me_6)$_2$$Ru_2$(dhbq)$Cl_2$] (60 mg, 0.08 mmol), AgO_3SCF_3 (43 mg, 0.016 mmol), tpt (17 mg, 0.05 mmol), and the aromatic molecule (fluoranthene 6 mg, 0.03 mmol; triphenylene 6 mg, 0.03 mmol).

[fluoranthene⊂25][O_3SCF_3]$_6$. Yield 55 mg (51%). ^{1}H NMR (400 MHz, acetone-d_6): δ (ppm) = 8.37 (m, 24H, H_α, H_β), 6.85 (dd, 2H, $^3J_{H\text{-}H}$ = 3.15, 5.39 Hz, H_g), 6.58 (d, 2H, $^3J_{H\text{-}H}$ = 8.10 Hz, H_g), 6.47 (d, 2H, $^3J_{H\text{-}H}$ = 6.60 Hz, H_g), 6.04 (s, 6H, H_q), 5.36 (dd, 2H, $^3J_{H\text{-}H}$ = 7.51 Hz, H_g), 5.14 (m, 2H, H_g), 2.16 (s, 108H, CH_3). ^{13}C{^{1}H} NMR (100 MHz, acetone-d_6): δ (ppm) = 184.3, 153.7, 144.1, 138.3, 135.3, 134.5, 127.3, 127.2, 125.6, 123.8, 122.1, 120.7, 120.6, 102.5, 94.3, 15.2. IR (cm^{-1}): 1628(w), 1518(vs), 1374(s), 1257(s), 1157(w), 1031(m), 811(w), 638(m). Anal. Calc. for $C_{148}H_{148}Cl_6N_{12}O_{30}F_{18}S_6Ru_6$ ·4H_2O: C, 44.44; H, 3.93; N, 4.20. Found: C, 44.47; H, 4.41; N, 4.32%.

[triphenylene⊂25][O_3SCF_3]$_6$. Yield: 50 mg (49%). ^{1}H NMR (400 MHz, acetone-d_6): δ (ppm) = 8.30 (dd, 12H, $^3J_{H\text{-}H}$ = 5.08 Hz, H_α), 8.20 (dd, 12H, H_β), 7.59 (dd, 6H, $^3J_{H\text{-}H}$ = 4.68 Hz, H_g), 6.14 (s, 6H, H_q), 5.32 (dd, 6H, H_g), 2.15 (s, 108H, CH_3). ^{13}C{^{1}H} NMR (100 MHz, acetone-d_6): δ (ppm) = 184.6, 169.2, 153.5, 144.5, 128.4, 126.3, 125.9, 123.2, 108.6, 103.5, 94.6, 15.5. IR (cm^{-1}): 1759(s), 1523(m), 1448(s), 1224(s), 1032(m), 904(s). Anal. Calc. for $C_{150}H_{150}N_{12}O_{30}F_{18}S_6Ru_6$: C, 48.15; H, 4.05; N, 4.49. Found: C, 48.36; H, 4.06; N, 4.09%.

General synthesis of [aromatic⊂26][O_3SCF_3]$_6$

These carceplex systems are prepared in the same procedure as described above for [aromatic⊂**23**][O_3SCF_3]$_6$ using [(η^6-C_6Me_6)$_2$$Ru_2$(dchq)$Cl_2$] (60 mg, 0.07 mmol), AgO_3SCF_3 (39 mg, 0.015 mmol), tpt (16 mg, 0.05 mmol), and aromatic molecules (fluoranthene 6 mg, 0.03 mmol; triphenylene 6 mg, 0.03 mmol).

[fluoranthene⊂26][O_3SCF_3]$_6$. Yield: 77 mg (77%). ^{1}H NMR (400 MHz, acetone-d_6): δ (ppm) = 8.36 (m, 24H, H_α, H_β), 6.86 (m, 2H, H_g), 6.50 (m, 4H, H_g), 5.38 (m, 2H, H_g), 5.08 (m, 2H, H_g), 2.20 (s, 108H, CH_3). ^{13}C{^{1}H} NMR (100 MHz, acetone-d_6): δ (ppm) = 178.1, 169.0, 153.8, 144.6, 127.3, 127.2, 126.4, 124.2, 122.7, 121.1, 121.0, 107.3, 95.1, 15.8. IR (cm^{-1}): 1623(br), 1574(w), 1500(vs), 1372(s), 1263(s), 1152(m), 1031(s), 866(w), 811(w), 637(m). Anal. Calc. for $C_{148}H_{142}Cl_6N_{12}O_{30}F_{18}S_6Ru_6$: C, 45.32; H, 3.65; N, 4.29. Found: C, 37.93; H, 3.45; N, 3.64%.

[triphenylene⊂26][O_3SCF_3]$_6$. Yield: 55 mg (56%). ^{1}H NMR (400 MHz, acetone-d_6): δ (ppm) = 8.33 (dd, 12H, $^3J_{H\text{-}H}$ = 5.00 Hz, H_α), 8.27 (dd, 12H, H_β), 7.58 (dd, 6H, $^3J_{H\text{-}H}$ = 6.12 Hz, H_g), 5.12 (dd, 6H, H_g), 2.19 (s, 108H, CH_3). ^{13}C{^{1}H} NMR (100 MHz, acetone-d_6): δ (ppm) = 177.1, 167.6, 163.7, 152.4, 143.2, 126.0, 125.5, 123.2, 110.9, 106.4, 94.1, 14.8. IR (cm^{-1}): 1709(s), 1411(m), 1217(s), 1093(s), 1032(m), 906(s), 787(s). Anal. Calc. for $C_{150}H_{144}N_{12}O_{30}F_{18}S_6Cl_6Ru_6$: C, 45.63; H, 3.68; N, 4.26. Found: C, 45.32; H, 3.76; N, 4.21%.

7.2.8 Prisms with functionalized pyrenyl derivatives, **a-i⊂23**

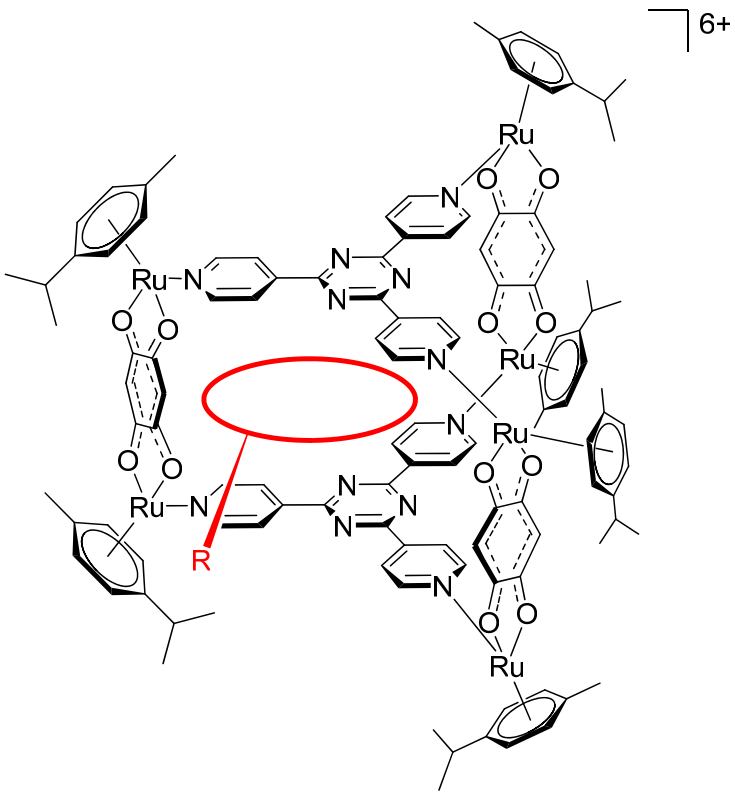

General synthesis of [a–i⊂23][O_3SCF_3]$_6$

[(η^6-*p*-^{i}PrC$_6$H$_4$Me)$_2$Ru$_2$(dhbq)Cl$_2$] (50 mg, 0.0736 mmol) and AgO_3SCF_3 (38 mg, 0.147 mmol) was stirred in MeOH (30 mL) for 2 h, thereafter the solution was filtered into a suspension of tpt (15 mg, 0.049 mmol) and pyrenyl (1-pyrenebutanol 6.8 mg, 0.025 mmol; 1-pyrenemethyl butanoate 7.5 mg, 0.025 mmol; 1-pyrenebutyric acid 7.1 mg, 0.025 mmol; 1-pyrenemethylamine 6.7 mg, 0.025 mmol; *N*-hexadecylpyrene-1-sulfonamide 12.6 mg, 0.025 mmol; 1-(4,6-dichloro-1,3,5-triazin-2yl)pyrene 8.8 mg, 0.025 mmol; pyrenyl ethacrynic amide 12.7 mg, 0.025 mmol; 2-(pyren-1-ylmethylcarbamoyl) phenyl acetate 9.7 mg, 0.025 mmol) in MeOH (10 mL). The mixture was stirred at RT for 18 h. The MeOH was removed under reduced pressure and then the product re-dissolved in CH_2Cl_2 before being filtered. The filtrate was reduced to about 5 mL and the product precipitated with Et_2O and collected by filtration as a red powder.

[a⊂23][O_3SCF_3]$_6$. Yield: 68 mg (77%). ^{1}H NMR (400 MHz acetone-d_6): δ (ppm) = 8.58 (d, 12H, $^3J_{H-H}$ = 6.39 Hz, H_α), 8.07 (br, 12H, H_β), 7.24 (d, 1H, $^3J_{H-H}$ = 4.43 Hz, H_g), 7.11 (m, 1H, H_g), 6.99 (br, 1H, H_g), 6.91 (br, 1H, H_g), 6.57 (br, 1H, H_g), 6.34(br, 1H, H_g), 6.22 (d, 12H, $^3J_{H-H}$ = 6.24 Hz, H_{ar}), 6.18 (s, 6H, H_q), 6.13 (br, 2H, H_g), 6.00 (d, 12H, H_{ar}), 5.85 (br, 1H, H_g), 2.98 (sept, 6H, $^3J_{H-H}$ = 6.91 Hz, CH), 2.62 (br, 2H, H_g), 2.50 (br, 2H, H_g), 2.22 (s, 18H, CH_3), 1.62 (br, 2H, H_g), 1.39 (d, 36H, CH_3). ^{13}C{^{1}H} NMR (100 MHz, acetone-d_6): δ (ppm) = 184.3, 167.9, 154.0, 143.5, 124.3, 104.2, 102.1, 99.4, 84.0, 82.4, 31.3, 21.7, 17.3. IR (cm^{-1}): 1524(s), 1377(s), 1258(s), 1224(w), 1159(w), 1030(m), 811(w), 638(w). MS (ESI-MS) *m/z*: 1062.42 [**a⊂23** + $(O_3SCF_3)_3]^{3+}$, 759.32 [**a⊂23** + $(O_3SCF_3)_2]^{4+}$. UV-visible (MeOH): λ_{max} 495 (45500), 351 (42300), 304 (81000), 281 (57500), 271 (54300) nm.

[b⊂23][O_3SCF_3]$_6$. Yield: 78 mg (88%). ^{1}H NMR (400 MHz acetone-d_6): δ (ppm) = 8.58 (d, 12H, $^3J_{H-H}$ = 6.4Hz H_α), 8.06 (br, 12H, H_β), 7.03 (d, 1H, $^3J_{H-H}$ = 8.8 Hz, H_g), 6.95 (d, 1H, $^3J_{H-H}$ = 6.8 Hz, H_g), 6.87 (d, 1H, $^3J_{H-H}$ = 8.4 Hz, H_g), 6.52 (d, 1H, $^3J_{H-H}$ = 8.8 Hz, H_g), 6.22 (d, 12H, $^3J_{H-H}$ = 6.4 Hz, H_{ar}), 6.18 (s, 6H, H_q), 6.00 (d, 12H, H_{ar}), 3.76 (d, 2H, $^3J_{H-H}$ = 5.2 Hz, H_g), 2.98 (sept, 6H, $^3J_{H-H}$ = 6.8 Hz, CH), 2.52 (t, 2H $^3J_{H-H}$ = 7.2 Hz, H_g), 2.22 (s, 18H, CH_3), 1.63 (m, 2H, H_g), 1.47 (m, 2H, H_g), 1.39 (d, 36H, $^3J_{H-H}$ = 7.2 Hz, CH_3). ^{13}C{^{1}H} NMR (100 MHz, acetone-d_6): δ (ppm) = 185.1, 168.6, 154.8, 144.3, 137.5, 130.7, 130.1, 128.9, 128.4, 128.0, 127.6, 127.1, 126.6, 126.6, 125.7, 125.4, 125.4, 125.1, 124.0, 123.8, 123.7, 123.2, 120.8, 105.0, 102.9, 100.2, 84.8, 83.1, 62.3, 33.7, 33.2, 32.1, 22.5, 18.1. IR (cm^{-1}): 1523(s), 1377(s), 1258(s), 1224(w), 1159(w), 1030(m), 811(w), 638(w). MS (ESI-MS) *m/z*: 1057.79 [**b⊂23** + $(O_3SCF_3)_3]^{3+}$, 756.09 [**b⊂23** + $(O_3SCF_3)_2]^{4+}$. UV-visible (MeOH): λ_{max} 493 (44800), 342 (47300), 308 (80800), 275 (64300).

[c⊂23][O_3SCF_3]$_6$. Yield: 49 mg (56%). ^{1}H NMR (400 MHz acetone-d_6): δ (ppm) = 8.59 (br, 12H, H_α), 8.22 (br, 12H, H_β), 6.20 (d, 12H, $^3J_{H-H}$ = 6.21 Hz, H_{ar}), 6.14 (s, 6H, H_q), 5.99 (d, 12H, H_{ar}), 2.98 (sept, 6H, $^3J_{H-H}$ = 6.96 Hz, CH), 2.22 (s, 18H, CH_3), 1.40 (d, 36H,

CH_3). $^{13}C\{^1H\}$ NMR (100 MHz, acetone-d_6): δ (ppm) = 185.2, 154.0, 124.4, 104.1, 101.9, 99.2, 83.8, 82.3, 31.4, 21.6, 17.3. IR (cm^{-1}): 1524(s), 1377(s), 1259(s), 1225(w), 1161(w), 1031(m), 812(w), 639(w). MS (ESI-MS) *m/z*: 1043.41 [**c**⊂**23** + $(O_3SCF_3)_3]^{3+}$, 745.07 [**c**⊂**23** + $(O_3SCF_3)_2]^{4+}$. UV-visible (MeOH): λ_{max} 494 (43100), 341 (54300), 309 (83200), 275 (73200) nm.

[d⊂23][O_3SCF_3]$_6$. Yield: 64 mg (72%). ^1H NMR (400 MHz acetone-d_6): δ (ppm) = 8.58 (d, 12H, $^3J_{H\text{-}H}$ = 6.54 Hz, H_α), 8.10 (br, 12H, H_β), 7.14 (d, 1H, $^3J_{H\text{-}H}$ = 9.11 Hz, H_g), 6.98 (d, 1H, $^3J_{H\text{-}H}$ = 7.42 Hz, H_g), 6.92 (d, 1H, $^3J_{H\text{-}H}$ = 8.88 Hz, H_g), 6.33 (dd, 1H, $^3J_{H\text{-}H}$ = 7.41 Hz, H_g), 6.26 (br, 1H, H_g), 6.22 (d, 12H, $^3J_{H\text{-}H}$ = 6.31 Hz, H_{ar}), 6.19 (m, 1H, H_g), 6.16 (s, 6H, H_q), 6.08 (d, 1H, $^3J_{H\text{-}H}$ = 7.56 Hz, H_g), 6.00 (d, 12H, $^3J_{H\text{-}H}$ = 6.31 Hz, H_{ar}), 5.85 (d, 1H, $^3J_{H\text{-}H}$ = 7.53 Hz, H_g), 3.80 (s, 3H, H_g), 2.98 (sept, 6H, $^3J_{H\text{-}H}$ = 6.94 Hz, CH), 2.54 (m, 4H, H_g), 2.23 (s, 18H, CH_3), 1.67 (m, 2H, H_g), 1.40 (d, 36H, $^3J_{H\text{-}H}$ = 6.94 Hz, CH_3). $^{13}C\{^1H\}$ NMR (100 MHz, acetone-d_6): δ (ppm) = 185.2, 183.1, 168.8, 154.9, 144.4, 128.6, 127.9, 127.4, 126.7, 126.5, 125.9, 125.5, 125.3, 125.2, 124.1, 123.6, 123.2, 123.1, 120.9, 105.1, 102.9, 84.8, 83.3, 52.3, 34.3, 32.2, 26.9, 22.6, 18.2. IR (cm^{-1}): 1731(w), 1523(vs), 1376(s), 1258(s), 1159(w), 1057(w), 1030(m), 811(w), 638(m). MS (ESI-MS) *m/z*: 1067.10 [**d**⊂**23** + $(O_3SCF_3)_3]^{3+}$, 1674.70 [**d**⊂**23** + $(O_3SCF_3)_4]^{2+}$. UV-visible (CH_2Cl_2): λ_{max} 494 (46100), 342 (83800), 298 (113100), 275 (147200), 242 (260800), 211 (274300) nm.

[e⊂23][O_3SCF_3]$_6$. Yield: 59 mg (65%). ^1H NMR (400 MHz acetone-d_6): δ (ppm) = 8.54 (br, 12H, H_α), 8.00 (br, 12H, H_β), 6.20 (d, 12H, $^3J_{H\text{-}H}$ = 6.02 Hz, H_{ar}), 6.18 (s, 6H, H_q), 5.98 (d, 12H, H_{ar}), 2.97 (sept, 6H, $^3J_{H\text{-}H}$ = 6.68 Hz, CH), 2.21 (s, 18H, CH_3), 1.39 (d, 36H, CH_3). $^{13}C\{^1H\}$ NMR (100 MHz, acetone-d_6): δ (ppm) = 184.4, 154.1, 124.3, 104.3, 102.2, 99.3, 83.9, 82.4, 31.3, 21.7, 17.3. IR (cm^{-1}): 1523(s), 1377(s), 1258(s), 1224(w), 1159(w), 1030(m), 811(w), 638(w). MS (ESI-MS) m/z: 1081.40 [**e**⊂**23** + $(O_3SCF_3)_3]^{3+}$,

773.81 [**e⊂23** + $(O_3SCF_3)_2$]$^{4+}$. UV-visible (MeOH): λ_{max} 491 (49200), 373 (51000), 300 (99300), 271 (67300) nm.

[f⊂23][O_3SCF_3]$_6$. Yield: 61 mg (65%). ^{1}H NMR (400 MHz acetone-d_6): δ (ppm) = 8.63 (br, 12H, H_α), 8.42 (br, 12H, H_β), 6.22 (d, 12H, $^3J_{H\text{-}H}$ = 6.46 Hz, H_{ar}), 6.02 (s, 6H, H_q), 6.01 (d, 12H, H_{ar}), 2.99 (sept, 6H, $^3J_{H\text{-}H}$ = 6.93 Hz, CH), 2.25 (s, 18H, CH_3), 1.40 (d, 36H, CH_3). $^{13}C\{^1H\}$ NMR (100 MHz, acetone-d_6): δ (ppm) = 184.3, 154.3, 124.8, 104.2, 102.0, 99.3, 83.9, 82.4, 31.4, 21.8, 17.5. IR (cm^{-1}): 1523(s), 1377(s), 1258(s), 1224(w), 1158(w), 1030(m), 811(w), 638(w). MS (ESI-MS) *m/z*: 1134.48 [**f⊂23** + $(O_3SCF_3)_3$]$^{3+}$, 813.63 [**f⊂23** + $(O_3SCF_3)_2$]$^{4+}$. UV-visible (MeOH): λ_{max} 492 (38700), 351 (41100), 301 (76400), 281 (65800) nm.

[g⊂23][O_3SCF_3]$_6$. Yield: 75 mg (78%). ^{1}H NMR (400 MHz acetone-d_6): δ (ppm) = 8.56 (br, 12H, H_α), 8.36 (br, 2H, H_g), 8.00 (br, 12H, H_β), 7.56 (br, 2H, H_g), 7.23 (br, 1H, H_g), 7.09 (br, 1H, H_g), 6.80 (br, 1H, H_g), 6.20 (d, 12H, $^3J_{H\text{-}H}$ = 6.08 Hz, H_{ar}), 6.18 (s, 6H, H_q), 6.05 (br, 2H, H_g), 5.99 (d, 12H, H_{ar}), 5.83 (br, 2H, H_g), 5.79 (br, 2H, H_g), 5.18 (s, 2H, H_g), 4.52 (br, 2H, H_g), 2.98 (sept, 6H, $^3J_{H\text{-}H}$ = 6.93 Hz, CH), 2.53 (q, 2H, $^3J_{H\text{-}H}$ = 7.07 Hz, H_g), 2.23 (s, 18H, CH_3), 1.39 (d, 36H, CH_3), 1.21 (t, 3H, H_g). $^{13}C\{^1H\}$ NMR (100 MHz, acetone-d_6): δ (ppm) = 184.3, 167.6, 154.0, 124.3, 104.2, 102.0, 99.2, 83.9, 82.5, 31.3, 21.7, 17.3. IR (cm^{-1}): 1524(s), 1377(s), 1259(s), 1225(w), 1159(w), 1031(m), 811(w), 638(w). MS (ESI-MS) m/z: 1138.42 [**g⊂23** + $(O_3SCF_3)_3$]$^{3+}$, 816.32 [**g⊂23** + $(O_3SCF_3)_2$]$^{4+}$. UV-visible (MeOH): λ_{max} 492 (44700), 341 (56300), 309 (83900), 275 (76000) nm.

[h⊂23][O_3SCF_3]$_6$. Yield: 66 mg (72%). ^{1}H NMR (400 MHz acetone-d_6): δ (ppm) = 9.12 (br, 1H, H_g), 8.56 (br, 12H, H_α), 7.97 (br, 12H, H_β), 7.73 (br, 2H, H_g), 7.39 (br, 2H, H_g), 7.25 (br, 1H, H_g), 6.95 (br, 2H, H_g), 6.19 (br, 19H, H_{ar}, H_q, H_g), 5.99 (br, 13H, H_{ar}, H_g),

4.79 (br, 2H, H_g), 2.98 (sept, 6H, $^3J_{H\text{-}H}$ = 6.64 Hz, CH), 2.26 (s, 18H, CH_3), 1.41 (d, 36H, CH_3). $^{13}C\{^1H\}$ NMR (100 MHz, acetone-d_6): δ (ppm) = 184.2, 167.6, 153.9, 124.3, 104.1, 101.9, 83.9, 82.5, 65.3, 31.3, 21.7, 17.3, 14.8. IR (cm^{-1}): 1524(s), 1377(s), 1258(s), 1224(w), 1158(w), 1030(m), 811(w), 637(w). MS (ESI-MS) m/z: 1083.46 [**h⊂23** – CH_3CO + $(O_3SCF_3)_3]^{3+}$, 775.34 [**h⊂23** – CH_3CO + $(O_3SCF_3)_2]^{4+}$. UV-visible (MeOH): λ_{max} 495 (43400), 350 (45700), 342 (45600), 306 (81200), 281 (58500), 276 (57600) nm.

[i⊂23][O_3SCF_3]$_6$. Yield 78 mg (85%). ^1H NMR (400 MHz acetone-d_6): δ (ppm) = 8.56 (br, 12H, H_α), 8.03 (br, 12H, H_β), 7.08 (br, 1H, H_g), 6.79 (br, 2H, H_g), 6.38 (br, 4H, H_q), 6.21 (d, 12H, $^3J_{H\text{-}H}$ = 6.11 Hz, H_{ar}), 6.21 (br, 2H, H_q), 6.06 (br, 1H, H_g), 5.99 (d, 12H, H_{ar}), 5.80 (br, 2H, H_g), 5.54 (br, 1H, H_g), 5.06 (br, 2H, H_g), 2.98 (sept, 6H, $^3J_{H\text{-}H}$ = 6.89 Hz, CH), 2.20 (s, 18H, CH_3), 1.74 (s, 12H, H_g), 1.38 (d, 36H, CH_3). $^{13}C\{^1H\}$ NMR (100 MHz, acetone-d_6): δ (ppm) = 185.0, 154.9, 125.2, 105.0, 100.2, 84.8, 83.0, 32.0, 22.5, 18.1. IR (cm^{-1}) : 1524(s), 1377(s), 1259(s), 1161(w), 1030(m), 811(w), 638(w). MS (ESI-MS) m/z: 1705.13 [**i⊂23** + $(O_3SCF_3)_4]^{2+}$, 1088.44 [**i⊂23** + $(O_3SCF_3)_3]^{3+}$. UV-visible (MeOH): λ_{max} 491 (50600), 383 (90200), 362 (68700), 345 (47100), 301 (88300), 290 (106000), 278 (71500) nm.

Cytotoxicity study of supramolecular prism encapsulating functionalized pyrenyl derivatives

Human A2780 ovarian carcinoma cells were obtained from the European Centre of Cell Cultures (ECACC, Salisbury, UK) and maintained in culture as described by the provider. The cells were routinely grown in RPMI 1640 medium with GlutaMAX™ containing 5% fetal calf serum (FCS) and antibiotics (penicillin and ciproxin) at 37 °C and 5% CO_2. For the evaluation of growth inhibition, the cells were seeded in 96-well plates ($25x10^3$ cells per well) and grown for 24 h in complete medium. Complexes were added to the required concentration and added to the cell culture for 72 h incubation. Solutions of the compounds were applied by diluting a freshly prepared stock solution of the corresponding compound in aqueous RPMI medium with GlutaMAX™ (20 mM).

Following drug exposure, 3-(4,5-dimethylthiazol-2-yl)-2,5-diphenyl-2*H*-tetrazolium bromide (MTT) was added to the cells at a final concentration of 0.25 mg/ml and incubated for 2 h, then the culture medium was aspirated and the violet formazan (artificial chromogenic precipitate of the reduction of tetrazolium salts by dehydrogenases and reductases) dissolved in DMSO. The optical density of each well (96-well plates) was quantified three times in tetraplicates at 540 nm using a multiwell plate reader (iEMS Reader MF, Labsystems, US), and the percentage of surviving cells was calculated from the ratio of absorbance of treated to untreated cells. The IC_{50} values for the inhibition of cell growth were determined by fitting the plot of the logarithmic percentage of surviving cells against the logarithm of the drug concentration using a linear regression function. The median value and the median absolute deviation were obtained from the Excel™ software (Microsoft ™).

8. References

1. Z. Huaizhi, N. Yuantao, *Gold Bulletin* **2001**, *31*, 24
2. A. Yarnell, *Chemical & engineering news* **2005**, *83*, 3
3. in *Cancer Statistics 2009*, American Cancer Society.
4. Available from: http://ec.europa.eu/health/ph_information/dissemination/diseases/cancer_en.htm.
5. J. S. Sebolt-Leopold, J. M. English, *Nature* **2006**, *441*, 457
6. B. Rosenberg, L. V. Camp, T. Krigas, *Nature* **1965**, *205*, 698
7. P. M. Takahara, A. C. Rosenzweig, C. A. Frederick, S. J. Lippard, *Nature* **1995**, 649
8. P. J. Dyson, G. Sava, *Dalton Trans.* **2006**, 1929
9. T. Boulikas, M. Vougiouka, *Oncol. Rep.* **2003**, *10*, 1663
10. L. S. Hollis, A. R. Amundsen, E. W. Stern, *J. Med. Chem.* **1989**, *32*, 128
11. M. B. Kloster, J. C. Hannis, D. C. Muddiman, N. Farrell, *Biochemistry* **1999**, *38*, 14731
12. B. Lippert, ed. *Cisplatin, Chemistry and Biochemistry of a Leading Anti-Cancer Drug*. 1999, Wiley-VCH, Weinheim.
13. K. S. Lovejoy, R. C. Todd, S. Zhang, M. S. McCormick, J. A. D'Aquino, J. T. Reardon, A. Sancar, K. M. Giacomini, S. J. Lippard, *Proc. Natl. Acad. Sci. U. S. A.* **2008**, *105*, 8902
14. E. I. Montero, S. Diaz, A. M. Gonzalez-Vadillo, J. M. Perez, C. Alonso, C. Navarro-Ranninger, *J. Med. Chem.* **1999**, *42*, 4264
15. G. Natile, M. Coluccia, *Coord. Chem. Rev.* **2001**, *216-217*, 383
16. F. P. Dwyer, E. C. Gyarfas, W. P. Rogers, J. H. Koch, *Nature* **1952**, *170*, 190
17. M. Galanski, V. B. Arion, M. A. Jakupec, B. K. Keppler, *Curr. Pharm. Des.* **2003**, *9*, 2078
18. I. Kostova, *Curr.Med.Chem* **2006**, *13*, 1085
19. M. J. Clarke, *Met. Ions Biol. Syst.* **1980**, *11*, 231
20. M. J. Clarke, *Coord. Chem. Rev.* **2003**, *236*, 209
21. A. Bergamo, L. Messori, F. Piccioli, M. Cocchietto, G. Sava, *Invest. New Drugs* **2003**, *21*, 401
22. S. Kapitza, M. Pongratz, M. A. Jakupec, P. Heffeter, W. Berger, L. Lackinger, B. K. Keppler, B. Marian, *J. Cancer. Res. Clin. Oncol.* **2005**, *131*, 101
23. A. Bergamo, G. Sava, *Dalton Trans.* **2007**, 1267
24. F. Lentz, A. Drescher, A. Lindauer, M. Henke, R. A. Hilger, C. G. Hartinger, M. E. Scheulen, C. Dittrich, B. K. Keppler, U. Jaehde, *Anti-Cancer Drugs* **2009**, *20*, 97
25. B. Therrien, *Coord. Chem. Rev.* **2009**, *253*, 493
26. R. E. Morris, R. E. Aird, P. d. S. Murdoch, H. Chen, J. Cummings, N. D. Hughes, S. Parsons, A. Parkin, G. Boyd, D. I. Jodrell, P. J. Sadler, *J. Med. Chem.* **2001**, *44*, 3616

27. C. S. Allardyce, P. J. Dyson, D. J. Ellis, S. L. Heath, *Chem. Commun.* **2001**, 1396
28. H. Chen, J. A. Parkinson, R. E. Morris, P. J. Sadler, *J. Am. Chem. Soc.* **2003**, *125*, 173
29. F. Wang, H. Chen, S. Parsons, I. D. H. Oswald, J. E. Davidson, P. J. Sadler, *Chem. Eur. J.* **2003**, 5810
30. C. Scolaro, C. G. Hartinger, C. S. Allardyce, B. K. Keppler, P. J. Dyson, *J. Inorg. Biochem.* **2008**, 1743
31. B. Therrien, W. H. Ang, F. Cherioux, L. Vieille-Petit, L. Juillerat-Jeanneret, G. Suss-Fink, P. J. Dyson, *J. Cluster Sci.* **2007**, *18*, 741
32. M.-G. Mendoza-Ferri, C. G. Hartinger, R. E. Eichinger, N. Stolyarova, K. Severin, M. A. Jakupec, A. A. Nazarov, B. K. Keppler, *Organometallics* **2008**, *27*, 2405
33. M. G. Mendoza-Ferri, C. G. Hartinger, M. A. Mendoza, M. Groessl, A. E. Egger, R. E. Eichinger, J. B. Mangrum, N. P. Farrell, M. Maruszak, P. J. Bednarski, F. Klein, M. A. Jakupec, A. A. Nazarov, K. Severin, B. K. Keppler, *J. Med. Chem.* **2009**, *52*, 916
34. F. Schmitt, P. Govindaswamy, G. Suss-Fink, W. H. Ang, P. J. Dyson, L. Juillerat-Jeanneret, B. Therrien, *J. Med. Chem.* **2008**, *51*, 1811
35. F. Schmitt, P. Govindaswamy, O. Zava, G. Süss-Fink, L. Juillerat-Jeanneret, B. Therrien, *J. Biol. Inorg. Chem.* **2009**, *14*, 101
36. Y. Matsumura, H. Maeda, *Cancer. Res.* **1986** *46* 6387
37. H. Maeda, *Advan. Enzyme Regul.* **2001**, *41*, 189
38. S. Svenson, D. A. Tomalia, *Adv. Drug Deliv. Rev.* **2005**, *57*, 2106
39. N. Malik, E. G. Evagorou, R. Duncan, *Anti-Cancer Drugs* **1999**, *10*, 767
40. N. W. S. Kam, T. C. Jessop, P. A. Wender, H. Dai, *J. Am. Chem. Soc.* **2004**, *126*, 6850
41. N. W. S. Kam, Z. Liu, H. Dai, *J. Am. Chem. Soc.* **2005**, *127*, 12492
42. Z. Liu, W. Cai, L. He, N. Nakayama, K. Chen, X. Sun, X. Chen, H. Dai, *Nat. Nanotechnol.* **2007**, *2*, 47
43. K. Ajima, T. Murakami, Y. Mizoguchi, K. Tsuchida, T. Ichihashi, S. Iijima, M. Yudasaka, *ACS Nano* **2008**, *2*, 2057
44. S. Dhar, L. Zhuang, J. Tomale, H. Dai, S. J. Lippard, *J. Am. Chem. Soc.* **2008**, *130*, 11467
45. C. Lu, R. Perez-Soler, B. Piperdi, G. L. Walsh, S. G. Swisher, W. R. Smythe, H. J. Shin, J. Y. Ro, L. Feng, M. Truong, A. Yalamanchili, G. Lopez-Berestein, W. K. Hong, A. R. Khokhar, D. M. Shin, *J. Clin. Oncol.* **2005**, *23*,
46. A. R. Kennedy, A. J. Florence, F. J. McInnesb, N. J. Wheate, *Dalton Trans.* **2009**, 7695
47. Y. Zhao, M. S. Bali, C. Cullinane, A. I. Day, J. G. Collins, *Dalton Trans.* **2009**, 5190
48. C. Sanchez-Cano, M. J. Hannon, *Dalton Trans.* **2009**, 10702
49. G. Winkhaus, H. Singer, *J. Organomet. Chem.* **1967**, *7*, 487
50. R. A. Zelonka, M. C. Baird, *Can. J. Chem.* **1972**, *50*, 3063
51. M. A. Bennett, A. K. Smith, *Dalton Trans.* **1974**, 233
52. D. A. Tomalia, H. Baker, J. R. Dewald, M. Hall, G. Kallos, S. Martin, J. Roeck, J. Ryder, P. Smith, *Polym. J.* **1985**, *17*, 117

53. C. J. Hawker, J. M. J. Frechet, *J. Am. Chem. Soc.* **1990**, *112*, 7638
54. C. C. Lee, J. A. MacKay, J. M. J. Fréchet, F. C. Szoka, *Nature Biotech.* **2005**, *23*, 1517
55. D. A. Tomalia, L. A. Reyna, S. Svenson, *Biochem. Soc. Trans.* **2007**, *35*, 61
56. U. Boas, J. B. Christensen, P. M. H. Heegaard, *Dendrimers in Medicine and Biotechnology: New Molecular Tools*. 2006: RSC Publishing.
57. F. Aulenta, W. Hayes, S. Rannard, *Eur. Polym. J.* **2003**, *39*, 1741
58. J. B. Wolinsky, M. W. Grinstaff, *Adv. Drug Deliv. Rev.* **2008**, *60*, 1037
59. A. Agarwal, S. Saraf, A. Asthana, U. Gupta, V. Gajbhiye, N. K. Jain, *Int. J. Pharm.* **2008**, *350*, 3
60. E. R. Gillies, J. M. J. Fréchet, *Drug Discov. Today* **2005**, *10*,
61. M. Liu, J. M. J. Fréchet, *PSTT* **1999**, *2*, 393
62. B. A. J. Jansen, J. van des Zwan, J. Reedijk, H. d. Dulk, J. Brouwer, *Eur. J. Inorg. Chem.* **1999**, 1429
63. T. Kapp, A. Dullin, R. Gust, *J. Med. Chem.* **2006**, *49*, 1182
64. W. H. Ang, E. Daldini, L. Juillerat-Jeannerat, P. J. Dyson, *Inorg. Chem.* **2007**, *46*, 9048
65. L. Carter, D. L. Davies, J. Fawcett, D. R. Russell, *Polyhedron* **1993**, *12* 1123
66. A. J. Steedman, A. K. Burrell, *Acta Crystallogr. Sect.* **1997**, *C 53*, 864
67. C. A. Vock, C. Scolaro, A. D. Phillips, R. Scopelitti, G. Sava, P. J. Dyson, *J. Med. Chem.* **2006**, *49* 5552
68. J.-M. Lehn, *Supramolecular Chemistry - Concepts and Perspectives*. 1995, Weinheim: Wiley-VCH.
69. D. Philp, J. F. Stoddart, *Angew. Chem., Int. Ed. Engl.* **1996**, *35*, 1154
70. J.-M. Lehn, *Proc. Natl. Acad. Sci. U.S.A.* **2002**, *99*, 4763
71. G. M. Whitesides, M. Boncheva, *Proc. Natl. Acad. Sci. U.S.A.* **2002**, *99*, 4769
72. F. J. Hof, *Proc. Natl. Acad. Sci. U.S.A.* **2002**, *99*, 4775
73. M. Fujita, J. Yazaki, K. Ogura, *J. Am. Chem. Soc.* **1990**, *112*, 5645
74. P. J. Stang, B. Olenyuk, *Acc. Chem. Res.* **1997**, *30*, 502
75. P. J. Stang, D. H. Cao, S. Saito, A. M. Arif, *J. Am. Chem. Soc.* **1995**, *117*,
76. P. J. Stang, K. Chen, *J. Am. Chem. Soc.* **1995**, *117*, 1667
77. P. J. Stang, A. M. Arif, *J. Am. Chem. Soc.* **1995**, *117*, 8793
78. P. J. Stang, J. A. Whiteford, *Organometallics* **1994**, *13*, 3776
79. J. A. Whiteford, C. V. Lu, P. J. Stang, *J. Am. Chem. Soc.* **1997**, *119*, 2524
80. R. V. Slone, D. I. Yoon, R. M. Calhoun, J. T. Hupp, *J. Am. Chem. Soc.* **1995**, *117*, 11813
81. M. Fujita, S. Nagao, M. Iida, K. Ogata, K. Ogura, *J. Am. Chem. Soc.* **1993**, *116*, 1574
82. X.-Y. Yu, M. Maekawa, M. Kondo, S. Kitagawa, G.-X. Jin, *Chem. Lett.* **2001**, 168
83. M. Schweiger, S. Russell-Siedel, A. M. Arif, P. J. Stang, *Angew. Chem., Int. Ed.* **2001**, *40*, 3467
84. S. Derossi, M. Casanova, E. Lengo, E. Zangrando, M. Stener, E. Alessio, *Inorg. Chem.* **2007**, *46*, 11243
85. R. V. Slone, K. D. Benkstein, S. Bélanger, J. T. Hupp, I. A. Guzei, A. L. Rheingold, *Coord. Chem. Rev.* **1998**, *171*, 221

86. H. Yan, G. Süss-Fink, A. Neels, H. Stoeckli-Evans, *Dalton Trans.* **1997**, 4345
87. C. J. Kuehl, S. D. Huang, P. J. Stang, *J. Am. Chem. Soc.* **2001**, *123*, 9634
88. R. Kramer, K. Polborn, C. Robl, W. Beck, *Inorg. Chim. Acta* **1992**, *198-200*, 415
89. P. Annen, S. Schildberg, W. S. Sheldrick, *Inorg. Chim. Acta* **2000**, *307*, 115
90. S. Korn, W. S. Sheldrick, *Inorg. Chim. Acta* **1997**, *254*, 85
91. H. Chen, M. M. Olmstead, D. P. Smith, M. F. Maestre, R. H. Fish, *Angew. Chem., Int. Ed. Engl.* **1995**, *34*, 1514
92. K. Yamanari, S. Yamamoto, R. Ito, Y. Kushi, A. Fuyuhiro, N. Kubota, T. Fukuo, R. Arakawa, *Angew. Chem., Int. Ed.* **2001**, *40*, 2268
93. K. Yamanari, R. Ito, S. Yamamoto, T. Konno, A. Fuyuhiro, K. Fujioka, R. Arakawa, *Inorg. Chem.* **2002**, *41*, 6824
94. L.-M. Lehaire, R. Scopelliti, L. Herdeis, K. Polborn, P. Mayer, K. Severin, *Inorg. Chem.* **2004**, *43*, 1609
95. Z. Grote, L.-M. Lehaire, R. Scopelliti, K. Severin, *J. Am. Chem. Soc.* **2003**, *125*, 13638
96. H. Piotrowski, K. Severin, *Proc. Natl. Acad. Sci. U. S. A.* **2002**, *99*, 4997
97. L.-M. Lehaire, R. Scopelliti, K. Severin, *Angew. Chem., Int. Ed.* **2002**, *41*, 1419
98. T. Kusukawa, M. Fujita, *Angew. Chem., Int. Ed.* **1998**, *37*, 3142
99. T. Kusukawa, M. Yoshizawa, M. Fujita, *Angew. Chem., Int. Ed.* **2001**, *40*, 1879
100. T. Kusukawa, M. Fujita, *J. Am. Chem. Soc.* **2002**, *124*, 13576
101. K. Nakabayashi, M. Kawano, M. Yoshizawa, S. Ohkoshi, M. Fujita, *J. Am. Chem. Soc.* **2004**, *126*, 16694
102. M. Kawano, Y. Kobayashi, T. Ozeki, M. Fujita, *J. Am. Chem. Soc.* **2006**, *128*, 6558
103. K. Nakabayashi, M. Kawano, T. Kato, T. Furukawa, S. Ohkoshi, T. Hozumi, M. Fujita, *Chem.: Asian J.* **2007**, *2*, 164
104. K. Ono, M. Yoshizawa, M. Akita, T. Kato, Y. Tsunobuchi, S. Ohkoshi, M. Fujita, *J. Am. Chem. Soc.* **2009**, *131*, 2782
105. T. Sawada, M. Yoshizawa, S. Sato, M. Fujita, *Nat. Chem.* **2009**, *1*, 53
106. R. Kieltyka, P. Englebienne, J. Kakhoury, C. Autexier, N. Moitessier, H. F. Sleiman, *J. Am. Chem. Soc.* **2008**, *130*, 10040
107. T. Kusukawa, M. Fujita, *J. Am. Chem. Soc.* **1999**, *121*, 1397
108. M. Yoshizawa, M. Tamura, M. Fujita, *J. Am. Chem. Soc.* **2004**, *126*, 6846
109. S. Tashiro, M. Tominaga, M. Kawano, B. Therrien, T. Ozeki, M. Fujita, *J. Am. Chem. Soc.* **2005**, *127*, 4546
110. M. Yoshizawa, Y. Takeyama, T. Kusukawa, M. Fujita, *Angew. Chem., Int. Ed.* **2002**, *41*, 1347
111. M. Yoshizawa, M. Tamura, M. Fujita, *Science* **2006**, *312*, 251
112. T. Yamaguchi, M. Fujita, *Angew. Chem., Int. Ed.* **2008**, *47*, 2067
113. Y. Nishioka, T. Yamaguchi, M. Kawano, M. Fujita, *J. Am. Chem. Soc.* **2008**, *130*, 8160
114. W. H. Ang, Z. Grote, R. Scopelliti, L. Juillerat-Jeanneret, K. Severin, P. J. Dyson, *J. Organomet. Chem.* **2009**, *694*, 968
115. M. J. Hannon, V. Moreno, M. J. Prieto, E. Moldrheim, E. Sletten, I. Meistermann, C. J. Isaac, K. J. Sanders, A. Rodger, *Angew. Chem., Int. Ed.* **2001**, *40*, 879
116. Y.-F. Han, W.-G. Jia, Y.-J. Lin, G.-X. Jin, *Organometallics* **2008**, *27*, 5002

117. L. A. Berben, M. C. Faia, N. R. M. Crawford, J. R. Long, *Inorg. Chem.* **2006**, *45*, 6378
118. J. Mattsson, P. Govindaswamy, J. Furrer, Y. Sei, K. Yamaguchi, G. Süss-Fink, B. Therrien, *Organometallics* **2008**, *27*, 4346
119. B. Therrien, G. Suss-Fink, P. Govindaswamy, A. K. Renfrew, P. J. Dyson, *Angew. Chem., Int. Ed. Engl.* **2008**, *47*, 3773
120. P. Govindaswamy, J. Furrer, G. Süss-Fink, B. Therrien, *Z. Anorg. Allg. Chem.* **2008**, *634*, 1349
121. S. Kitagawa, S. Kawata, *Coord. Chem. Rev.* **2002**, *224*, 11
122. M. D. Ward, *Inorg. Chem.* **1996**, *35*, 1712
123. A. K. Gupta, A. Gupta, A. Choudhury, *Indian J. Chem.* **2002**, *41A*, 2076
124. O. Zava, J. Mattsson, B. Therrien, P. J. Dyson, *Chem. Eur. J.* **2010**, *16*, 1428
125. F. Linares, M. A. Galindo, S. Galli, M. A. Romero, J. A. R. Navarro, E. Barea, *Inorg. Chem.* **2009**, *48*, 7413
126. M. Fujita, D. Ogura, M. Miyazawa, H. Oka, K. Yamaguchi, K. Ogura, *Nature* **1995**, *378*, 469
127. H. Ito, T. Kusukawa, M. Fujita, *Chem. Lett.* **2000**, 598
128. P. J. Stang, B. Olenyuk, D. C. Muddiman, R. D. Smith, *Organometallics* **1997**, *16*, 3094
129. X. Chi, A. J. Guerin, R. A. Haycock, C. A. Hunter, L. D. Sarson, *Chem. Commun.* **1995**, 2563
130. S. Roche, C. Haslam, H. Adams, S. L. Heath, J. A. Thomas, *Chem. Commun.* **1998**, 1681
131. A. Marquis-Rigault, A. Dupont-Gervais, P. N. W. Baxter, A. V. Dorsselaer, J.-M. Lehn, *Inorg. Chem.* **1996**, *35*, 2307
132. K. Kumazawa, K. Biradha, T. Kusukawa, T. Okano, M. Fujita, *Angew. Chem., Int. Ed.* **2003**, *42*, 3909
133. K. Umemoto, K. Yamaguchi, M. Fujita, *J. Am. Chem. Soc.* **2000**, *122*, 7150
134. M. Fujita, M. Tominaga, A. Hori, B. Therrien, *Acc. Chem. Res.* **2005**, *38*, 371
135. C. J. Kuehl, T. Yamamoto, S. R. Seidel, P. J. Stang, *Org. Lett.* **2002**, *4*, 913
136. Y. K. Kryschenko, S. R. Seidel, D. C. Muddiman, A. I. Nepomuceno, P. J. Stang, *J. Am. Chem. Soc.* **2003**, *125*, 9647
137. P. Govindaswamy, D. Linder, J. Lacour, G. Süss-Fink, B. Therrien, *Chem. Commun.* **2006**, 4691
138. P. Govindaswamy, G. Süss-Fink, B. Therrien, *Organometallics* **2007**, *26*, 915
139. P. Govindaswamy, J. Furrer, G. Süss-Fink, B. Therrien, *Z. Anorg. Allg. Chem.* **2008**, *634*, 1349
140. S. Tsuzuki, K. Honda, T. Uchimura, M. Mikami, K. Tanabe, *J. Am. Chem. Soc.* **2002**, *124*, 104
141. J.-Q. Wang, C.-X. Ren, G.-X. Jin, *Chem. Commun.* **2005**, 4738
142. L. Hernandez-Folgado, D. Baretic, I. Piantanida, M. Marjanovic, M. Kralj, T. Rehm, C. Schmuck, *Chem. Eur. J.* **2010**, *16*, 3036
143. P. J. Dyson, W. H. Ang, L. J. Parker, A. De Luca, L. Juillerat-Jeanneret, C. J. Morton, M. L. Bello, M. W. Parker, *Angew. Chem., Int. Ed.* **2009**, *48*, 3854
144. S. Leroy-Lhez, F. Fages, *Eur. J. Org. Chem* **2005**, 2684
145. D. H. Wu, A. Chen, C. S. Johnson, *J. Magn. Reson. A.* **1995**, *115*, 123

146. C. S. J. Johnson, *Prog. Nucl. Magn. Reson. Spectrosc.* **1999**, *34*, 203
147. D. Ajami, J. J. Rebek, *Angew. Chem., Int. Ed.* **2007**, *46*, 9283
148. J.-F. Lemonnier, S. Floquet, A. Kachmar, M.-M. Rohmer, M. Bénard, J. Marrot, E. Terazzi, C. Piguet, E. Cadot, *Dalton Trans.* **2007**, 3043
149. N. P. E. Barry, J. Furrer, J. Freudenreich, G. Süss-Fink, B. Therrien, *Eur. J. Inorg. Chem.* **2010**, 725
150. A. F. A. Peacock, P. J. Sadler, *Chem. -Asian J.* **2008**, *3*, 1890
151. C. G. Hartinger, P. J. Dyson, *Chem. Soc. Rev.* **2009**, *38*, 391
152. P. J. Dyson, *Chimia* **2007**, *61*, 698
153. G. Süss-Fink, *Dalton Trans.* **2010**, *39*, 1673
154. F. M. Winnik, *Chem. Rev.* **1993**, *93*, 587
155. J. Mattsson, P. Govindaswamy, A. K. Renfrew, P. J. Dyson, P. Štěpnička, G. Süss-Fink, B. Therrien, *Organometallics* **2009**, *28*, 4350
156. N. P. E. Barry, F. Edafe, P. J. Dyson, B. Therrien, *Dalton Trans.* **2010**, 2816
157. A. L. Harris, X. Yang, A. Hegmans, L. Povirk, J. L. Ryan, L. Kelland, N. P. Farrell, *Inorg. Chem.* **2005**, *44*, 9598
158. Z. Ma, J. Roy Choudhury, M. W. Wright, C. S. Day, G. Saluta, G. L. Kucera, U. Bierbach, *J. Med. Chem.* **2008**, *51*, 7574
159. A. V. Klein, T. W. Hambley, *Chem. Rev.* **2009**, *109*, 4911
160. C. T. Supuran, A. Scozzafava, A. Casini, *Med. Res. Rev.* **2003**, *23*, 146
161. A. Thiry, C. T. Supuran, B. Masereel, J.-M. Dogné, *J. Med. Chem.* **2008**, *51*, 3051
162. H.-W. Lo, F. Ali-Osman, *Curr. Opin. Pharmacol.* **2007**, *7*, 367
163. W. H. Ang, A. De Luca, C. Chapuis-Bernasconi, L. Juillerat-Jeanneret, L. B. M., P. J. Dyson, *ChemMedChem.* **2007**, *2*, 1799
164. J. D. Hayes, J. U. Flanagan, I. R. Jowsey, *Ann. Rev. Pharmacol. Toxicol.* **2005**, *45*, 51
165. C. A. Puckett, J. K. Barton, *Biochem. J.* **2008**, *409-416*, 11711
166. O. Briz, M. A. Serrano, N. Rebollo, B. Hagenbuch, P. J. Meier, H. Koepsell, J. J. Marin, *Mol. Pharmacol.* **2002**, *61*, 853
167. D. L. Bourdet, D. R. Thakker, *Pharm. Res.* **2006**, *23*, 1165
168. M. A. Bennett, T. N. Huang, T. W. Matheson, A. K. Smith *Inorganic Synthesis* Ed H. D. Kaesz, John Wiley & Sons Inc., **1982**, *21*, 74
169. H. L. Anderson, S. Anderson, J. K. M. Sanders, *J. Chem. Soc., Perkin Trans.* **1995**, *1*, 2231
170. G. M. Sheldrick, *Acta Crystallogr.* **2008**, *A64*, 112
171. L. J. Farrugia, *J. Appl. Crystallogr.* **1997**, *30*, 565
172. C. F. Macrae, P. R. Edgington, P. McCabe, E. Pidcock, G. P. Shields, R. Taylor, M. Towler, J. van de Streek, *J. Appl. Crystallogr.* **2006**, *39*, 453
173. P. Govender, N. C. Antonels, J. Mattsson, A. K. Renfrew, P. J. Dyson, J. R. Moss, B. Therrien, G. S. Smith, *J. Organomet. Chem.* **2009**, *694*, 3470

Appendix

1 X-ray crystallography structures

Crystallographic data of solved structures in this thesis can be retrieved from the Cambridge Crystallographic Data Centre (CCDC). Given in the table below is the compound number with corresponding CCDC number.

Compound	CCDC number	Found on page	Found in reference
5	CCDC-723508	28	[173]
[**17**][$O_3SCF_3]_4$	CCDC-721012	47	[155]
[**22**][$O_3SCF_3]_4$	CCDC-721013	49	[155]
[pyrene⊂**23**][$O_3SCF_3]_6$	CCDC-685450	72	[118]
[benzo[*e*]pyrene⊂**23**][$O_3SCF_3]_6$	CCDC-662926	72	[118]

2. List of publications

J. Mattsson, P. Govindaswamy, J. Furrer, Y. Sei, K. Yamaguchi, G. Süss-Fink, B. Therrien. Encapsulation of aromatic molecules in hexanuclear arene ruthenium cages: A strategy to build up organometallic carceplex Prisms with a dangling arm standing out. *Organometallics* **2008**, *27*, 4346

J. Mattsson, P. Govindaswamy, A. K. Renfrew, P. J. Dyson, P. Štěpnička, G. Süss-Fink, B. Therrien. Synthesis, molecular structure, and anticancer activity of cationic arene ruthenium metalla-rectangles. *Organometallics* **2009**, *28*, 4350

P. Govender, N. C. Antonels, J. Mattsson, A. K. Renfrew, P. J. Dyson, J. R. Moss, B. Therrien, G. S. Smith. Anticancer activity of multinuclear arene ruthenium complexes coordinated to dendritic polypyridyl scaffolds. *J. Organomet. Chem.* **2009**, *694*, 3470

M. Auzias, J. Mattsson, B. Therrien, G. Süss-Fink. New dinuclear $Ru_2(CO)_4$ sawhorse-type complexes containing bridging carboxylato ligands. *Z. Anorg. Allg. Chem.* **2009,** *635*, 115

O. Zava, J. Mattsson, B. Therrien, P. J. Dyson. Evidence for drug release from a metalla-cage delivery vector following cellular internalization. *Chem. Eur. J.* **2010**, *16*, 1428

J. Mattsson, O. Zava, A. K. Renfrew, Y. Sei, K. Yamaguchi, P. J. Dyson, B. Therrien. Drug delivery of lipophilic pyrenyl derivatives by encapsulation in a water soluble metalla-cage. *Dalton Trans.* **2010,** In Press